UNIVERSITY OF ALBERTA

PUNCHING SHEAR CAPACITY OF SLAB-COLUMN CONNECTIONS WITH STEEL-FIBRE REINFORCEMENT UNDER LATERAL CYCLIC LOADING

BY

SASCHA KEN SCHREIBER

A thesis submitted to the Faculty of Graduate Studies and Research in partial fulfillment of the requirements for the degree of MASTER OF SCIENCE

IN

STRUCTURAL ENGINEERING

DEPARTMENT OF CIVIL AND ENVIRONMENTAL ENGINEERING

EDMONTON, ALBERTA

SPRING 2001

National Library of Canada
Acquisitions and Bibliographic Services
395 Wellington Street
Ottawa ON K1A 0N4
Canada

Bibliothèque nationale du Canada
Acquisitions et services bibliographiques
395, rue Wellington
Ottawa ON K1A 0N4
Canada

Your file Votre référence

Our file Notre référence

The author has granted a non-exclusive licence allowing the National Library of Canada to reproduce, loan, distribute or sell copies of this thesis in microform, paper or electronic formats.

L'auteur a accordé une licence non exclusive permettant à la Bibliothèque nationale du Canada de reproduire, prêter, distribuer ou vendre des copies de cette thèse sous la forme de microfiche/film, de reproduction sur papier ou sur format électronique.

The author retains ownership of the copyright in this thesis. Neither the thesis nor substantial extracts from it may be printed or otherwise reproduced without the author's permission.

L'auteur conserve la propriété du droit d'auteur qui protège cette thèse. Ni la thèse ni des extraits substantiels de celle-ci ne doivent être imprimés ou autrement reproduits sans son autorisation.

0-612-60493-4

Canada

University of Alberta

Library Release Form

Name of Author: Sascha Ken Schreiber

Title of Thesis: Punching Shear Capacity of Slab-Column Connections with Steel-Fibre Reinforcement under Lateral Cyclic Loading

Degree: Master of Science

Year this Degree Granted: 2001

Permission is hereby granted to the University of Alberta Library to reproduce single copies of this thesis and to lend or sell such copies for private, scholarly or scientific purposes only.

The author reserves all other publication and other rights in association with the copyright in the thesis, and except as herein before provided, neither the thesis nor any substantial portion thereof may be printed or otherwise reproduced in any material form whatever without the author's prior written permission.

S. Schreiber

Sascha Schreiber
50 Knudson Drive
Kanata, ON
K2K 2L6
Canada

Date: April 25, 2001

UNIVERSITY OF ALBERTA

FACULTY OF GRADUATE STUDIES AND RESEARCH

The undersigned certify that they have read, and recommend to the Faculty of Graduate Studies and Research for acceptance, a thesis entitled PUNCHING SHEAR CAPACITY OF SLAB-COLUMN CONNECTIONS WITH STEEL-FIBRE REINFORCEMENT UNDER LATERAL CYCLIC LOADING submitted by SASCHA KEN SCHREIBER in partial fulfillment of the requirements for the degree of MASTER OF SCIENCE in STRUCTURAL ENGINEERING.

Dr. S. D. B. Alexander (Supervisor)

Dr. A. E. Elwi

Dr. W. A. Lipsett

Date: April 24, 2001

ABSTRACT

The effect of steel fibre reinforcement on the seismic performance of an interior slab-column connection was investigated experimentally. Two full-scale isolated slab-column connections were tested under cyclic lateral loading to determine the effect of adding corrugated steel fibres to the concrete on the shear capacity of the connection. The addition of steel fibres increased the shear and flexural capacity, increased the torsional stiffness, and significantly increased the ductility of the connection. It is concluded that the addition of steel fibres is a practical alternative to increase the shear capacity of slabs in both new construction and rehabilitation projects.

ACKNOWLEDGEMENT

Sincere gratitude and appreciation is expressed to Prof. Scott D.B. Alexander for his guidance, supervision and encouragement throughout the course of this research. Appreciation is also due to the members of the examination committee, Profs. Alaa. E. Elwi and William. A. Lipsett, for their constructive input in this work.

The author would like to thank Richard Helfrich at the I. F. Morrison Structural Engineering Laboratory of the University of Alberta for his brilliant technical assistance in this project. Many thanks to Malika A. Ali for her help with figures in this work.

Financial support for this study was provided by the federal government of Canada through the National Science and Engineering Research Council and by Read Jones Christoffersen Ltd. of Edmonton, and is greatly appreciated.

Table of Contents

Chapter	Page
1. Introduction	1
Description of the Problem	1
Objectives and Scope	2
Organization of the Report	3
2. Background	4
2.1 Introduction	4
2.2 Literature Survey	4
2.2.1 Swamy and Ali (1982)	4
2.2.2 Durrani and Diaz (1992)	7
2.2.3 Alexander and Simmonds (1992)	9
2.2.4 Shaaban and Gesund (1994)	11
2.2.5 McHarg et. al. (2000)	13
2.3 Discussion of Previous Test Results	14
3. Experimental Program	17
3.1 Objectives of Testing	17
3.2 Experimental Program	17
3.3 Design of the Experiments	18
3.4 Materials	20
3.4.1 Concrete	20
3.4.2 Reinforcement	21

3.4.2.1 Deformed Bar Reinforcement 21

3.4.2.2 Steel Fibre Reinforcement 22

3.5 Fabrication of the Specimens 23

3.6 Testing 24

3.6.1 Test Set-up 24

3.6.1.1 Column Support 24

3.6.1.2 Vertical Edge Links 24

3.6.1.3 Slab Edge Restraints 25

3.6.1.4 Loading 26

3.6.2 Instrumentation 27

3.6.2.1 Internal Measurements 27

3.6.2.2 External Measurements 28

3.6.3 Test Procedure 29

4. Test Results and Observations 56

4.1 General 56

4.2 General Behaviour of the Test Specimens 57

4.2.1 Observations made during the Test 57

4.2.2 Observations at Failure 57

4.3 Test Results 59

4.3.1 Statics 59

4.3.2 Support Reactions and Equilibrium 60

4.3.3 Edge Restraints 61

4.3.4 Lateral Load-Drift Response 62

4.3.5 Stiffness and Ductility of the Connection 64

4.3.6 Slab Deflections and Rotations 66

4.3.7 Internal Forces and Strains 68

5. Discussion of Test Results 104

5.1 Effects of Steel Fibres 104

5.2 Comparison of Test Results to Code Provisions 105

5.3 Comparison of Test Results to the Strip Model 107

5.4 Slab Forces at Peak Lateral Load 109

5.5 Degradation of the Stiffness of the Connection 112

5.6 Proposed Design Equation 114

6. Summary, Conclusions and Recommendations 119

6.1 Summary 119

6.2 Conclusions 120

6.3 Recommendations 122

List of References 124

Appendix A 126

Appendix B 130

List of Tables

Table		Page
3.1	Concrete Strengths	31
3.2	Effective Depths of Slab Reinforcement	32
3.3	Reinforcement Ratios	32
3.4	Properties of Reinforcement Steel	32
4.1	Horizontal Static Check	72
4.2	Vertical Static Check	72
4.3	Vertical Load in edge Boundary Condition Links	73
4.4	Moment Check around Connection	74
4.5	North-South Edge Restraints	75
4.6	East-West Edge Restraints	76
4.7	Comparison of Load-Drift Response	77
4.8	Comparison of Vertical Slab Deflections – Vertical LVDT's	78
4.9	Comparison of Measured Rotations across E-W Slab Centreline	79
4.10	Calculation of Column Drift at mid-height for each Cycle	80
4.11	Comparison of Measured North and South Slab Edge Rotations	81
4.12	Comparison of North-South Top Bar Strains	82
4.13	Comparison of North-South Bottom Bar Strains	83
4.14	Comparison of East-West Bar Strains	84
5.1	Calculation of Effective Slab Width after each Cycle	116

List of Figures

Figure		Page
3.1	Prototype Flat Plate Structure	33
3.2	Slab Deflection under Gravity Loads	34
3.3	Geometry of Specimen	35
3.4	Column Reinforcement Layout	36
3.5	Slab Reinforcement – Bottom Mat (N-S Direction)	37
3.6	Slab Reinforcement – Bottom Mat (E-W Direction)	37
3.7	Slab Reinforcement – Top Mat (N-S Direction)	38
3.8	Slab Reinforcement – Top Mat (E-W Direction)	38
3.8A	Detail of Reinforcement of Slab	39
3.9	Overall Test Set-up	40
3.10	Lateral Load Test Frame	41
3.10A	Detail of Column Support	42
3.11	Deflection of Prototype under Lateral Load	43
3.12	North-South Slab Edge Boundary Condition	44
3.13	Detail of Vertical Link	45
3.14	Deflected Shape of Model	46
3.15	Slab Edge Restraining System	47
3.16	Plan of Specimen	48
3.17	Elevation of Specimen	48
3.18	Top Mat Gauge Locations (N-S Direction)	49
3.19	Top Mat Gauge Locations (E-W Direction)	50

3.20	Bottom Mat Gauge Locations (N-S Direction)	51
3.21	Bottom Mat Gauge Locations (E-W Direction)	52
3.22	Position of Vertical LVDT's	53
3.23	Position of Cable Transducers	54
3.24	Position of RVDT's	55
4.1	Final Crack Pattern of Steel Fibre Specimen	85
4.2	Final Crack Pattern of Control Specimen	86
4.3	Load in Vertical Edge Boundary Links vs. Lateral Drift – Steel Fibre Specimen	87
4.4	Load in Vertical Edge Boundary Links vs. Lateral Drift – Control Specimen	87
4.5	Free-Body Diagram of Specimen	88
4.6	Sum of Loads in North-South Edge Restraints vs. Lateral Drift – Steel Fibre Specimen	89
4.7	Sum of Loads in North-South Edge Restraints vs. Lateral Drift – Control Specimen	89
4.8	Sum of Loads in East-West Edge Restraints vs. Lateral Drift – Steel Fibre Specimen	90
4.9	Sum of Loads in East-West Edge Restraints vs. Lateral Drift – Control Specimen	90
4.10	Horizontal Load vs. Lateral Drift – Steel Fibre Specimen	91
4.11	Horizontal Load vs. Lateral Drift – Control Specimen	91
4.12	Horizontal Load vs. Lateral Drift – Post Peak Response	92
4.13	Gravity Load Redistribution at Pushover – Steel Fibre Specimen	93
4.14	Gravity Load Redistribution at Pushover – Control Specimen	93
4.15	Stiffness of Connection for each Drift Cycle	94

4.16	Slab Deflections – Steel Fibre Specimen	95
4.17	Slab Deflections – Control Specimen	95
4.18	Slab Rotations – Steel Fibre Specimen	96
4.19	Slab Rotations – Control Specimen	96
4.20	Yielded Bar Locations at Failure in Top Mat – Steel Fibre Specimen	97
4.21	Yielded Bar Locations at Failure in Top Mat – Control Specimen	98
4.22	Yielded Bar Locations at Failure in Bottom Mat – Steel Fibre Specimen	99
4.23	Peak Moments in North-South Top Bars – Steel Fibre Specimen	100
4.24	Peak Moments in North-South Top Bars – Control Specimen	101
4.25	Peak Moments in North-South Bottom Bars – Steel Fibre Specimen	102
4.26	Peak Moments in North-South Bottom Bars – Control Specimen	103
5.1	Location of Compression Struts	117
5.2	Free Body Diagram of Slab Cantilever	117
5.3	Effective Width of Slab after each Cycle	118
A.1	Figure A.1	129
A.2	Figure A.2	129
B.1	Edge Boundary Links	131
B.2	Bottom Column	131
B.3	Bottom Support	132
B.4	Lateral Jack and Edge Restraints	132
B.5	Top Support	133
B.6	Twisting Restraints	133
B.7	Lateral Drift of Steel Fibre Specimen	134

B.8 Cracks at 60 mm Drift – Steel Fibre Specimen 135

B.9 Cracks at 60 mm Drift – Control Specimen 135

B.10 Cracks at Pushover – Steel Fibre Specimen 136

B.11 Cracks at Pushover, Underside of Slab – Steel Fibre Specimen 136

B.12 Cracks at Failure – Control Specimen 137

B.13 Cracks at Failure, Underside of Slab – Control Specimen 137

B.14 Cracks at Failure – Control Specimen 138

B.15 Cracks at Failure, Underside of Slab – Control Specimen 138

List of Symbols

A_s	Total area of reinforcement steel
a	Depth of compression block
B	Slab perimeter supported on one column
b	Column perimeter
b	Width of slab
b_0	Perimeter of critical section
C	Cracking factor
c	Column width
c_1	Column width perpendicular to lateral load
c_2	Column width parallel to lateral load
D	Column deflection due to slab rotation
d	Effective depth of slab
E	Modulus of Elasticity
e	Distance from centroid of critical section to critical perimeter
F	Mass of steel fibres per unit volume of concrete
f'_c	Concrete compressive strength
f_{ct}	Tensile splitting strength of concrete
f_{sp}	Splitting strength of concrete
f_u	Ultimate strength of flexural reinforcement
f_y	Yield strength of flexural reinforcement
h	Slab thickness

ID	Inter-story drift
I_c	Moment of inertia of column
I_{slab}	Effective moment of inertia of slab
J	Polar moment of inertia of critical section
jd	Distance between bar and stress block
K	Stiffness of connection
k_s	Slab stiffness
L	Slab bay width
M	Moment due to lateral load (unbalanced Moment)
M_s	Flexural capacity of radial strips
M_{fib}	Moment capacity resulting from post cracking tension capacity due to fibre reinforcement
M_{neg}	Negative moment capacity of radial strip
M_{pos}	Positive moment capacity of radial strip
M_{res}	Resisting negative moment at connection
P_s	Punching shear load transferred to column by radial strip
Q	Failure criterion
T	Tensile force in reinforcement bar
V	Lateral force
V	Shear force due to gravity loads
V_c	Shear capacity of concrete
v_c	Shear resistance provided by the concrete
v_s	Shear transfer per unit length of radial strip

W_f	Percentage of fibres by weight of concrete
w	Internal shear capacity of slab
w_c	Unit weight of plain concrete
α	Angle of rotation of slab at column
α_1	Ratio of average stress in compression block to the concrete compressive strength
Δ	Inter-story drift in %
ΔD	Column deflection
γ_v	Fraction of unbalanced moment transferred as shear
ρ	Reinforcement ratio

1. INTRODUCTION

1.1 Description of the Problem

In most multi-story reinforced concrete buildings, shear walls or other core structures specifically designed for that purpose resist lateral loads due to wind and particularly earthquake. The remaining structural elements are then designed only for gravity loads; however, during an earthquake event these elements are subjected to and must be able to sustain lateral drift. In flat-slab buildings, inter-story deflections give rise to a moment at the slab-column joint. A portion of this moment is transferred as shear to the slab in the joint region. Since the ultimate strength of flat-slab buildings is frequently governed by the shear or punching capacity of the slab-column connection, an increase in shear due to lateral drift will likely reduce the shear capacity available for gravity loads.

There are a number of options available to the designer to increase punching shear capacity, including changes of geometry in the joint region and the use of shear reinforcement. Punching shear failure is primarily due to the inability of the concrete to sustain large tensile stresses. Appropriately changing the geometry of the joint region will distribute the tensile stresses over a larger surface around the column, thereby reducing peak tensile stresses. The use of drop panels, capitals, deeper slabs or larger columns is often impractical and difficult to construct leading to the use of shear reinforcement. One potential method of increasing the punching shear capacity is the use of steel fibre reinforced concrete. Steel fibres significantly improve the deformation properties of

concrete; they reduce crack widths and deflection. Even after cracking, fibre reinforced concrete can maintain a viable tensile capacity. Finally, the brittle strain behaviour of concrete is made more ductile, resulting in a more gradual failure.

In construction, steel fibres may have many advantages over conventional types of shear reinforcement, including simplicity and flexibility. The use of steel fibres as shear reinforcement does not require any preparation whatsoever; steel fibre reinforced concrete can be mixed at the job site and then placed like ordinary concrete. Steel fibre reinforced concrete can find application in new construction as well as in rehabilitation projects.

To date, Canadian building codes have not recognized the improvement in punching shear strength of slab-column connections due to the addition of steel fibres.
Several tests on the punching shear capacity of steel fibre reinforced concrete under gravity load have been undertaken. It is the purpose of this experiment to investigate the punching shear capacity of slab-column connections subjected to multiple cycles of lateral deflection.

1.2 Objectives and Scope

The research program involved the design, preparation, construction and testing of two full-scale specimens simulating an interior isolated slab-column connection subjected to lateral cyclic loading to study the effect of incorporating steel fibre into the concrete on

punching shear capacity. For that purpose one specimen contained steel fibre reinforced concrete, while the other specimen acted as a "control" specimen without steel fibres. Both specimens were loaded until failure under numerous increasing cycles of lateral drift.

The primary objective of the experiment was to measure, observe and subsequently compare the behaviour of the two specimens. Variables of particular interest were the shear capacity, the initial stiffness, the deterioration of load capacity and the ductility of the connection at failure. This required the design and construction of an effective test-set up to correctly model the behaviour of an interior slab-column connection under both gravity and lateral loads.

1.3 Organization of the Report

Chapter 2 outlines the work of some previous research conducted on the subject and reviews proposed recommendations. Chapter 3 presents a detailed description of the test specimen and the experimental program. Details of fabrication, instrumentation and test procedure are being presented. Test results, observations and a comprehensive description of specimen behaviour are given in Chapter 4. These results are discussed in Chapter 5. Finally, in Chapter 6, a summary of the test results and conclusions or recommendations drawn upon those are presented.

2. BACKGROUND

2.1 Introduction

Provision of shear reinforcement in slab-column connections proves to be an essential requirement for seismic resistant buildings. In the 1999 ACI 421 Draft Report on the design of slabs subjected to seismic and dynamic forces, it is shown that the use of shear capitals in flat slabs may not improve the punching strength of the slab in an earthquake. Indeed, drop panels and shear capitals enhance the punching strength of a slab but do not improve its ductility, an essential characteristic for slabs in earthquake zones. Both, conventional shear reinforcement, such as stirrups, and other types of shear reinforcement like shear studs may be rather difficult and often impractical to place in slabs, especially thin slabs. This gave rise to great interest in the possibility of using steel fibres as an effective type of shear reinforcement. Various research projects on this topic have been undertaken in the past, some of which are presented and discussed here.

2.2 Literature Survey

2.2.1 Swamy and Ali (1982)

Swamy and Ali tested 19 full-scale models of isolated slab column connections of a typical prototype flat-plate structure. The test slabs modelled the moment region around the interior column and inside the line of contra-flexure. This resulted in a test specimen

slab size of 1800 x 1800 x 125 mm with a 150 x 150 mm column. All specimens were simply supported on all four edges of the slab and centrally loaded through a stub-column under gravity load only. The main variables studied were fibre volume, fibre location and flexural reinforcement distribution and fibre type. Concrete strengths were similar for both the fibre reinforced concrete and plain concrete and ranged between 45 MPa and 51 MPa. The first series of interest varied the steel fibre percentage by volume from 0 %, 0.6 %, 0.9 % to 1.2 % (0, 47, 70 and 94 kg/m^3), using crimped steel fibres throughout the whole specimen. The second series of interest used 0.9 % crimped steel fibres by volume in all specimens, but varied the location of the steel fibre concrete in the slab. One specimen contained fibres within a distance of three times the slab thickness (*3h)* around the column and the other contained fibres throughout the slab but only in the 60 mm depth of the tensile face. The last series of interest investigated the differences in behaviour of crimped, plain and hooked steel fibres.

The presence of steel fibres resulted in a significant, up to 58 %, reduction in tensile steel strains, although all slabs showed extensive yielding in the tension steel at 75-80 % of the maximum load. Influence of fibre reinforcement was also evident in the compression steel, which did not experience any yielding. Test results illustrate that fibre reinforcement substantially reduces deflection at all load stages, particularly after initial cracking, regardless if the fibres were distributed over the entire slab area or not. In contrast, variations of the distribution of flexural reinforcement did not affect deflection much.

The authors propose that the diagonal tension-cracking load is related to the load at which the compression steel strain begins to change direction since this occurs as a result of internal shear cracking developed within the critical section. Tension cracking loads observed in the steel fibre specimen were about 40 % higher than in the plain counterparts and the authors conclude that there is a beneficial effect of fibres in controlling and delaying the diagonal tension cracking.

Important reductions in concrete compressive strains at service loads were also achieved. Interestingly, the plain slab specimens were never able to reach the limiting strain of 0.0035 specified by the British concrete code, but the steel fibre specimens achieved strains well beyond this value. As with deflections and strains, fibres had the same effect on slab rotations. The fibre reinforced slabs sustained greater deformations at their failure loads.

At failure, plain slabs failed suddenly in punching with extensive spalling of the tension concrete, while fibre concrete slabs displayed a gradual and ductile punching failure with considerable post-cracking behaviour and residual load capacity. Here, ductility is defined as the ratio of the deflection at 25 percent of maximum load (after reaching maximum load) to the deflection at first crack (as visually observed). The authors found that with a fibre volume of about 1 %, ductility increased by about 100 %, crimped fibres being the most effective. Finally, fibres increased the ultimate punching shear loads from 23 to 42 % as the fibre volume changed from 0.6 to 1.2 %. Fibres in the tension zone only proved to be less effective; however, distributing fibres in a $3h$ wide region around the

column face was as effective as placing the fibres over the entire slab area. The inclusion of fibres progressively pushed the failure cone away from the column face thus enlarging the failure surface.

2.2.2 Durrani and Diaz (1992)

Four one-half scale interior slab-column connections with a slab span of 2.9 m and a 115 mm thickness with a 250 x 250 mm column were tested. The objective was to study the effect of steel fibre reinforcement on the behaviour of connections under simulated earthquake-type loading. The column of each specimen was extended to mid-height and the slab to mid-span. Plain concrete strengths were around 35 MPa. The main variable in this experiment was the fibre reinforcement ratio ranging from 0 (control specimen), 30, 60 to 90 kg/m^3 using 25 mm corrugated steel fibres. Using two different batches of concrete, steel fibre concrete was only placed in the immediate joint region extending 1.2 m away from the column, but including the column region itself. Flexural reinforcement was identical for all specimens. During each test, the specimens were loaded with full gravity dead load and 30 % of the design live load as to simulate the service load condition under the earthquake event. The lateral load was applied at the top of the column and reactions were measured at the edge of the slab and at the column base. Each specimen was subjected to several cycles of increasing lateral displacement until failure.

Two of the specimens featuring the highest fibre reinforcement ratios, 60 and 90 kg/m^3, experienced a flexural failure mode. The two other specimens, 30 kg/m^3 fibre content and plain concrete, both failed in punching shear. The authors conclude that the test result suggest a beneficial effect of using fibre reinforcement in interior slab-column connections, the optimum amount of reinforcement lying between 30 and 60 kg/m^3 fibre content.

The load-drift response for all specimens was linear up to 1 % drift, beyond this point there was a gradual loss of stiffness. All specimens reached their peak load at a 4.5 % drift level; the 60 and the 90 kg/m^3 specimens were able to retain 90 % of the peak load until failure. Overall, the 60 and the 90 kg/m^3 specimens experienced a similar load-drift response, indicating that a fibre content exceeding 90 kg/m^3 will not provide further benefits. The authors propose that a higher concentration of fibres may result in weaker bond with the concrete and a result thereof a large number of fibres pulled out instead of yielding.

The fibre specimens showed higher strength above a 2 % drift and continued to do so until a 4 % drift was reached. Between 3.5 and 4 % drift the non-fibre specimen displayed a sudden loss of load capacity and hence failed. The other specimens were able to carry significant loads up to a 6 % drift. It can be said that presence of fibres increased the strength of the connection by 24 to 39 %. Noteworthy is the convergence in stiffness of all three fibre reinforced specimen; nevertheless their stiffness was higher at all load stages than the plain specimen.

Durrani and Diaz defined ductility as the ratio of maximum drift during a given cycle to that at first yield of the slab reinforcement. The 30 kg/m^3 and the 60 kg/m^3 specimens both had a ductility 2.3 times higher at peak load than at 1.5 % drift, the ductility of the 90 kg/m^3 specimen was 2.8 times higher, and the plain specimen achieved a ductility increase of only 1.2 times.

In conclusion the authors find, that the tensile strength of the concrete matrix is increased by the use of fibre reinforcement and the early disintegration under load reversals is prevented. The most important effects were the increase of shear strength and drift capacity.

2.2.3 Alexander and Simmonds (1992)

Alexander and Simmonds tested full-scale isolated interior slab-column connections under gravity loading. The principal variables were the concrete clear cover for the top mat of the reinforcement and the density of the corrugated steel fibre reinforcement. Of the six specimens, three had a concrete cover of 11 mm, and the remaining series 38 mm, being approximately half and twice the usual concrete cover for slabs, respectively. The steel-fibre reinforcement densities selected were 0, 30 and 60 kg/m^3 for each series. Concrete strengths ranged from 33 to 38 MPa.

During the test, it was observed that adding steel fibres significantly increased both the load capacity and the ductility of the connection. Test results indicate that a fibre content of 30 kg/m^3 increased the ultimate strength of the connection by about 20 % compared to the specimen with no fibres. Doubling the fibre content to 60 kg/m^3 led to a further gain of only 7 %. Similarly, the deflections at ultimate load showed increases of about 40 % and an additional 12 % for fibre contents of 30 and 60 kg/m^3, respectively. It can be concluded that relatively moderate amounts of steel fibres are sufficient to improve the performance of a slab-column connection. Further observations showed an increase in structural stiffness throughout the uncracked and cracked behaviour to the onset of the formation of a folding mechanism within the plate. At this point the specimen carried 20 to 25 % more load than the specimen without fibre reinforcement. The addition of fibres also changed the nature of failure. While the plain concrete specimen punched instantaneously at maximum load the fibre concrete specimen split apart gradually over a period of five minutes as the load fell off. Interestingly, the specimen containing 60 kg/m^3 of fibres with a clear cover of 38 mm experienced a sudden failure.

The authors propose a theory on how the steel fibre reinforcement contributes to the increase in punching strength. According to the bond model also developed by Alexander and Simmonds (1991), the punching shear load transferred to the column by the radial strips in the slab P_s is proportional to $\sqrt{M_s v_s}$, where M_s is the flexural capacity of the radial strip and v_s the shear transfer per unit length. From test observations, the authors conclude that the increased flexural capacity in the plastic deformation stage was solely due to the increased deformations. Further, at the location of plastic hinges in the slab,

only the conventional reinforcement was able to bridge the cracks, hence the steel fibres did not contribute significantly to the moment capacity at yield lines. At the column face, a yield line crossed all the radial strips meaning that the fibre reinforcement did not contribute to M_s but the increase in shear capacity must be attributed to an increase intensity of shear transfer v_s provided by the steel fibres. This shear transfer between plate and strip can occur due to the force gradient in the bar reinforcement or due to the gradient in the moment capacity resulting from the post cracking tension capacity due to the fibre reinforcement M_{fib}. The force gradients in the conventional reinforcement were measured and it was determined that the fibre reinforcement did not alter them in any significant way. Hence, the authors deduce that fibre reinforcement increases the magnitude of v_s mainly through the gradient M_{fib}.

2.2.4 Shaaban and Gesund (1994)

Shaaban and Gesund tested the punching capacity of several isolated slab-column connections under a uniform load with the only variable being the amount of steel fibre reinforcement in the slab concrete. All specimens were designed to fail in punching shear and the design was based on the criterion developed by Gesund and Kaushik (1970):

$$Q = \frac{10\rho^2 f_y d^2}{bB\sqrt{f'_c}} \tag{2.1}$$

where ρ = reinforcement ratio, b = column perimeter, B = slab perimeter supported on one column, d = effective depth of slab, f_y = tensile strength of flexural reinforcement and

f'_c = compressive strength of concrete. The dimensionless failure criterion parameter Q value of less than 2 indicates that a flexural type failure would occur, Q between 2 and 4 means that failure could occur by either failure mechanism and Q greater than 4 indicates a probable punching shear failure. The specimens in this experimental program had a Q value of 4.2.

No formal discussion about the test results has been provided, however it can be deduced that the addition of fibres did increase the ultimate punching strength of the connection. Shabaan and Gesund note that neither the shape, nor the inclination of the failure surface was affected by the presence of steel fibres. The inclination of the failure surface with respect to the horizontal in their tests ranged from 16 to 20 degrees. Other reports have concluded that the inclination of the failure surface is about 20 degrees (Shehata 1990) and 18.5 degrees (Gardner 1990) for plain concrete.

The authors propose a theoretical way of predicting the punching shear strength of steel fibre reinforced flat plates based on ACI 318-89. According to the ACI 318-89 the shear strength of the slab V_c for a square column in SI units is given by:

$$V_c = 0.33\sqrt{f'_c}\, b_0 d \qquad (2.2)$$

where $b_0 = 4(c+d)$ = punching perimeter for a square column, d = effective depth of the slab and c = column width. For slabs containing steel fibre it is suggested that $0.33\sqrt{f'_c}$ should be replaced by the splitting strength f_{sp} of the concrete derived by the same authors in 1993:

$$f_{sp} = \left(0.025W_f + 0.57\right)\sqrt{f'_c}$$

(2.3)

where W_f = the percentage of fibres by weight of concrete = weight of fibres divided by weight of concrete. Making the substitution yields:

$$V_c = FS\left[\left(0.025W_f + 0.57\right)\sqrt{f'_c}\right]b_0 d \quad 0 \le W_f \le 8$$

(2.4)

where FS is a safety factor. This equation is in SI units and is only proposed for square columns.

2.2.5 McHarg et al. (2000)

McHarg et al. tested six full-scale two-way slab specimens representing the 2.3 x 2.3 m column strip regions of an interior connection with a 4 m clear span and 225 x 225 mm column size under gravity load. The slab thickness was 150 mm. The flexural strength was over-designed by 10 % and the punching strength was under-designed having only 66 % of the required strength in order to ensure a punching type failure. Main variables were the location of steel fibre reinforcement and the distribution of the reinforcement bars in the top mat. All specimens had a concrete strength of 30 MPa and a fibre content of 39.4 kg/m^3, if fibres were added. In the test program there were two series of three specimens each, one having banded and the other distributed top reinforcement. For each series, there was one specimen with no fibres (N), one with fibres in the immediate

column region (FS), and the other with fibre reinforced concrete in the top slab cover only (FC).

The cracking loads for the N series were the lowest as expected, a 17% and 8% increase was observed for the FS and FC series, respectively. At full service loads, the FS series exhibited the stiffest behaviour followed by the FC series. The N series experienced the largest deflections. The ultimate strength of the connection was positively influenced by the addition of fibres with the FS series boasting the largest values and the FC series only having a small increase compared to the N specimen. In addition to increased punching shear strength, the presence of steel fibres resulted in a considerable reserve strength after failure. Substantial tensile resistance after cracking of the fibre reinforced concrete has been observed contributing to the post-peak resistance of the slab. The N specimen lost 50% of its load carrying capability at failure, while the FC specimen displayed an increase in post-failure resistance as the deflections increased. The FS series demonstrated the greatest ductility of all specimens; there was no sudden failure, instead general yielding with a horizontal load-deflection curve was observed suggesting a very ductile behaviour.

2.3 Discussion of Previous Test Results

Previous research clearly demonstrates that steel fibres are an effective and practical type of shear reinforcement in slabs. Steel fibre reinforcement not only increases the ultimate strength of slab-column connections, but also provides reserve strength after a punching

shear failure has occurred. It offers significant tensile resistance after cracking of the concrete resulting in improved post-peak strength.

Other important observations of the various experimental programs include the reduction in slab deflections and rotations at all load stages and the reduction of both tensile and compressive strains in the bar reinforcement. Also, fibres need only be placed in an appropriate area in the slab, usually beyond the critical section around the column, and not over the entire slab area to produce the desirable results. Fibres placed in the tension zone only, i.e. not throughout the entire depth of the slab by casting the slab in two stages, proved to be less effective except for crack control purposes.

Discrepancies in the findings in geometry of the failure surface can be found amongst the various research projects. Some results indicated that the failure cone expanded away from the column, thus increasing the failure surface and thereby reducing peak stresses. Other results have shown no difference in failure surfaces between steel fibre specimens and plain specimens.

Most of the previous research suggests that an optimum amount of steel fibres in the concrete lies between 30 to 60 kg/m^3. Amounts of fibres in the lower end of this range are consistently very effective, while amounts in excess of 60 kg/m^3 provide no additional benefits. High steel fibre concentrations appear to cause a loss in bond between each fibre and the concrete, frequently resulting in a complete pullout of the fibre. Also,

incorporating large amounts of fibres into the concrete makes it difficult to place and vibrate properly.

Most importantly, especially for earthquake situations, steel fibre reinforced slab-column connections experience a gradual and ductile punching shear failure. Non-shear reinforced connections undergo a precipitous punching failure, which may be catastrophic during an earthquake. Tests illustrated that the presence of steel fibres enabled the connection to accommodate very high inter-story drifts without loss in load capacity, even under cyclic loading. It is unclear whether steel fibre reinforced slab-column connections are able to sustain a large number of cycles of lateral drift without deterioration in load capacity.

Steel fibres have proven to increase the concrete toughness making the use of steel fibre concrete beneficial in seismic design. Although some slight increases in strength have been attributed to the addition of steel fibres in some previous experiments, steel fibres are not thought to contribute significantly to both the compressive and tensile strength of the concrete. Since code design equations are based on strength and not toughness, the beneficial effect of the use of steel fibres has not been included in the North American building codes to date.

3. EXPERIMENTAL PROGRAM

3.1 Objectives of Testing

The primary objective of this experiment is to investigate the benefit, if any, of using steel fibre-reinforced concrete to improve the punching shear capacity of a reinforced concrete two-way slab-column joint subjected to gravity and lateral loads.

3.2 Experimental Program

Two full-scale specimens were built to model an interior reinforced concrete slab-column connection representative of typical flat slab multi-story buildings. The two specimens were identical in design and testing procedure except that the first specimen contained steel fibres. The second "plain" specimen thus served as a control specimen for comparison purposes.

To permit a more comprehensive description of specimen behaviour a quasi-static test was selected as opposed to a pseudo-dynamic or dynamic test. Quasi-static tests allow the experiment to be interrupted to undertake measurements and visual descriptions like crack patterns. The inertial effects occurring during an earthquake were neglected and the strain rates were lower in this experiment resulting in a softer and weaker response of the specimen.

The dimensions of the two specimens were chosen as to accurately represent a typical multi-story flat slab building. The magnitude and location of the applied slab loading was selected in such manner that the resultant moment and shears at the column face would match those in a prototype slab-column connection. Finally, the lateral loading on the connection was such as to address a typical inter-story drift occurring during an earthquake.

3.3 Design of the Experiments

The prototype for these experiments was an interior slab-column connection located ten floors below the roof of a typical tall building. The top floor was not selected in order to create a more realistic condition at the connection, subjecting the compression stress block to axial load from the column. The prototype building had 4.5 m bays and a floor height of 3 m as illustrated in Figure 3.1. As the experiment was conducted on a full-scale model, the prototype dimensions were essentially retained. The model of the slab-column connection was terminated at mid-span, where the moment from lateral load is assumed zero, and at the mid-height of the column where the moment is zero.

At mid-span of the slab, under gravity loads, the slope of the deflected shape of the slab is zero as shown in Figure 3.2. The boundary condition provided at the slab edges, discussed in more detail in a subsequent section, allows for the slab to rotate. As a result, in the model, a zero slope cannot be achieved at this location under gravity loads. With the type of edge support provided in the experiment, the model can only represent a

section of the prototype slab, approximately 150 mm away from mid-span towards the column (see Figure 3.2) where the slope of the deflected shape is no longer zero. This leaves a 4.2 m x 4.2 m square slab with column stubs at its centre protruding 1.5 m to above and below the slab surface. The slab thickness was selected to be 152 mm (6") and the column size to be 355 x 355 mm, which are reasonable dimensions for this type of structure. The geometry of the specimen is illustrated in Figure 3.3.

The slab and column loading was determined according to the 1995 National Building Code of Canada. For residential type occupancies, a specified uniformly distributed live load of 1.9 kPa and a specified uniformly distributed superimposed dead load of 0.75 kPa was to act on the slab surface. However, during earthquakes only 50% of the live load is deemed present, resulting in a uniformly distributed design load of 1.7 kPa (unfactored). The axial load on the column, consisting of dead and live loads, was calculated for the ten floors above the column while considering all applicable load factors and was found to be 750 kN, factored.

In most cases the slab-column connection is not part of the lateral load resisting system. Shear walls in buildings usually resist earthquake loads. The slab-column connection must however accommodate a lateral deflection due to the earthquake while maintaining its gravity load capacity. The 1995 National Building Code of Canada stipulates that any structural member must be able to withstand a lateral deflection of no less than 2 % of the story height. In this case, for a story height of 3 m, the design inter-story drift shall be taken as 60 mm. For the geometry of the test specimens, the 60 mm drift translated to an

estimated lateral force V = 29.3 kN, assuming fully cracked condition, applied at the top of the column stub. This lateral force couple creates a moment to be transferred at the slab-column joint. The appropriate load combinations of the transferred lateral moment, together with the moments due to self-weight of the slab, superimposed dead load and a portion of the live load were taken to be the design moments for the slab. The specimen was then designed according to the Canadian concrete code, CSA standard A23.3-94. For both specimens, the slab and column were designed using normal density concrete of 30 MPa strength. A summary of the design calculations is presented in Appendix A.

3.4 Materials

3.4.1 Concrete

Although both the slab and the column were designed using 30 MPa concrete, the column concrete was proportioned to achieve a slightly higher strength than the slab concrete. This was to further ensure that the failure of the specimen would occur in the slab prior to failure in the column. The actual concrete strengths achieved during testing for the two specimens are shown in Table 3.1.

Concrete compressive strengths were determined by conducting a series of standard cylinder compression tests. ACI Committee 544 on fibre reinforced concrete found that the standard cylinder compression test is indeed applicable to fibre reinforced concrete. The split cylinder test has been performed to assess the uncracked tensile strength of the

concrete. After cracking, the split cylinder test indicated a residual tensile capacity of the steel fibre concrete, but not in the plain concrete.

3.4.2 Reinforcement

3.4.2.1 Deformed Bar Reinforcement

Both specimens had the same arrangement of deformed bar reinforcement. Columns were reinforced longitudinally with eight grade G30.12M-400 No. 20 deformed bars. A tie arrangement using two No. 10M ties was provided at 90 mm spacing in the joint region and at 120 mm otherwise. The tie/bar arrangement selected was deemed effective for an earthquake design. The column reinforcement layout as well as the tie arrangement is shown in Figure 3.4.

The slabs had top and bottom layers of reinforcement running in both directions. The bottom layer consisted of a uniform mat of G30.12M-400 No. 10 bars spaced at 300 mm intervals throughout except through the immediate column region. Since the maximum positive moment will occur near the mid-span of a slab, i.e. near the edge of the specimen, the bottom bars will have to develop their full capacity in this region requiring proper anchorage. To accomplish suitable anchorage, all bottom bars in the east-west direction had 180-degree hooks at their ends and all bottom bars running north to south, the direction of the applied lateral load, had 75 x 75 x 6 mm steel plates welded to their ends. Integrity steel was provided in the immediate column region consisting of two

hooked No. 15M bars each way. The bottom bar layout is illustrated in Figures 3.5 and 3.6.

The top mat consisted of fourteen No. 15M bars, ten in the column strip and the remaining four in the middle strip. Bars in the immediate column region were continuous to provide adequate anchorage. The bars lengths were then shortened in two increments moving away from the column region. Bar lengths and bar spacing are shown in Figures 3.7 and 3.8. The reinforcement ratios are given in Table 3.3. The effective depths of both the bottom and top mats are tabulated in Table 3.2 and illustrated in Figure 3.7 A. The actual material properties of the reinforcement steel as tested are presented in Table 3.4.

3.4.2.2 Steel Fibre Reinforcement

Two inch (50.8 mm) long and 4 mm wide corrugated steel fibres were added to the slab concrete in the first specimen. The fibres were present in the entire slab except in the column region. To improve the hard concrete properties, a fibre content in excess of 25 kg/m^3 or 0.33 % by volume is necessary (Maidl 1995). The efficiency of the fibres then increases with increasing fibre content until an upper limit of fibre content is reached due to workability of the concrete. The technical limit, depending on placing method and application type, lies between 50 and 100 kg/m^3 beyond which the difficulties in workability lead to irregularities in the concrete with subsequent consequences for the concrete properties (Maidl 1995). For this experiment a steel fibre content of 40 kg/m^3 has been chosen.

3.5 Fabrication of the Specimens

Specimens were cast in three stages. The lower column was cast using concrete mixed on site. Control cylinders were also taken. Before casting the slab concrete, the lower column form was stripped and the column was positioned below the slab form, which was held at the correct height using scaffolding. The column was aligned so that the slab soffit coincided with the top level of the lower column stub.

Next, the slab reinforcement was tied and the slab concrete was cast. Slab concrete was ordered in one batch from a concrete plant to guarantee uniformity. Steel fibres for the first specimen were added to the concrete at the plant. In the first specimen the slab concrete mix was not placed in the column region in order to make the experiment relevant to rehabilitation projects, where concrete cannot be replaced in the column region. This was achieved by using rough and irregular Styrofoam blocks placed into the column region to prevent the slab concrete from flowing into the area while casting. Care was taken to ensure that the interface of the slab concrete at the column was rough and would provide a good bond with the column concrete to be cast in the third stage. Control cylinders for the slab concrete were also taken.

In the third stage, the column form was aligned with the bottom column and the top column concrete was mixed and cast. Again, control cylinders were taken. The specimen was cured for seven days after the formwork had been stripped.

3.6 Testing

3.6.1 Test Set-up

Figure 3.9 shows a picture of the specimen outlining the various components of the overall test-set-up. The main components, discussed in more detail in the following sections, are the support at the bottom of the column, the vertical edge links at the north and south slab edges, the slab edge restraints, and the various loading points on the specimen. Additional pictures of the test set-up are shown in Appendix B.

3.6.1.1 Column Support

A pin-type support (Figure 3.10 and 3.10 A) was provided at the end of the bottom column using a ball and socket and a roller, the column being held in place by the horizontal load cell. Such an assembly allowed free rotation of the specimen, while restricting vertical and horizontal translation at the bottom of the column stub.

3.6.1.2 Vertical Edge Links

Under lateral load only, at mid-span between columns, the prototype slab would rotate but not deflect vertically while the building as a whole moves horizontally as shown in Figure 3.11. To model the prototype slab deflection, specially designed vertical edge

links, illustrated in Figure 3.12, located at the north and south edges of the slab were provided which would allow rotation as well as horizontal translation but no vertical deflection. Specific details of these vertical edge links are given in Figure 3.13. These links were only engaged after the gravity load had been applied and the slab was allowed to deflect. This boundary condition was designed to allow the specimen to behave as in an actual building under an earthquake event and the model was expected to behave as demonstrated in Figure 3.14.

Further, the specimen was prevented from sliding sideways by means of the lateral load system (Figure 3.10). The construction of steel rods and jacks provided on both the north and south sides would control any horizontal movement of the top column. Finally, the specimen was prevented from twisting around the column axis by providing rollers along the east and west edges of the slab.

3.6.1.3 Slab Edge Restraints

In effect, the specimen only models a portion of the slab and not an entire floor in a building. The model is discontinuous in the positive moment region, the mid-span of the prototype slab. Without any type of restraint at the slab edges, the model slab essentially behaves as a cantilever framing into the column. No positive moment would occur in this type of arrangement. To provide the appropriate positive moment at the slab edge, a system of sixteen vertical columns secured to all top edges of the slab and connected horizontally by adjustable tie-rods, shown in Figure 3.15, was provided. At the beginning

of the test, these tie-rods were pre-tensioned to create the desired positive moment that would occur under the gravity load in the slab.

3.6.1.4 Loading

The gravity load, consisting of superimposed dead load and live load, was added to the slab by means of sixteen concrete blocks, each weighing 1.87 kN. These were hung from chains on the underside of the slab, simulating a uniformly distributed load (see Figures 3.16 and 3.17).

Axial load on the column, replicating the weight of a ten-story building, was provided by a 36 mm diameter Dywidag Post-tensioning bar through the centre of the column (Figure 3.10), post-tensioned with the help of a jack at the top to a load of 750 kN kept constant during the test.

The lateral force, producing the desired lateral drift of the column, acted on the top of the column in the north-south direction. This force was applied primarily in tension, using 1" threaded bars and two reciprocating jacks mounted on a strong frame on either side of the column, able to travel in both directions (see Figure 3.10). Only one jack was engaged to pull on the column at any given time while the other travelled along. Pins at the columns and at the strong frame ensure that the lateral force was not coupled with any moment applied to the column.

3.6.2 Instrumentation

3.6.2.1 Internal Measurements

To address the internal behaviour of the slab, at total of 86 strain gauges on the deformed bars were used, 28 on the bottom bars (1-28) and the remainder on the top bars (29-86). An epoxy adhesive suitable for high elongations was used to attach the gauges to the reinforcement. It was felt that this adhesive would give the gauges their best chance of surviving cyclic loading. Of these 86 gauges, 69 in the steel fibre specimen and 77 in the control specimen were functioning at the start of the test. All of theses functioning gauges remained operational until the end of the test.

Strain gauge locations on the top bars in the direction of the lateral load (north-south direction) are given in Figure 3.18. The gauges were placed to monitor the strains caused by the moment imbalance due to the lateral load across the entire slab from east to west. Further, to follow the strain distribution across the slab form north to south, gauges have been applied along the long bars through the column region. Finally, to measure force gradients in the vicinity of the column, gauges have been placed along the perimeter of the critical section.

The strain gauge locations on the top bars in the east-west direction displayed in Figure 3.19 follow the same concept. A smaller number of gauges was used in this direction

simply because no significant strains were anticipated as no lateral load occurred in this plane.

Gauge layouts for the bottom reinforcement in the north-south and the east-west planes are shown in Figures 3.20 and 3.21, respectively. Again, in the direction of lateral load the strains due to moment imbalance were investigated by placing gauges across the slab. Special attention was given to the critical section around the column.

3.6.2.2 External Measurements

External measurements include deflections and rotations of slab and column, support reactions as well as monitoring the applied load. The horizontal drift of the specimen was measured with a cable transducer fastened to the top of the column and to an unloaded column. Figure 3.22 gives the locations of the eleven vertical Linear Variable-Differential Transformers (LVDT's) used to assess the overall deflection of the slab, and Figure 3.23 presents an effective way of employing two cable transducers each on both the north and south edges of the slab to assess the rotation of the slab at these edges. Rotations of the slab along the east-west axis through the column and rotations of the column near the joint itself were measured using six Rotation Variable-Differential Transformers (RVDT's) as shown in Figure 3.24.

At the bottom of the column, a vertical and a horizontal load cells were installed to monitor the reaction at that support (Figure 3.10 A). Support reactions were also

measured in each link of the edge boundary condition support using a total of eight load cells (Figure 3.13). Load cells in the two bars used to apply the lateral load allowed the observation of the lateral load applied to the specimen (Figure 3.10). The axial load in the column due to the post-tensioning bar was monitored using a pressure transducer. Finally, the forces in the slab edge restraining system were also observed with a load cell in each bar (Figure 3.15).

A total of 120 data channels were required to collect the data. Data collection was facilitated using a FLUKE data acquisition system, recording all readings electronically into a computer file.

3.6.3 Test Procedure

Before testing, the specimen was placed on temporary supports and not allowed to deflect, move or rotate in any way. Next, the entire test apparatus was installed and the data acquisition system connected. Then, all temporary supports were removed and the slab was allowed to deflect under its own weight with the edge restraints engaged, but the edge boundary condition links remained loose. An initial reading of all the data was taken at this point. The blocks simulating the gravity load were then put into place and a second set of readings was taken. Adjustment of the edge restraining system followed to create the desired positive moments due to gravity loads. At the same time the axial column load was applied. Another set of data was collected. Lastly, the edge boundary condition links were tightened just enough to be snug, but not taking any load. After another reading, the specimen was now ready for testing to commence.

The purpose of the test was to subject the specimen to repeat cycles of increasing horizontal drift, alternating in the north and south direction, until a significant loss of stiffness was observed. Using a manual pump, the active horizontal jack pulled the column in one direction until the desired level of drift was achieved while the other jack moved along passively. The hydraulic pressure was then released in steps until the specimen returned to its neutral point. Then the opposite jack was engaged to pull the column in the other direction, achieving the same drift there.

During the test, the horizontal load was plotted against the horizontal drift at the top of the column yielding a hysteretic loop for each cycle. Enough intermediate readings were taken to outline hysteretic loops for at least three cycles within each increment of north-south drift. The endpoints of each loop were monitored for loss of stiffness. If no significant loss of stiffness was observed the drift was increased to the next increment, otherwise the specimen was subjected to more cycles until it eventually became stable. Lateral drift increments of 6 mm, 12 mm, 18 mm, 24 mm, 30 mm (1 % drift), 45 mm, 60 mm (2 % drift), 90 mm (3 % drift) and finally 120 mm (4 % drift) were scheduled. The loading rate was kept at about 1 complete cycle per five minutes.

Before each new increment in lateral drift the column was always brought back to its neutral position with no horizontal load acting on the specimen. At this point the edge boundary condition links were loosened briefly to remove any gravity load that had been redistributed to the edge links over the course of the drift cycle.

Specimen	Concrete Strength (MPa)						
	Compressive Strength f'_c			Splitting Strength f'_{ct}			Residual f'_{ct}
	Top Column	Bottom Column	Slab	Top Column	Bottom Column	Slab	Slab
1 (steel fibre)	40.3	39.5	37.6 (48)	3.4	2.3	3.7	0.9
2 (control)	40.0	40.0	34.1 (25)	3.8	3.8	3.0	0

Notes: Concrete strengths correspond to those at time of testing. Numbers in parentheses indicate slab concrete age in days.

Table 3.1 Concrete Strengths

Specimen	Effective Depths (mm)					
	Top Steel			Bottom Steel		
	E-W d'	N-S d'	Average d'_{ave}	E-W d	N-S d	Average d_{ave}
1 (steel fibre)	54	38	46	105	116	111
2 (control)	54	38	46	105	116	111

Table 3.2 Effective Depths of Slab Reinforcement

Specimen	Reinforcement Ratios % ρ								
	Top E-W		Top N-S		Bottom E-W		Bottom N-S		Column
	Column Strip	Middle Strip	Column Strip	Middle Strip	Column Strip	Middle Strip	Column Strip	Middle Strip	
1 (steel fibre)	0.97	0.38	0.83	0.33	0.32	0.32	0.28	0.28	1.90
2 (control)	0.97	0.38	0.83	0.33	0.32	0.32	0.28	0.28	1.90

Table 3.3 Reinforcement Ratios

Specimen	No. 15M Bar			No. 10M bar		
	Yield Strength f_y (MPa)	Ultimate Strength f_u (MPa)	Modulus of Elasticity E (MPa)	Yield Strength f_y (MPa)	Ultimate Strength f_u (MPa)	Modulus of Elasticity E (MPa)
1 (steel fibre)	425	610	195000	480	760	235000
2 (control)	460	702	227000	440	700	231000

Table 3.4 Properties of Reinforcement Steel

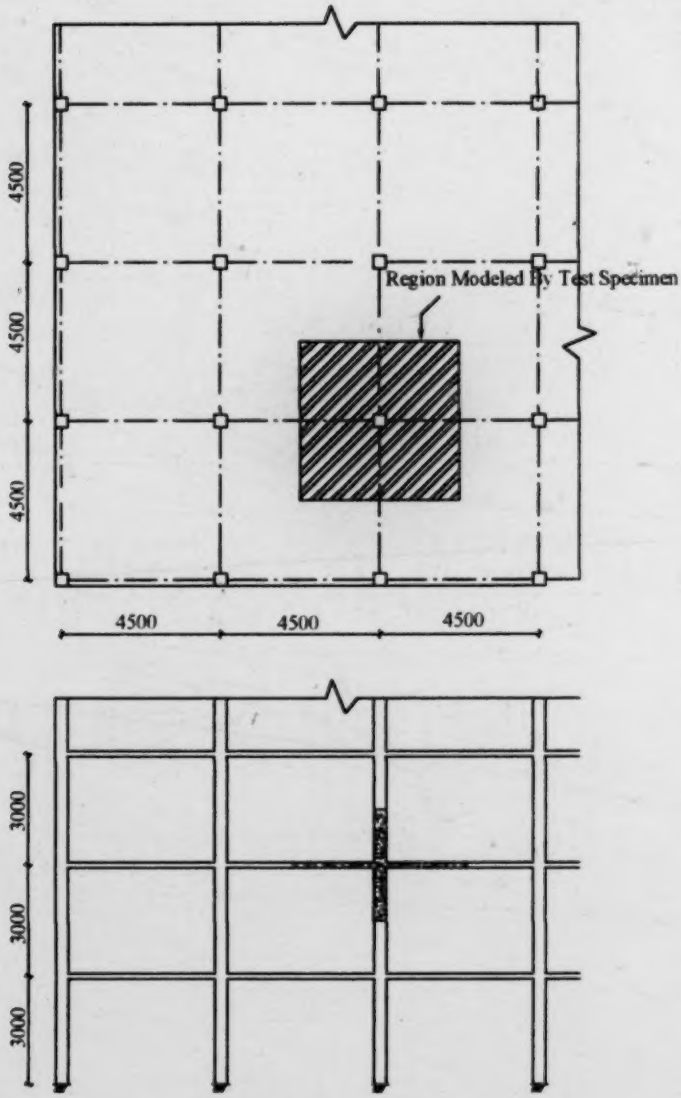

Figure 3.1 Prototype Flat Plate Structure

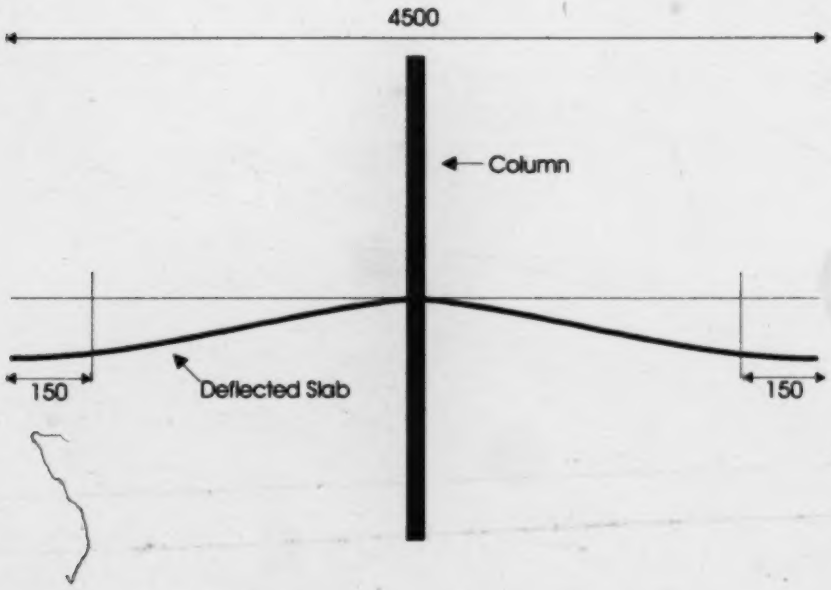

Figure 3.2 Slab Deflection under Gravity Loads

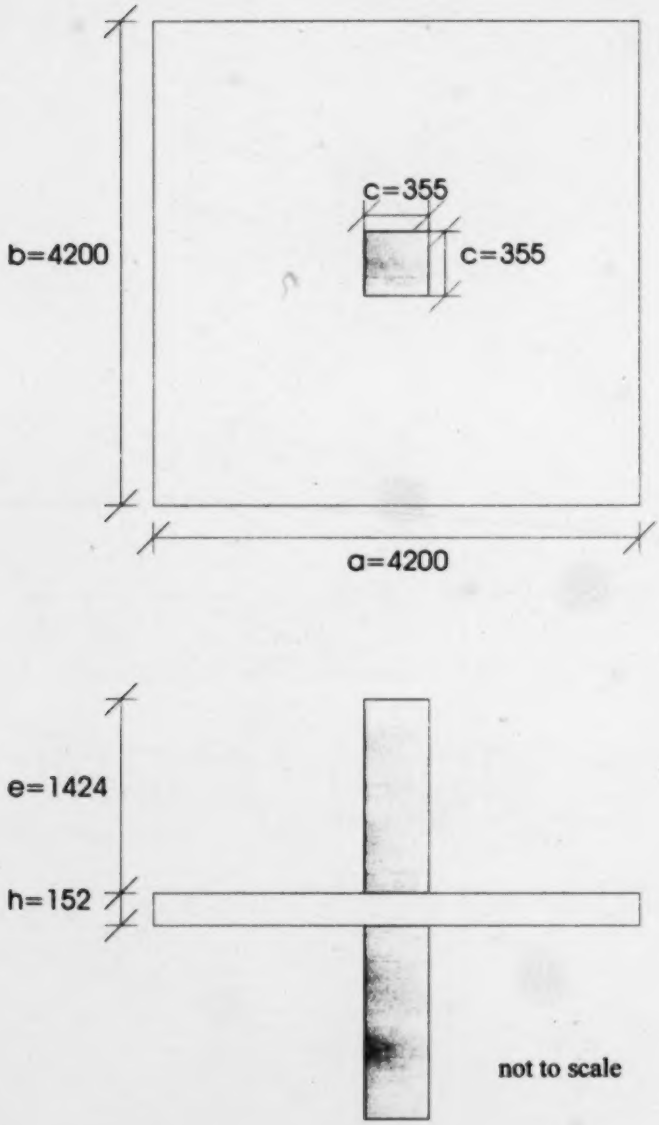

Figure 3.3 Geometry of Specimen (mm)

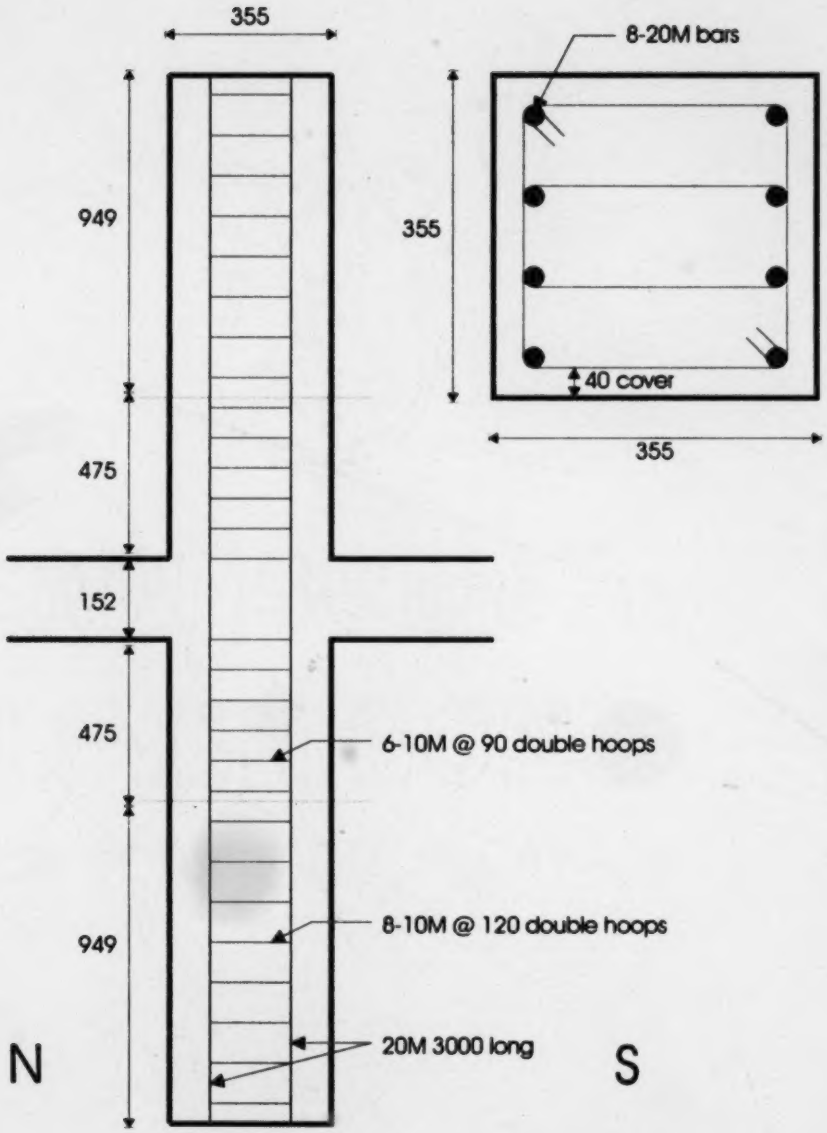

Figure 3.4 Column Reinforcement Layout

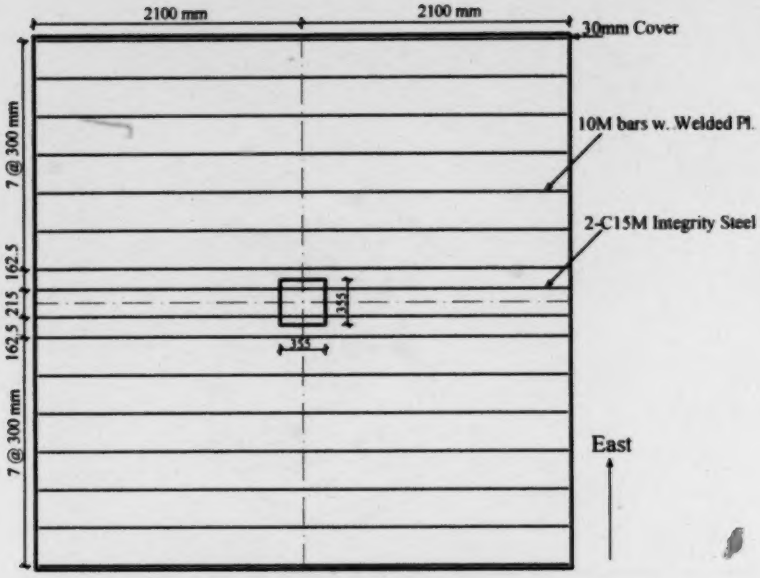

Figure 3.5 Slab Reinforcement - Bottom Mat (N-S Direction)

C = Hooked Bar (180 deg)

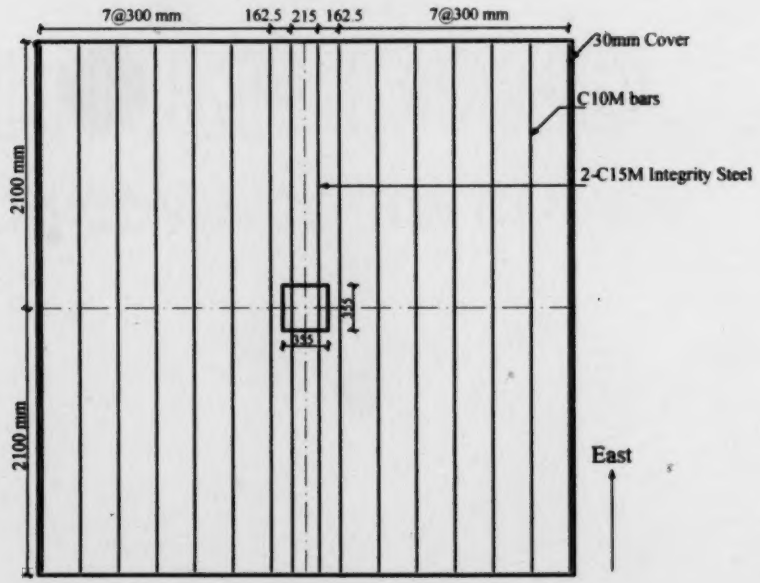

Figure 3.6 Slab Reinforcement - Bottom Mat (E-W Direction)

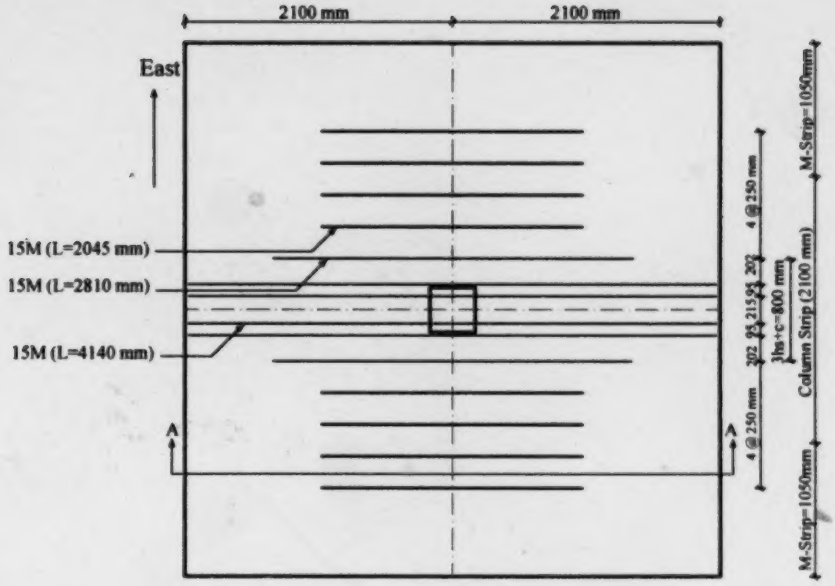

Figure 3.7 Slab Reinforcement - Top Mat (N-S Direction)

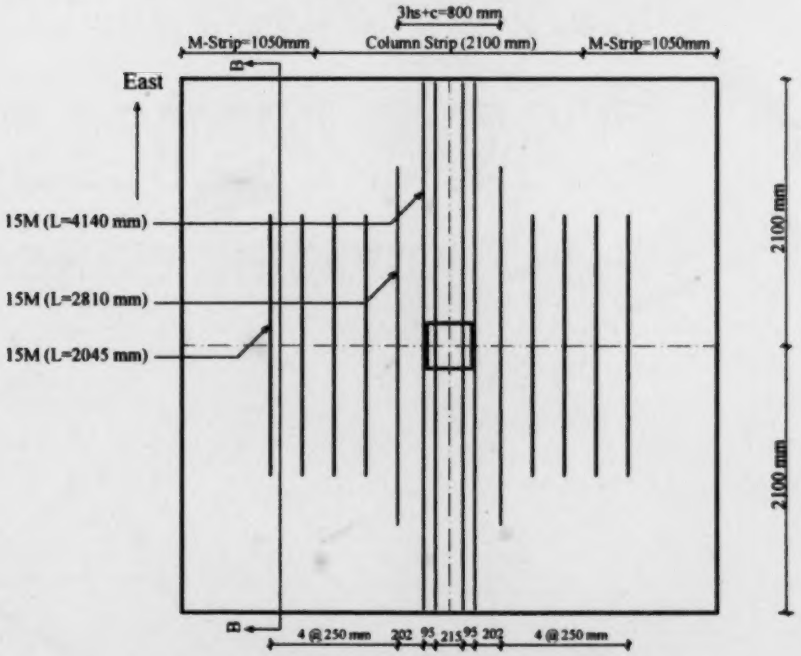

Figure 3.8 Slab Reinforcement - Top Mat (E-W Direction)

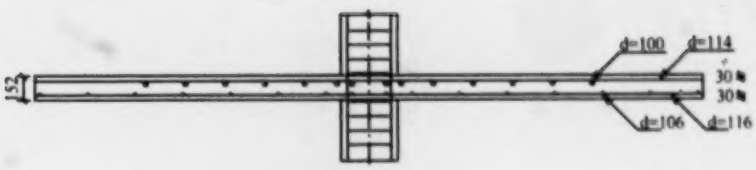

Section A-A of Figure 3.7

Figure 3.8 A Detail of Reinforcement of Slab

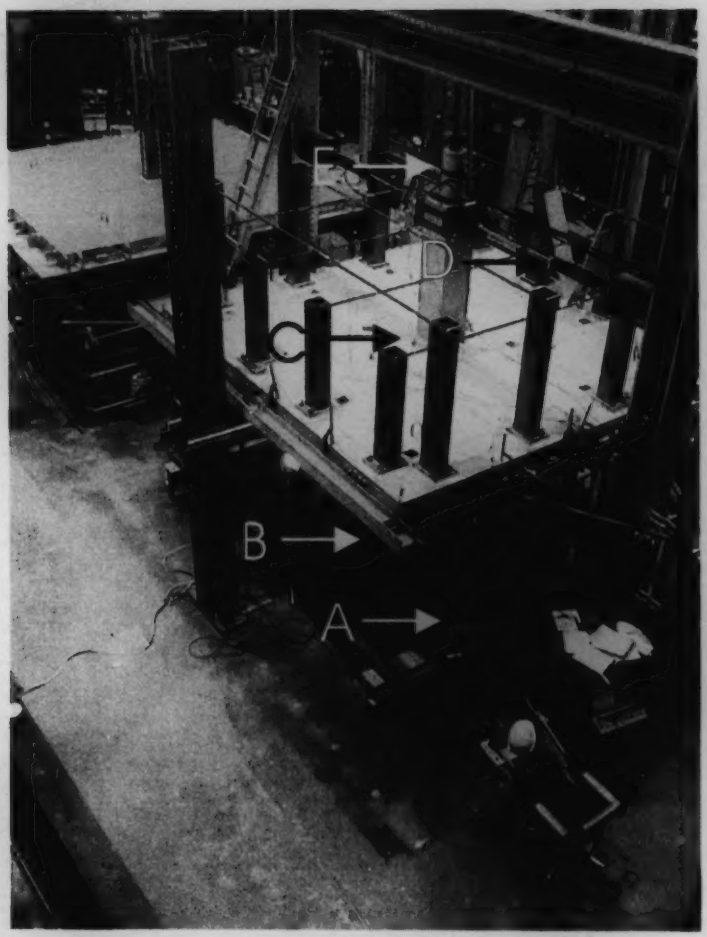

A = Edge Links (see Figure 3.12 and 3.13)
B = Slab Twisting Restraint
C = Slab Edge Restraint (see Figure 3.15)
D = Horizontal Load Assembly (see Figure 3.10)
E = Vertical Jack (see Figure 3.10)
Not seen: Bottom Support of Column (see Figure 3.10 A)

Figure 3.9 Overall Test Set-up

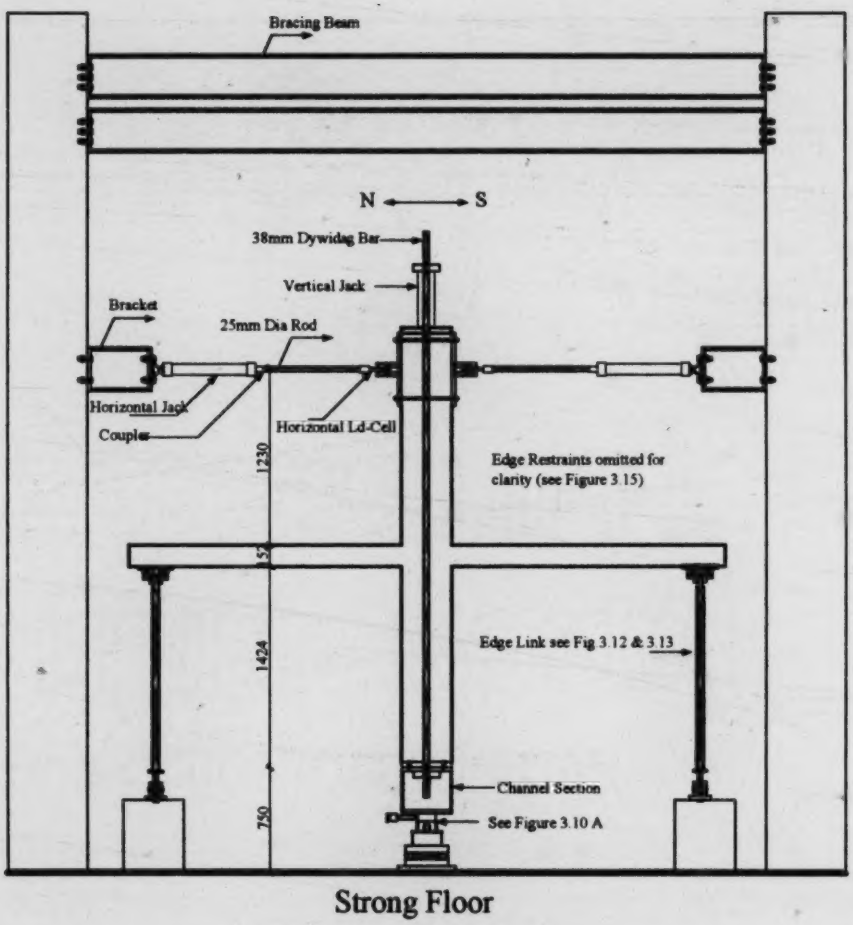

Figure 3.10 Lateral Load Test Frame

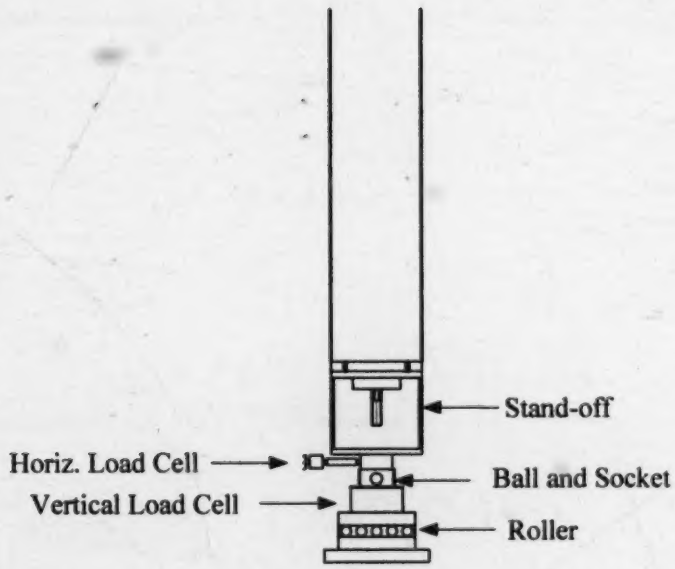

Figure 3.10 A Detail of Column Support

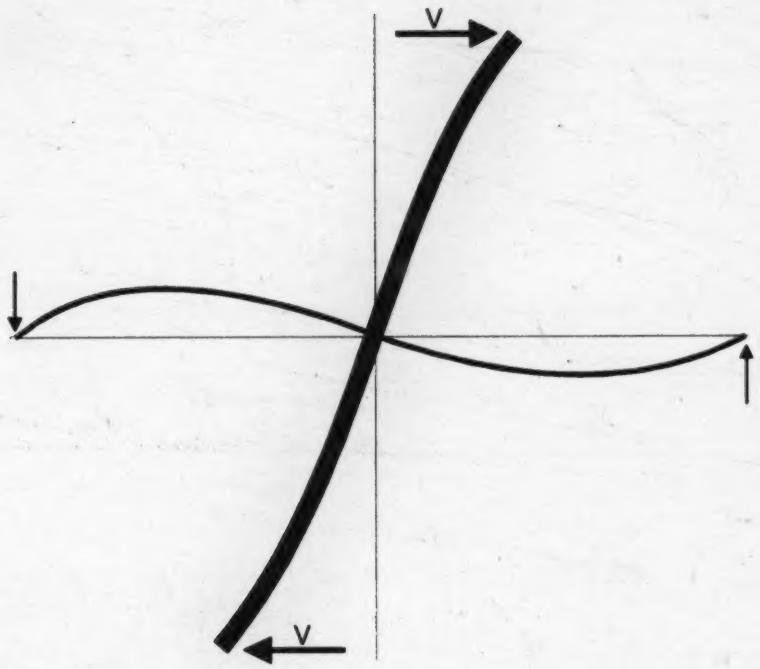

Figure 3.11 Deflection of Prototype under Lateral Load

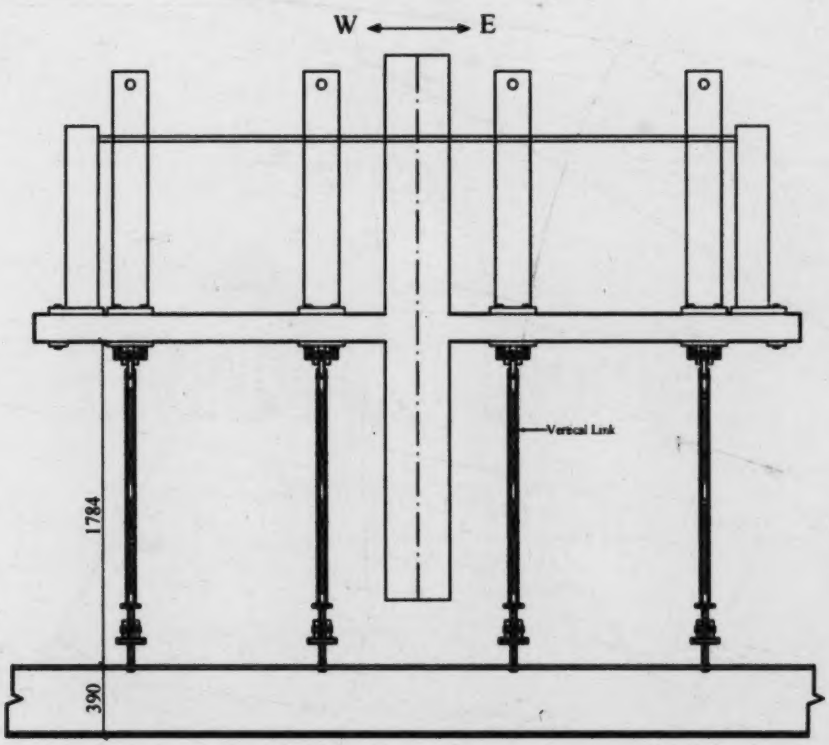

Figure 3.12 North-South Slab Edge Boundary Condition

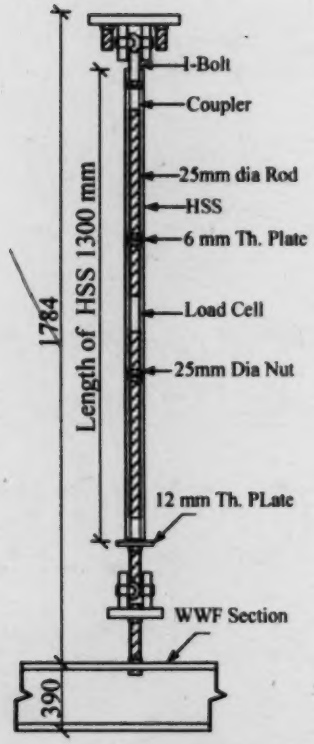

Figure 3.13 Detail of Vertical Link

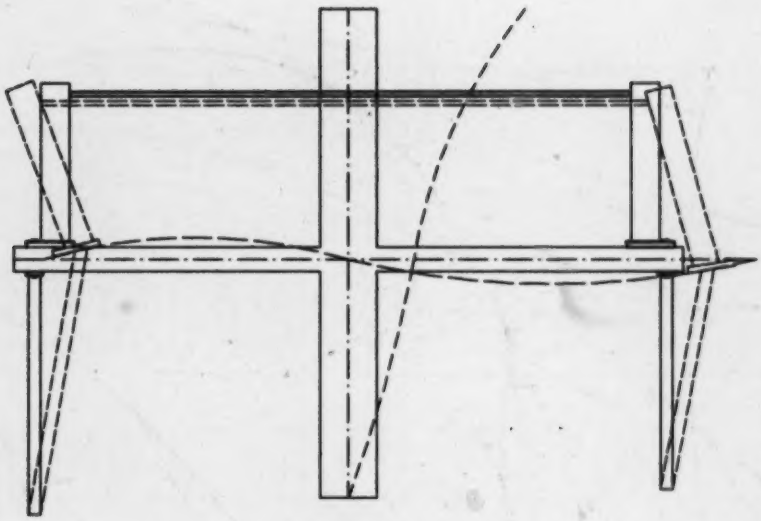

Figure 3.14 Deflected Shape of Model

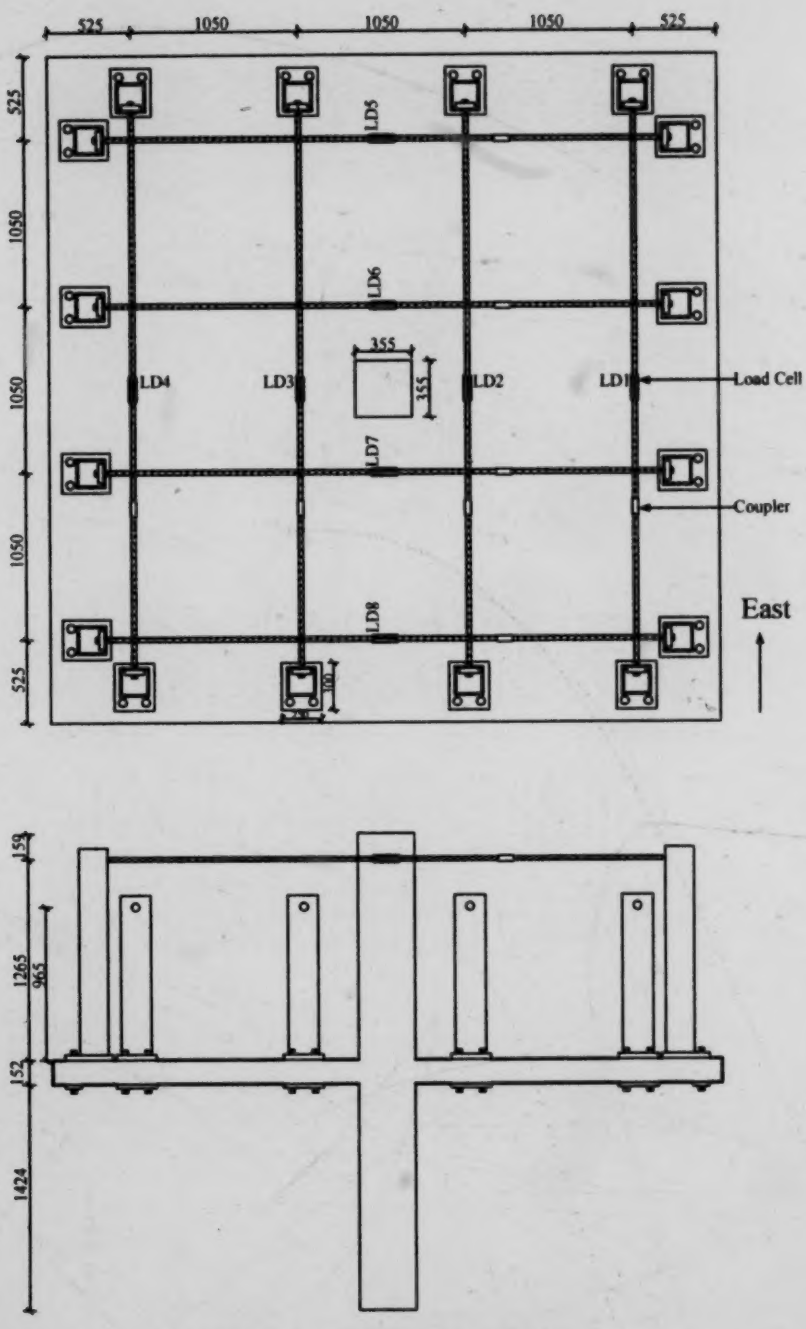

Figure 3.15 Slab Edge Restraining System

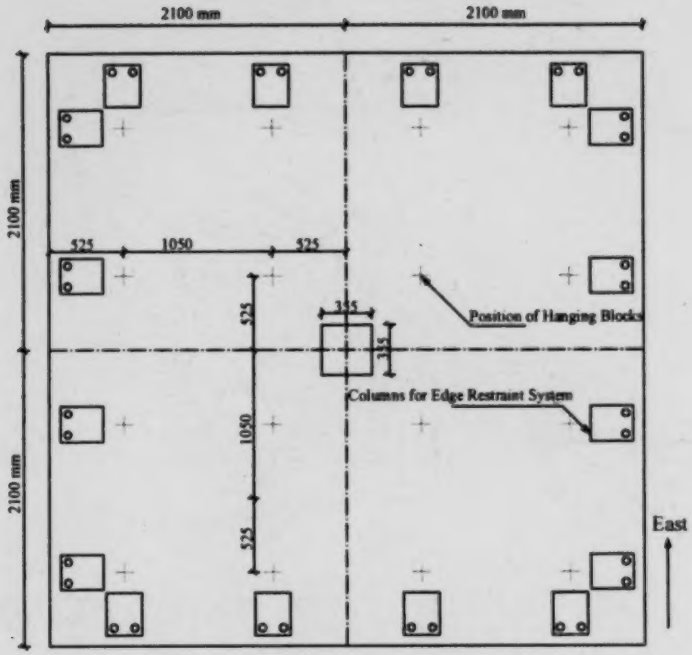

Figure 3.16 Plan of Specimen

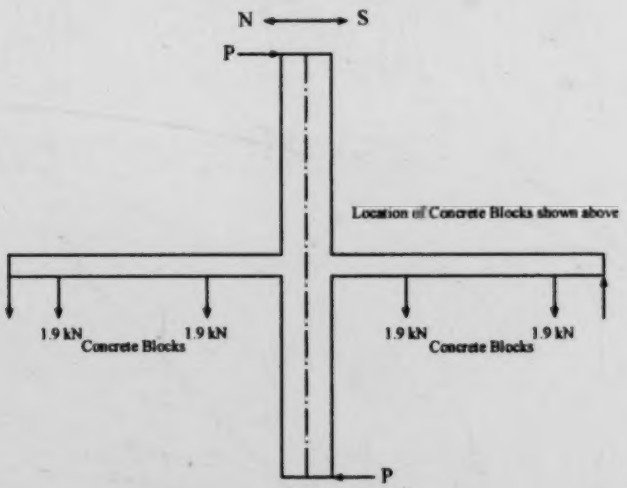

Figure 3.17 Elevation of Specimen

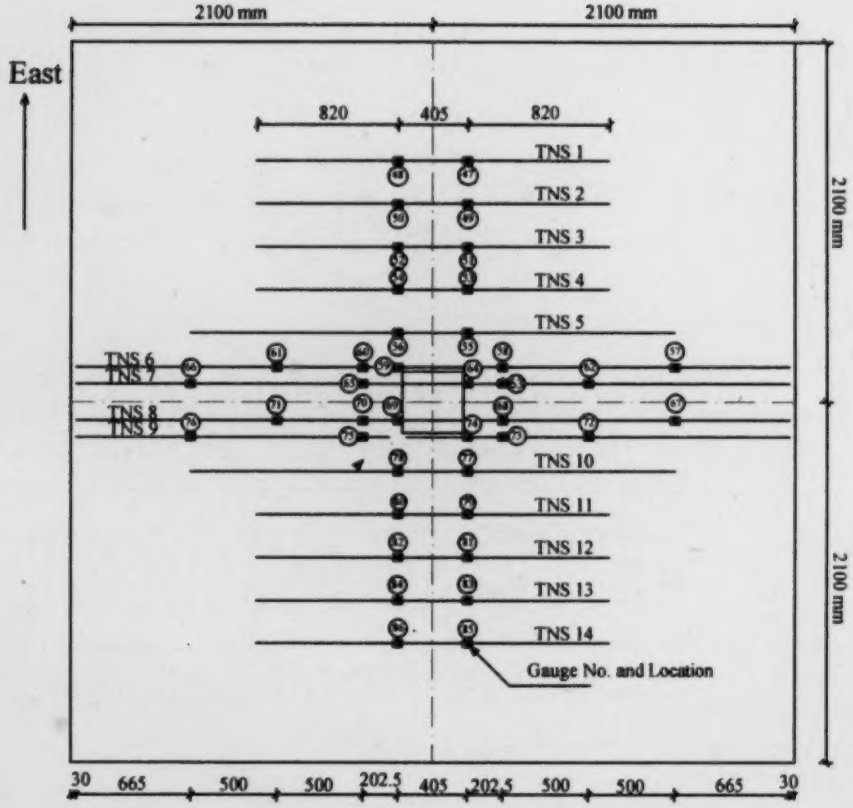

Figure 3.18 Top Mat Strain Gauge Locations (N-S Direction)

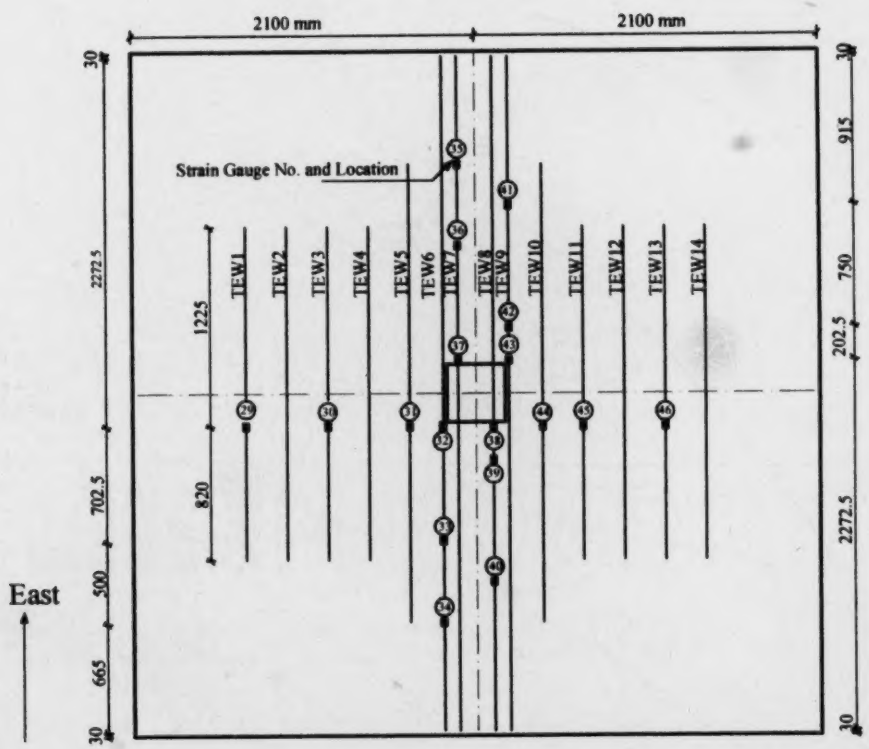

Figure 3.19 Top Mat Strain Gauge Locations (E-W Direction)

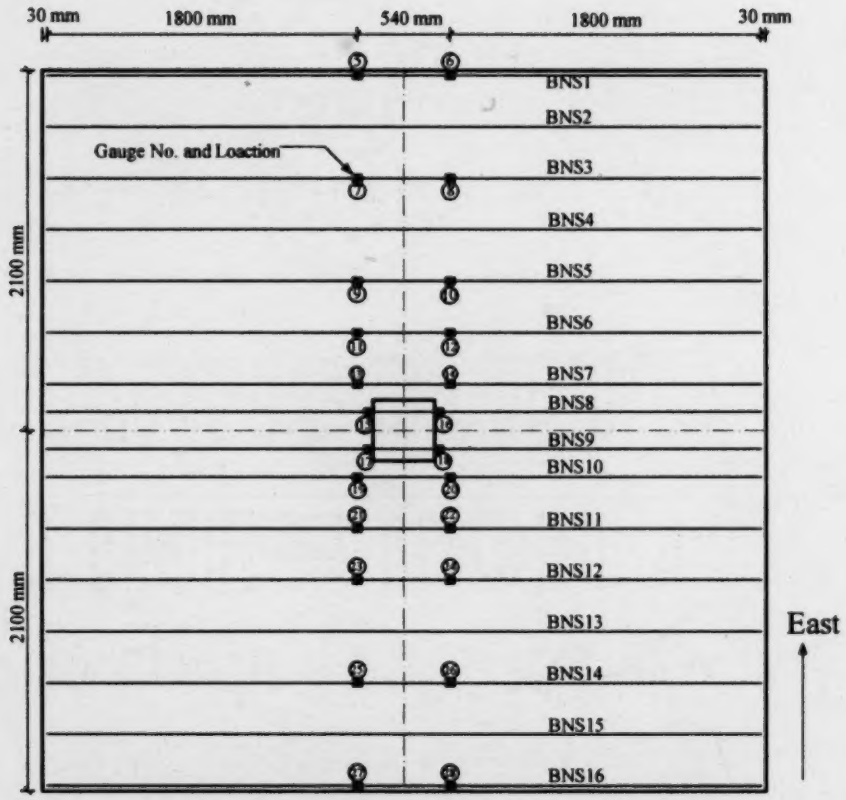

Figure 3.20 Bottom Mat Strain Gauge Locations (N-S Direction)

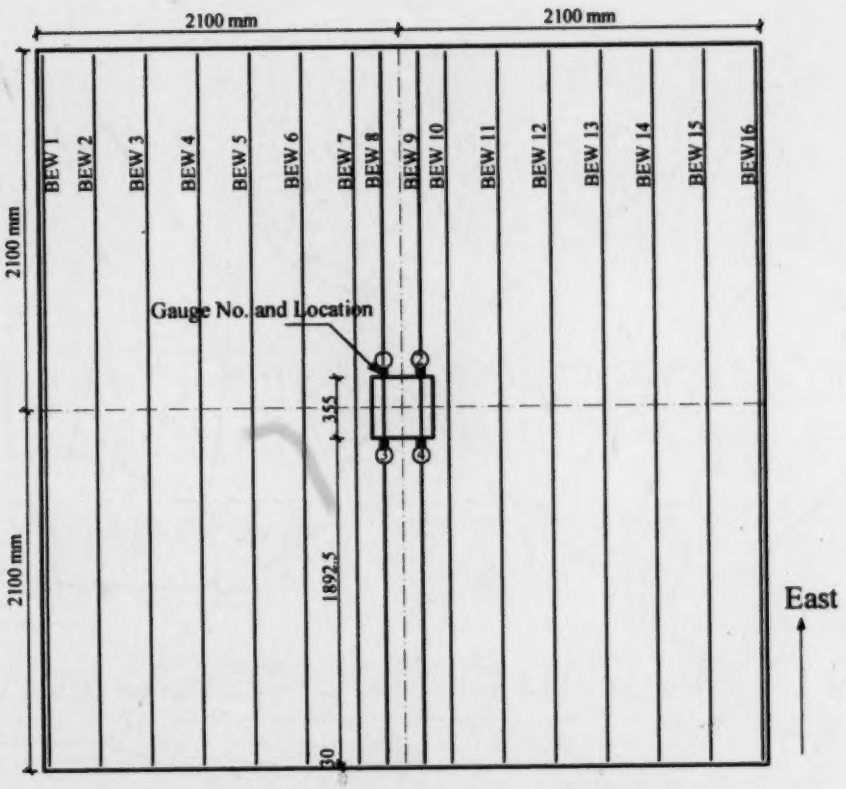

Figure 3.21 Bottom Mat Strain Gauge Locations (E-W Direction)

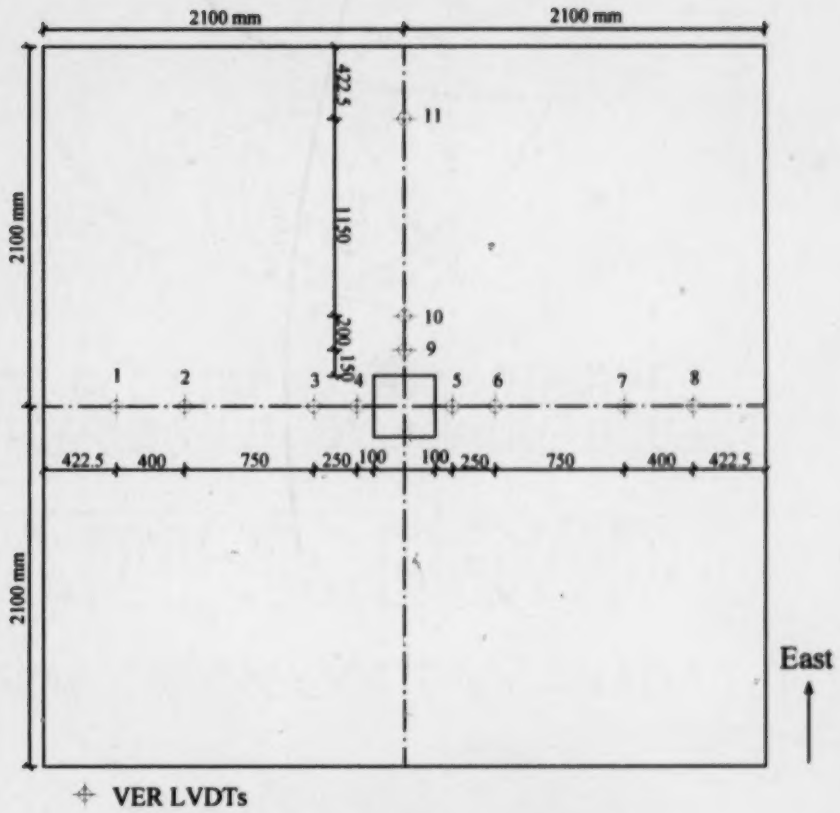

Figure 3.22 Position of Vertical LVDT's (Underside of Slab)

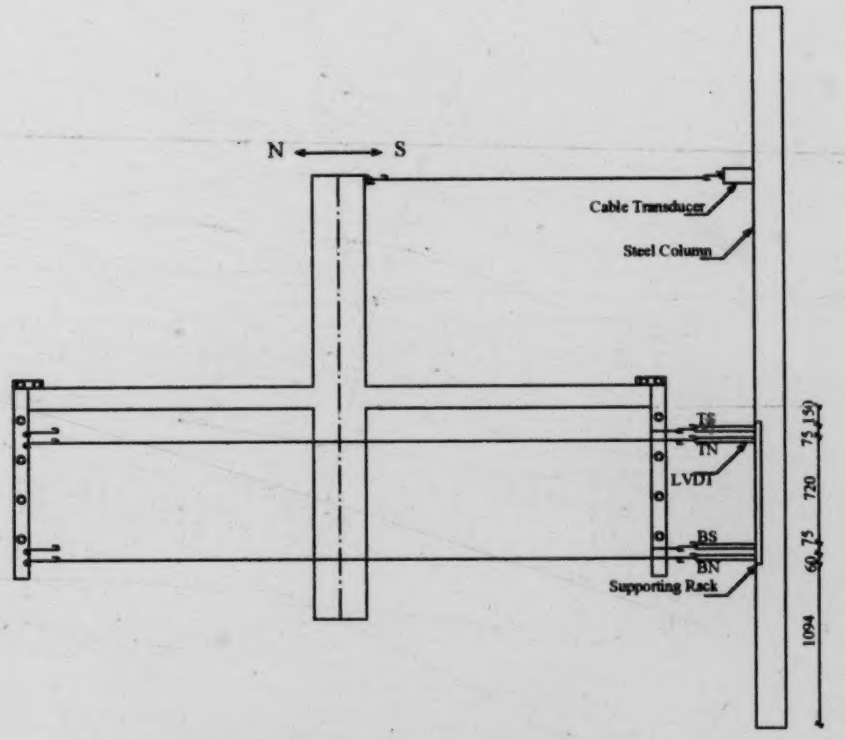

Figure 3.23 Position of Cable Transducers

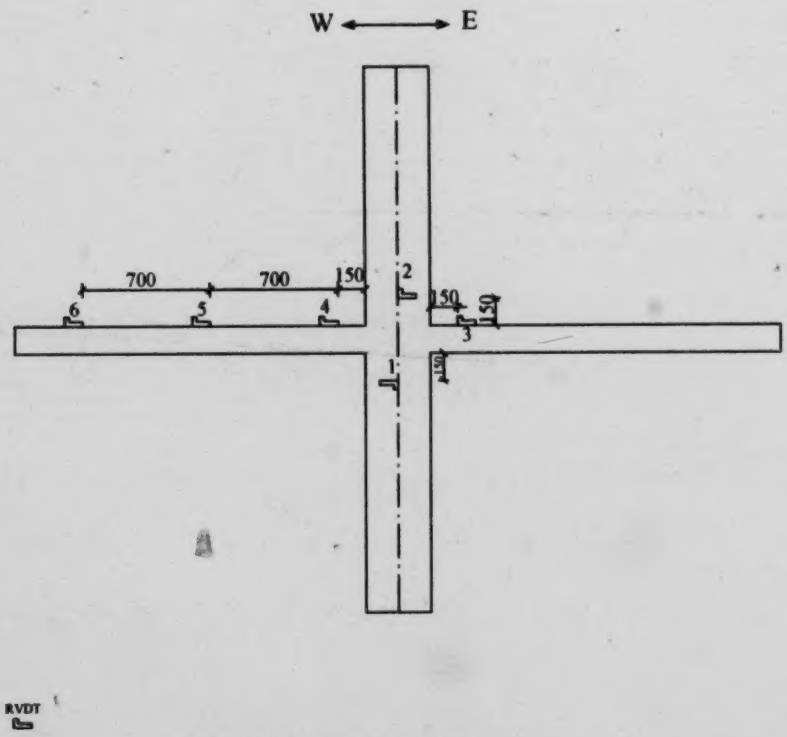

Figure 3.24 Position of RVDT's

4. TEST RESULTS AND OBSERVATIONS

4.1 General

The same test procedure was followed for both specimens. First, the gravity load was applied by attaching the concrete blocks to the slab. Then, once the slab had deflected under its gravity load, the edge links were engaged. Initially, the threaded bars of the edge restraining system were pre-stressed the same amount in both specimens. Each specimen was subjected to the same number of cycles of lateral drift and the loading rate was kept as consistent as possible. During the test the axial load on the column was closely monitored and the links of the edge boundary condition were reset after each drift cycle to allow the slab to deflect under its own weight.

As discussed in the previous chapter most of the observations made during the test resulted from the electronic collection of data from a wide range of instrumentation. This data is analysed and discussed in section 4.3. First however, a qualitative description made from notes and observations while testing is featured in section 4.2. These observations include the general behaviour of the specimens including crack patterns and the mode of failure. Appendix B shows numerous pictures of both specimens made during the course of the experiment.

4.2 General Behaviour of the Test Specimen

4.2.1 Observations made during the Test

A schematic drawing of the crack pattern occurring at the end of the test of the steel fibre specimen and at failure of the control specimen is given in Figures 4.1 and 4.2, respectively. During the course of the experiment, the steel fibre specimen displayed noticeable radial cracking after the 24 mm drift cycles. Very few additional cracks occurred during the 30 mm cycle. At 60 mm drift the same radial crack lines extended outward towards the edge of the slab and more cracks were formed. The 90 mm and 120 mm cycles brought few additional cracks but crack widths increased significantly from 1.25 mm at the 60 mm drift level to over 2.5 mm at the 120 mm drift level.

The control specimen suffered extensive radial cracking around the column at a lateral drift increment of only 12 mm. At 24 mm drift these radial cracks extended outward in every direction and at 30 mm drift the cracks generally reached the edge of the slab. The 60 mm drift cycles produced a significant number of additional cracks and crack widths of up to 1.8 mm were observed near the column edges.

4.2.2 Observations at Failure

The steel fibre specimen sustained numerous alternating cycles at 4 % drift or 120 mm lateral displacement without any significant loss of stiffness or softening. Although there

was considerable cracking with a crack along the column face opening significantly (up to 4 mm), no other signs of acute distress were apparent. The connection did not show any loss of load carrying capability nor did any spalling of concrete occur. Since no failure occurred at 4 % drift the next step was to proceed to a complete pushover of the column.

During the pushover, the lateral load applied to the column continuously increased until it reached a peak load of 51.5 kN at a lateral deflection of 152.3 mm. Beyond this point, while the drift increased, the lateral force required remained essentially constant or declined slightly. In fact, the connection withstood significant additional drift with a slight reduction in lateral load, showing properties of plastic behaviour. At a drift of 224.5 mm or more than 7 % drift with a lateral load of 42.3 kN, the horizontal jack ran out of stroke. The lateral load had to be removed immediately and the column jumped back to its 120 mm drift position.

The connection never displayed any signs of an imminent classic punching failure; the slab remained essentially intact. Failure seemed to start to occur along the interface between the slab and the column where a crack opened significantly. Subsequent loading cycles at 4 % or 120 mm drift level demonstrated that the connection was still able to carry the gravity load although the connection now was less stiff and required a smaller lateral force especially in the direction of the previous pushover.

At the 3 % (90 mm) drift level the control specimen was cracked extensively on both the top and the underside of the slab. No significant softening of the connection in between cycles was observed however. The specimen visually showed signs of distress and "crunching" noises were noted at the peaks of the 90 mm cycle. Some spalling of the concrete occurred on the underside of the slab. Because failure seemed imminent, a much slower loading rate was used in the next drift cycle. The 4 % (120 mm) drift level was never reached, the connection failed suddenly with "plump" sound and a classic U-shaped punching failure on the north side of the column at 110.3 mm drift. At failure the load dropped suddenly from its peak value of 45.6 kN and the column continued to "fall over" in the direction it was pushed.

4.3 Test Results

4.3.1 Statics

Simple static checks have been performed to monitor closure of all load cell readings. Loads applied to the specimen had to be accounted for at the support reactions. Horizontal equilibrium was achieved when the sum of the applied load from the two lateral jacks at the top of the column was equal to support reaction at the horizontal load-cell at the bottom of the column. Deviations from this equilibrium are a measured error and are reported in Table 4.1. For the steel fibre specimen errors in the horizontal equilibrium were 10 % or less. The control specimen had a higher error percentage ranging from 12 to 14 %.

A reason for the observed errors is the fact that the restraint system provided to prevent the slab from twisting around the axis of the column offered some load resistance in the horizontal plane. At higher lateral drift, the friction between the slab and these restraints became noticeable and may have acted as horizontal supports. During testing of the steel fibre specimen, these restraints were loosened intermittently to mitigate such an error, but during the test of the control specimen this was omitted explaining larger errors there. This was not thought to be detrimental to the objective of comparing the two specimen as the required lateral drift was deflection and not load driven

Errors in the vertical equilibrium are shown in Table 4.2. The self-weight of the slab plus the applied gravity load should equal the vertical support reactions. Vertical supports are the vertical load-cell at the foot of the column and each link of the edge boundary system. The summation of load readings of all the supports should have resulted in the known weight of the entire specimen. Errors here were insignificant.

4.3.2 Support Reactions and Equilibrium

The vertical reactions at the north and south edge boundary conditions (vertical edge links) are summarized in Table 4.3. In Figures 4.3 and 4.4, these vertical reactions have been plotted against the lateral drift for both, the north and south edge of each specimen. It became evident that the edge links were taking higher loads with increasing drifts. With increasing drift, the slab softened and a larger portion of the gravity loads was

redistributed away from the column into these edge links. In the prototype structure all of the gravity load must frame into the column. Hence, it was important to loosen these edge links after each increment to remove any accumulated and to allow the slab to deflect.

Figure 4.5 shows the free-body diagram of the specimen. If moments are taken around the point O, the horizontal load taken out by the twist restraint has no effect as its line of action passes through point O. This moment equilibrium helps to assess whether there is indeed a real error in the horizontal load cells readings or whether these horizontal load errors are in fact unmeasured loads. As previously mentioned, the vertical load cells had relatively small errors and the bottom load cell is deemed very reliable. Table 4.4 shows the peak horizontal and vertical forces acting on the specimen at each drift cycle and the resulting moment equilibrium. Errors in moment equilibrium are less then 10 % for the steel fibre specimen and 12-13 % for the control specimen as observed in the horizontal static check. This suggests there is in fact an error in the horizontal load cell readings, most likely resulting from the load cells at the top of the column.

4.3.3 Edge Restraints

To simulate the positive moment at the edge of the slab in the specimen, corresponding to the mid-span location in the prototype, edge restraints have been provided. The forces in the edge restraints in the north-south direction for each drift cycle are shown in Figures 4.6 and 4.7 for the steel fibre specimen and the control specimen, respectively. Figures 4.8 and 4.9 show the east-west directions of these restraints. Peak values for each drift

increment are given in Tables 4.5 (north-south) and 4.6 (east-west). Loads in the edge restraints remained fairly constant throughout the test, increasing slightly with increasing lateral drift. This increase shows that the lateral moment affected the positive moment in the slab. Cyclic lateral loading softened the slab in the negative moment region and as a result, a slightly larger fraction of the gravity load panel moment was redistributed to the positive moment region. The positive moments at the slab edge were close to the positive design moment of 18.7 kN. In the north-south direction it can be seen that due to cracking of the slab, the internal forces redistributed towards the edge of the slab as the outlying edge restraints 1 and 4 took on a greater share of the load with each increase in drift. In the east-west direction it was noted that the restraints were more heavily loaded on the side opposite to the direction of lateral displacement while the restraints on the opposite side were unloaded.

4.3.4 Lateral Load-Drift Response

Plotting the applied lateral load against the column drift yields an elliptically shaped hysteretic loop for each cycle. Due to cracking of the concrete and redistribution of internal forces, the horizontal load required to achieve the same deflection may be lower in a subsequent cycle. If this occurs, the connection is becoming less stiff or softening. The loss of stiffness may continue for several cycles at constant drift before becoming stable with the peaks of the hysteretic loops converging.

The lateral load-drift response or hysteretic loops for both specimens are shown in Figures 4.10 and 4.11. These figures do not reveal a drastic difference in behaviour between the two specimens, except at the point of peak lateral load. From the aspect of load-drift response, both specimens performed equally well at all drift cycles up to and including the 90 mm drift cycles. The hysteretic loops all reached a stable response after usually three alternating cycles at the same drift. Table 4.7 compares the range of the lateral load required to complete one stable cycle for each drift increment. As seen in the hysteretic plots, the load ranges required to achieve a given drift cycle are nearly equal for both specimens. At the 90 mm cycles, the load range of the control specimen appeared to become smaller than that of the steel fibre specimen.

The control specimen experienced a classic punching shear failure at only 110.3 mm drift, explaining the greater loss of stiffness observed at the 90 mm drift cycle compared to the steel fibre specimen, which performed perfectly well beyond a 120 mm drift. The steel fibre specimen, revealing no signs of distress at 120 mm drift demonstrated ductile properties until the end of the test at 224.5 mm drift. Up to this point, the specimen experienced a gradual loss of stiffness, where the lateral deflection continued to increase, while the lateral load dropped slowly. The steel fibre specimen thus had a much larger energy absorption capabilities than the control specimen. Energy absorption can be described in terms of work done which is the product of the deflection and the applied load.

While the failure of the control specimen was of a catastrophic nature, the steel fibre specimen appeared to withstand several post peak cycles at 120 mm drift (see Figure 4.12) with no further stiffness degradation after only a couple of cycles. In fact, the connection retained 40.8 % of its stiffness in the direction of the complete pushover and 85.2 % in the other direction (Table 4.7).

As the slab becomes softer, a portion of the gravity loads were redistributed towards the edge of the slab and carried by the edge links In Figures 4.13 and 4.14 the vertical load in the bottom column is plotted against the increasing lateral drift during the pushover for the steel fibre and the control specimen, respectively. The steel fibre specimen gradually redistributed some of the gravity load towards the slab edges when the connection started to soften. Before the end of the test, about 20 % of the gravity loads were redistributed. In contrast, the control specimen encountered a sudden loss of gravity load in the column of 40 % at failure.

4.3.5 Stiffness and Ductility of the Connection

The stiffness of the connection could be experimentally determined from measuring the moment due to the lateral forces and the rotation of the connection. The stiffness K is related to these variables by the following simple relationship: $M = K \alpha$; M being the moment due to lateral load and α being the rotation of the column. The moment due to lateral load was calculated by multiplying the applied lateral force at the bottom of the

column with the story height and the column rotation at the joint was measured using two RVDT's, above and below the slab, where the average of the two readings was taken.

The calculated stiffness of both specimens for each drift cycle is shown in Figure 4.15. Both specimens show a 1/3 reduction in stiffness as a result of cracking. Initially, the control specimen behaved stiffer but converged to the stiffness of the steel fibre specimen with increasing lateral drift. At 90 mm drift, it had a slightly lower stiffness than the steel fibre specimen. The slab of the control specimen cracked more extensively resulting in a proportionately greater loss of stiffness.

Ductility, the ability of a material to undergo large plastic deformations without fracture, is a desirable property for connections subjected to load reversals as during an earthquake. To compare the two specimens, ductility of the connection is defined as the ratio of maximum drift to that at first yield of the slab reinforcement. As will be discussed in a following section, the slab reinforcement in both specimens first yielded during the 60 mm drift cycles. The peak load of the steel fibre specimen occurred at 152.4 mm and the end of the test at 224.5 mm lateral deflection. For the other specimen both peak load and failure occurred at 110.3 mm. The ductility of the steel fibre specimen is then 1.92 at peak load and 3.74 at the end of the test; for the control specimen the ductility at both peak load and failure is 1.83. For the steel fibre specimen, this translates to a 4.9 % higher ductility at peak load and a 104.4 % higher ductility at the end of the test compared to the control specimen.

4.3.6 Slab Deflections and Rotations

Vertical slab deflections were measured by vertical LVDT's on the underside of the slab, on both its north-south and east-west centreline. A comparison of the measured slab deflections is presented in Table 4.8. Generally, the slab deflections were about 10 % lower in the steel fibre specimen than in the control specimen, once the slab had cracked (after the 6 mm cycles). As expected, no significant deflections occurred in the east-west direction of the slab where no lateral forces were applied.

In the direction of lateral load the deflected shape of the slab follows the expected behaviour of the prototype shown in Figure 3.11. To illustrate this point, in Figures 4.16 and 4.17 the deflection readings from the north-south LVDT's at 60 mm drift are marked at their respective locations of the slab, outlining its deflected shape. The curve of the deflected shape of the slab has a steep slope near the column; beyond this region the curve remains fairly smooth towards the edge of the slab. Hence, the slab deflected significantly near the connection where most of the softening occurred.

RVDT's were used to assess rotations of the slab and column. On the slab, these RVDT's were positioned at several locations along the east-west centreline of the slab. With increasing lateral deflection, the control specimen underwent larger rotations, especially in the immediate column region. As seen in Table 4.9, rotations there were up to 30 % larger than in the steel fibre specimen. This trend was less evident however at the slab edge, at RVDT 5, indicating that the control specimen suffered more extensive cracking

and was not able to distribute all the rotation away from the joint region. The steel fibres seemed to counter the effect of cracking and the specimen behaved more uniformly.

The graphs of the east-west centreline RVDT's showing the rotations at failure of the control specimen or at the end of the test of the steel fibre specimen, illustrate some interesting differences in behaviour between the two specimens. Figures 4.18 and 4.19 present the rotations of RVDT 4 located in the joint region and RVDT's 5 and 6 located away from the joint region for both specimens. In the steel fibre specimen all rotations continue to grow with increasing lateral deflection of the connection until the end of the test, where the entire connection was brought back to its neutral position. In the control specimen, at failure, RVDT 4 experience a sudden increase in rotation while RVDT's 5 and 6 encounter a sudden decrease in rotation. An explanation for this behaviour is that RVDT 4 lied within the punching failure perimeter, and the column without any support from the connection fell over a certain amount after failure while the slab returned towards its neutral position.

The two RVDT's attached to the column were used to measure the rotation at the joint and to calculate the stiffness of the connection as presented before. They were also effective in estimating the deflection of the column itself under the lateral load. As can be seen in Table 4.10 the column is not indefinitely stiff and its deflection is significant.

Two sets of two cable transducers were used to estimate the rotations at the north and south edges of the slab. In accordance with the rotations at the centreline of the slab and

the slab deflections, the edge rotations of the control specimen were expected to be larger than the steel fibre specimen. Results confirming this are presented in Table 4.11.

4.3.7 Internal Forces and Strains

Strains in the reinforcing bars were measured to determine when yielding of the reinforcement occurred, the distribution of the applied lateral moment across the slab and to compare strain values between the two specimens. Yielding of the top reinforcement occurred in both specimens at 60 mm lateral drift at the north and south faces of the column. In the steel fibre specimen yielding on those faces was of a local nature while in the control specimen yielding occurred across the entire column face. The yielded gauge locations in the top bars are given in Figures 4.20 and 4.21.

At 90 mm of lateral deflection, the yielded zones spread outwards in both specimens, now across the entire column face in the steel fibre specimen and towards the edges of the critical section $c + d$, the column dimension plus the effective depth of the slab, in the control specimen (Figure 4.21). The latter failed shortly thereafter with not much additional yielding observed in the gauges of the top bars. For the steel fibre specimen, at 120 mm drift, yielding spread around the column perimeter in a U-shaped fashion and these bars remained yielded while the drift increased further. Bottom bar yielding occurred only in the steel fibre specimen and at the north and south faces of the column as shown in Figure 4.22.

No yielding was measured outside the critical section $c + d$. In the steel fibre specimen, while lateral deflection continued to increase, yielding slowly propagated to neighbouring bars until nearly the entire joint was yielded prior to failure. In the control specimen this propagation of yielding was not seen as clearly.

A comparison of strains in the top bars running in the lateral (north-south) direction is given in Table 4.12. No clear observations could be deduced here, although the steel fibre specimen appears to have higher strains in those bars, especially in the first few cycles. The bottom bars (see Table 4.13) generally appear to have smaller strains in the steel fibre specimen. Again, the strain data was fairly scattered and no clear observations could be made.

Although no lateral loads were applied in the east-west direction, significant strains were observed in both the top and bottom bars in this direction, particularly in the joint region. East-west strains in the column region are tabulated in Table 4.14. These strains are due to the torsional moment transfer at the column side faces. As concrete cracks in that region, a need for a tensile component arises, creating tensile strains in the east-west bars. The steel fibres in the concrete played an active role in the torsional moment transfer, reducing the tensile stress demand on those bars. Measured strains in the steel fibre specimen were much lower than in the control specimen.

From the recorded strain data the force distribution in the top and bottom bars due to the lateral forces across the centreline slab was determined. The force in the steel bar and is

obtained directly from the strain readings by multiplying the strain with the Modulus of Elasticity and the cross-sectional area of each bar.

The bar force distribution for each drift cycle across the east-west column line in the top north-south bars is presented in Figure 4.23 for the steel fibre specimen Figure 4.24 for the control specimen. The bar force distribution in the bottom bars running in the same direction is presented in Figures 4.25 and 4.26 for both specimens. Up to 60 mm lateral deflection, the steel fibre specimen had higher bar forces in the centreline region. The control specimen experienced more cracking from the beginning of the test on and redistributed the forces over a larger region.

Comparing the bar force distribution between the 60 mm and 90 mm drift cycles (Figures 4.23 and 4.24), the propagation of yielded gauges across the column face can be seen. Yielding started to propagate across the face of the column during both cycles, and yielded bars essentially just elongate further without taking any additional load. This caused adjacent bars to take a larger share of the load hence the peak bar forces moved east and westward in the 90 mm cycle. At failure, the outlying bars in the control specimen were taken less than in the previous 90 mm cycle. The slab had deteriorated to a point where it was not longer to distribute the forces outward and engage all the bars.

Similar behaviour has been observed in the bottom bars. With higher drift intensity, peak bar forces moved away from the joint region. However, this behaviour was less pronounced for the steel fibre specimen here (Figures 4.25 and 4.26). Most of the lateral

moment was resisted by the bottom bars in the joint region as opposed to the control specimen, which spread its peak bar forces over a much wider region. At peak lateral load, both specimens had a similar bar force distribution.

Cycle	Specimen	Max. Error in Cycle (kN)	Max. Load in Cycle (kN)	% Error
6 mm	Steel Fibre	0.7	8.3	9
	Control	1.9	9.9	19
12 mm	Steel Fibre	0.8	15.1	6
	Control	2.4	17.3	14
18 mm	Steel Fibre	0.9	20.8	4
	Control	3.4	25.1	14
24 mm	Steel Fibre	0.9	26.5	3
	Control	4.0	29.6	13
30 mm	Steel Fibre	0.9	31.3	3
	Control	4.1	31.9	13
60 mm	Steel Fibre	1.6	43.8	4
	Control	5.8	44.6	13
90 mm	Steel Fibre	2.8	48.5	6
	Control	6.7	50.0	13
120 mm	Steel Fibre	5.1	52.0	10

Table 4.1 **Horizontal Static Check**

Cycle	Specimen	Max. Error in Cycle (kN)	Vert. Load in Cycle (kN)	% Error
6 mm	Steel Fibre	1.4	118.4	1
	Control	2.2	115.7	2
12 mm	Steel Fibre	2.7	118.4	2
	Control	2.5	115.7	2
18 mm	Steel Fibre	2.6	118.4	2
	Control	2.6	115.7	2
24 mm	Steel Fibre	3.0	118.4	3
	Control	2.5	115.7	2
30 mm	Steel Fibre	3.6	118.4	3
	Control	2.8	115.7	2
60 mm	Steel Fibre	3.2	118.4	3
	Control	3.5	115.7	3
90 mm	Steel Fibre	3.6	188.4	2
	Control	2.9	115.7	3
120 mm	Steel Fibre	4.7	118.4	4

Table 4.2 **Vertical Static Check**

Cycle	Specimen	Pushing North		Pushing South	
		Σ North Edge (kN)	Σ South Edge (kN)	Σ North Edge (kN)	Σ South Edge (kN)
		(Comp.)	(Tension)	(Tension)	(Comp.)
6mm	Steel Fibre	6.3	7.0	8.4	7.9
	Control	6.5	7.9	5.7	3.7
12mm	Steel Fibre	11.7	10.7	11.0	12.1
	Control	15.9	9.8	10.3	13.0
18mm	Steel Fibre	16.2	14.9	16.0	17.7
	Control	20.8	15.8	13.6	18.1
24mm	Steel Fibre	22.2	19.0	17.3	20.6
	Control	25.0	19.5	17.2	21.0
30mm	Steel Fibre	26.0	22.2	18.8	23.8
	Control	24.9	22.0	22.1	23.2
60mm	Steel Fibre	36.0	30.3	29.2	35.8
	Control	35.1	30.2	29.3	34.9
90mm	Steel Fibre	35.5	39.0	36.7	38.2
	Control	36.4	38.6	37.5	33.5
120mm	Steel Fibre	36.9	44.1	42.6	34.9
	Control	-	-	-	-
Pushover	Steel Fibre	39.6	47.9	-	-
	Control	-	-	39.7	26.0

Table 4.3 Vertical Load in Vertical Edge Links (Peak Values)

Cycle	Specimen	Horizontal Forces		Vertical Forces			Σof Moments about "O"	Applied Lateral Moment	Error %
		Top Column H1	Bottom Column H2	North Edge V1	South Edge V2	Bottom Column V3			
	Pushing North	(kN)	(kN)	Comp. (kN)	Tension (kN)	(kN)	(kNm)	(kNm)	
6 mm	Steel Fibre	9.0	8.3	5.0	6.0	118.2	4.6	26.4	17
	Control	11.7	9.9	6.6	6.9	115.3	5.7	31.4	18
12 mm	Steel Fibre	15.7	15.1	9.9	10.7	119.1	6.2	47.9	13
	Control	19.6	17.3	15.1	8.8	106.9	8.5	55.0	16
18 mm	Steel Fibre	21.7	20.8	17.5	12.5	110.8	5.2	66.1	8
	Control	28.4	25.1	20.4	15.3	108.1	10.3	79.9	13
24 mm	Steel Fibre	27.4	26.5	23.8	15.3	107.0	4.7	84.4	6
	Control	33.6	29.6	24.1	18.5	107.9	11.3	94.3	12
30 mm	Steel Fibre	32.0	31.3	28.8	16.2	102.9	7.6	99.6	8
	Control	35.7	31.9	23.5	22.3	111.6	11.9	101.5	12
60 mm	Steel Fibre	45.4	43.8	35.9	28.8	109.8	8.8	139.4	6
	Control	50.4	44.6	34.8	29.2	107.3	18.2	141.8	13
90 mm	Steel Fibre	51.1	48.5	34.7	39.0	120.9	8.2	154.2	5
	Control	56.7	50.0	35.9	38.1	116.2	17.5	158.9	11
120 mm	Steel Fibre	55.5	52.0	38.8	41.8	118.9	7.9	165.3	5

% Error compares the Sum of Moments around "O" with the applied lateral Moment

Table 4.4 Moment Check around Connection

Cycle	Specimen	Pushing North						Pushing South					
		Edge Restraint 1 (kN)	Edge Restraint 2 (kN)	Edge Restraint 3 (kN)	Edge Restraint 4 (kN)	Total Force in N-S Edge Restraints (kN)	Positive Moment at Edge (kNm)	Edge Restraint 1 (kN)	Edge Restraint 2 (kN)	Edge Restraint 3 (kN)	Edge Restraint 4 (kN)	Total Force in N-S Edge Restraints (kN)	Positive Moment at Edge (kNm)
6 mm	Steel Fibre	2.6	2.4	2.5	3.0	10.6	14.1	3.0	2.4	2.5	3.0	11.0	14.6
	Control	2.5	3.4	3.5	2.5	11.9	15.9	2.5	3.4	3.5	2.7	12.1	16.1
12 mm	Steel Fibre	2.7	2.6	2.5	2.8	10.6	14.2	2.7	2.4	2.7	3.0	10.8	14.4
	Control	2.0	3.4	3.0	2.5	10.9	14.6	2.2	3.4	3.2	2.5	11.3	15.0
18 mm	Steel Fibre	3.0	2.9	2.5	3.0	11.4	15.2	3.0	2.4	2.8	3.0	11.2	15.0
	Control	2.5	3.6	3.5	3.0	12.6	16.8	2.5	3.8	2.5	3.0	11.8	15.7
24 mm	Steel Fibre	2.8	2.8	2.5	2.5	10.6	14.1	2.8	2.4	2.6	3.0	10.9	14.6
	Control	2.7	3.9	3.5	3.5	13.6	18.2	2.7	3.9	3.5	3.5	13.6	18.2
30 mm	Steel Fibre	2.5	2.6	2.5	2.7	10.3	13.7	2.5	2.4	2.5	3.0	10.4	13.9
	Control	3.5	4.4	4.0	3.5	15.4	20.6	3.5	4.4	4.0	3.9	15.7	21.0
60 mm	Steel Fibre	3.4	2.9	2.6	3.6	12.5	16.7	3.2	2.5	2.7	3.7	12.0	16.1
	Control	3.2	4.5	3.6	3.1	14.4	19.2	2.6	4.0	4.0	4.1	14.8	19.7
90 mm	Steel Fibre	4.6	4.5	3.6	4.7	17.4	23.2	4.4	3.5	3.6	5.2	16.7	22.3
	Control	3.7	5.5	4.6	4.2	18.0	24.1	3.8	5.2	5.1	5.4	19.6	26.1
120 mm	Steel Fibre	4.4	4.4	3.6	4.7	17.0	22.7	4.5	3.8	3.8	5.7	17.8	23.7
Pushover	Steel Fibre	6.0	5.4	5.0	6.0	22.4	29.9						
	Control							5.0	6.4	6.0	6.6	23.9	31.9

Table 4.5 **North - South Edge Restraints (Averages)**

Cycle	Specimen	Pushing North						Pushing South					
		Edge Restraint 1 (kN)	Edge Restraint 2 (kN)	Edge Restraint 3 (kN)	Edge Restraint 4 (kN)	Total Force in E-W Edge Restraints (kN)	Positive Moment at Edge (kNm)	Edge Restraint 1 (kN)	Edge Restraint 2 (kN)	Edge Restraint 3 (kN)	Edge Restraint 4 (kN)	Total Force in E-W Edge Restraints (kN)	Positive Moment at Edge (kNm)
6 mm	Steel Fibre	3.9	3.9	4.0	3.4	15.1	14.2	3.0	3.7	4.0	3.9	14.5	13.6
	Control	2.4	4.9	4.5	2.4	14.2	13.3	1.9	4.4	4.6	2.9	13.8	13.0
12 mm	Steel Fibre	4.5	4.6	3.9	3.4	16.4	15.4	3.5	3.5	3.3	4.6	14.9	14.0
	Control	2.4	4.9	4.5	2.4	14.2	13.3	1.5	4.4	4.5	3.4	13.7	12.9
18 mm	Steel Fibre	4.5	5.0	3.9	3.1	16.6	15.5	2.9	3.6	4.4	4.9	15.8	14.8
	Control	2.9	6.0	4.9	2.6	16.4	15.4	1.5	4.7	5.9	4.4	16.5	15.4
24 mm	Steel Fibre	4.8	5.3	3.9	2.9	17.0	16.0	2.4	3.4	4.4	5.4	15.6	14.6
	Control	3.4	6.6	5.4	3.4	18.8	17.6	1.6	5.0	6.8	5.7	19.1	17.9
30 mm	Steel Fibre	5.2	5.8	3.5	2.4	16.9	15.9	1.9	3.4	4.9	5.5	15.8	14.8
	Control	3.6	7.3	5.4	2.9	19.2	18.0	1.5	5.0	7.1	5.8	19.4	18.2
60 mm	Steel Fibre	7.1	7.5	3.5	2.9	21.0	19.7	2.5	3.6	5.3	7.3	18.7	17.5
	Control	4.6	7.2	4.1	2.4	18.3	17.2	1.1	4.0	7.4	7.2	19.7	18.5
90 mm	Steel Fibre	8.5	8.1	3.6	2.8	23.0	21.6	2.1	3.8	6.4	8.3	20.5	19.3
	Control	5.3	7.3	3.6	2.4	18.7	17.5	1.0	3.7	8.9	6.0	19.6	18.4
120 mm	Steel Fibre	9.0	8.0	3.5	2.9	23.4	21.9	1.8	3.0	7.3	8.4	20.5	19.3
Pushover	Steel Fibre	10.2	9.7	4.4	4.4	28.7	26.9						
	Control							1.5	4.9	9.4	6.3	22.1	20.7

Table 4.6 **East - West Edge Restraints (Averages)**

Cycle	Specimen	Stable Lateral Load for Cycle		Load Range (kN)
		North (kN)	South (kN)	
6 mm	Steel Fibre	6.9	-8.2	15.2
	Control	9.3	-6.3	15.6
12 mm	Steel Fibre	14.6	-15.8	30.4
	Control	16.9	-13.8	30.6
18 mm	Steel Fibre	20.6	-20.8	41.5
	Control	23.4	-18.1	41.5
24 mm	Steel Fibre	25.3	-24.4	49.7
	Control	27.3	-22.3	49.6
30 mm	Steel Fibre	28.5	-29.4	57.9
	Control	30.7	-28.2	58.9
60 mm	Steel Fibre	36.6	-38.8	75.4
	Control	40.0	-36.3	76.3
90 mm	Steel Fibre	45.6	-43.7	89.3
	Control	44.5	-41.9	86.4
120 mm	Steel Fibre	45.8	-44.5	90.2
Pushover	Steel Fibre at 224.5 mm	42.4*		
	Control at 110.3 mm		-45.6	
Residual 120 mm	Steel Fibre	18.7	-37.9	56.5
	% of 120 mm	40.8 %	85.2 %	

Notes: * after reaching a peak load of 51.5 KN at 152.4 mm

Table 4.7 Comparison of Load - Drift Response

	Direction	North - South (Direction of Lateral Deflection)									East -West		
	LVDT	1	2	3	4	5	6	7	8	Average	9	10	11
	Location (m)	-1.6775	-1.2775	-0.6275	-0.2775	0.2775	0.5275	1.2775	1.6775	Difference	0.15	0.35	1.5
Cycle	Specimen												
6 mm	Steel Fibre	1.4	1.2	0.6	0.5	0.3	0.9	1.2	1.5		0	0.1	0.3
	Control	1.3	1.3	0.7	0.5	0.5	0.7	1.3	1.2		0	0	0.2
	% Difference	108	92	86	100	60	129	92	125	99			
12 mm	Steel Fibre	1.8	1.7	1.1	1.0	0.5	1.0	1.7	1.8		0.3	0.3	N/A
	Control	1.8	2.0	0.9	1.0	1.0	1.2	1.9	1.8		0	0.2	0.1
	% Difference	100	85	122	100	50	83	89	100	91			
18 mm	Steel Fibre	2.3	2.2	1.6	1.4	0.7	2.1	2.2	2.5		0	0.1	0.4
	Control	2.4	2.6	2.0	1.5	1.6	1.9	2.6	2.2		0	0.1	0.3
	% Difference	96	85	80	93	44	111	85	114	88	0		
24 mm	Steel Fibre	2.6	2.7	2.1	1.9	1.1	2.6	2.6	3.0		0.1	0.2	0.6
	Control	2.9	3.1	2.5	2.1	2.1	2.4	3.0	2.7		0	0.1	0.5
	% Difference	90	87	84	90	52	108	87	111	89			
30 mm	Steel Fibre	3.0	3.2	2.6	2.6	1.6	3.3	3.1	3.4		0.1	0.2	0.7
	Control	3.2	3.6	3	2.6	2.7	3.0	3.6	3.2		0	0	0.3
	% Difference	94	89	87	100	59	110	86	106	91			
60 mm	Steel Fibre	4.3	5.3	5.4	5.3	5.0	5.8	5.4	5.3		0.4	0.5	0.3
	Control	5.6	6.7	6.8	5.9	6.0	6.6	6.5	4.5		0.1	0.4	1.6
	% Difference	77	79	79	90	83	88	83	118	87			
90 mm	Steel Fibre	5.8	7.8	8.6	8.5	8.7	10.5	7.6	6.9		0.5	0.8	0.6
	Control	6.7	9.8	10.5	9.2	9.3	10.2	9.1	5.6		0.3	0.9	1.5
	% Difference	87	80	82	92	94	103	84	123	93			
120 mm	Steel Fibre	7.2	9.9	11.1	10.9	11.2	13.9	9.3	8.3		0.8	1.5	1.5
	Control	N/A	N/A	N/A	N/A	N/A	N/A	N/A	N/A		N/A	N/A	N/A
	% Difference	N/A	N/A	N/A	N/A	N/A	N/A	N/A	N/A		N/A	N/A	N/A
Actual Slab Deflections observed at Pushover													
	Steel Fibre	5.2	5.3	6.0	7.6	-8.3	-11.3	-7.3	N/A		2.0	1.7	1.7
	Control	-3.2	-6.0	-7.1	-6.6	6.8	6.5	5.9	3.6		2.9	2.3	2.8

Notes: % Difference is the ratio of the slab deflections of the steel fibre specimen compared to the control specimen in %
For the steel fibre specimen LVDT's Nos. 5, 6 and 8 do not give reliable readings.
For the control specimen LVDT No. 8 does not give reliable readings.

Table 4.8 **Comparison of Measured Slab Deflections - Vertical LVDT's**

Cycle	RVDT / Location / Specimen	4 150 mm E of Column (deg)	5 850 mm E of Column (deg)	6 1550 mm E of Column (deg)
6 mm	Steel Fibre	0.13	0.07	0.05
	Control	0.11	0.08	0.06
	% Difference	117	86	88
12 mm	Steel Fibre	0.26	0.14	0.11
	Control	0.20	0.13	0.07
	% Difference	129	111	151
18 mm	Steel Fibre	0.33	0.14	0.09
	Control	0.37	0.20	0.09
	% Difference	90	69	108
24 mm	Steel Fibre	0.43	0.16	0.12
	Control	0.55	0.23	0.19
	% Difference	77	70	64
30 mm	Steel Fibre	0.55	0.20	0.14
	Control	0.78	0.26	0.12
	% Difference	71	75	111
60 mm	Steel Fibre	1.21	0.45	0.30
	Control	2.41	0.57	0.43
	% Difference	50	78	69
90 mm	Steel Fibre	1.80	0.67	0.50
	Control	2.64	0.82	0.56
	% Difference	68	82	90
120 mm	Steel Fibre	2.52	0.92	0.64
	Control			
Actual Slab Rotations observed at Pushover				
	Steel Fibre	2.55	0.63	0.44
	Control	1.80	0.50	0.33

Note: % Difference is the ratio of the slab rotations of the steel fibre specimen compared to the control specimen in %

Table 4.9 **Comparison of Measured Rotation across the E-W Slab Centreline**

Cycle	RVDT / Location / Specimen	1 Column above Slab (deg)	2 Column below Slab (deg)	Drift at Column mid-height (mm)	Story Drift (mm)	Actual Column Deflection (mm)
6 mm	Steel Fibre	0.18	0.16	2.24	3	0.76
	Control	0.16	0.14	1.91	3	1.09
12 mm	Steel Fibre	0.37	0.32	4.49	6	1.51
	Control	0.30	0.26	3.65	6	2.35
18 mm	Steel Fibre	0.50	0.44	6.11	9	2.89
	Control	0.45	0.45	5.88	9	3.12
24 mm	Steel Fibre	0.66	0.64	8.48	12	3.52
	Control	0.64	0.57	7.90	12	4.10
30 mm	Steel Fibre	0.86	0.97	12.00	15	3.00
	Control	0.80	0.92	11.27	15	3.73
60 mm	Steel Fibre	1.86	1.62	22.75	30	7.25
	Control	1.78	1.60	22.14	30	7.86
90 mm	Steel Fibre	2.80	2.50	34.77	45	10.23
	Control	2.75	2.47	34.14	45	10.86
120 mm	Steel Fibre	3.80	3.42	47.30	60	12.70
	Control					

Table 4.10 Calculation of Column Drift at mid-height for each cycle in mm

Cycle	Specimen	North Edge	South Edge	Average Difference
6 mm	Steel Fibre	0.7	0.7	
	Control	1.1	0.8	
	% Difference	36	13	24
12 mm	Steel Fibre	N/A	N/A	
	Control	2.0	1.5	
	% Difference	N/A	N/A	N/A
18 mm	Steel Fibre	1.0	1.0	
	Control	2.5	2.5	
	% Difference	60	60	60
24 mm	Steel Fibre	1.5	2.0	
	Control	2.5	1.5	
	% Difference	40	-33	3
30 mm	Steel Fibre	1.4	1.5	
	Control	1.7	1.4	
	% Difference	18	-7	5
60 mm	Steel Fibre	2.7	2.5	
	Control	4.9	2.7	
	% Difference	45	7	26
90 mm	Steel Fibre	5.3	5.2	
	Control	8.0	6.0	
	% Difference	34	13	24
120 mm	Steel Fibre	8.6	6.5	
	Control	N/A	N/A	
	% Difference	N/A	N/A	N/A
Actual Slab Edge Rotations observed at Pushover				
	Steel Fibre	7.3	5.4	
	Control	5.5	3.8	

Note: % Difference shows the difference of the slab edge rotations of the steel fibre specimen compared to the control specimen in %

Table 4.11 Comparison of Measured North and South Slab Edge Rotations in 1000 rad
Horizontal Cable Transducers

Top North-South Bars
Steel Fibre Specimen
(Average Strains)

Bar	TNS 14	TNS 13	TNS 12	TNS 11	TNS 10	TNS 9/8	TNS 7/6	TNS 5	TNS 4	TNS 3	TNS 2	TNS 1
Cycle												
Dead Load	56	65	85		198	142	253	180		142	138	-20
Peak Strains 6 mm	67	82	111		289	420	554	319		173	164	-7
Peak Strains 12 mm	124	106	175		401	718	965	481		256	288	66
Peak Strains 18 mm	151	128	270		472	919	1166	590		310	390	163
Peak Strains 24 mm	168	146	309		552	1062	1349	679		343	459	211
Peak Strains 30 mm	174	166	344		657	1266	1524	780		379	528	277
Peak Strains 60 mm	247	271	557		1123	2174	2407	1353		549	884	722
Peak Strains 90 mm	437	420	679		1671	2657	3745	1836		686	1065	855
Peak Strains 120.1 mm	541	563	852		2057	1396	2141	2540		811	1164	916
Peak Strains 120.2 mm	545	550	894		1722	969	931	3061		733	885	648
Pushover	533	539	966		2152	1996	1554	6156		519	1120	803

Top North-South Bars
Control Specimen
(Average Strains)

Bar	TNS 14	TNS 13	TNS 12	TNS 11	TNS 10	TNS 9/8	TNS 7/6	TNS 5	TNS 4	TNS 3	TNS 2	TNS 1
Cycle												
Dead Load	35	30	39	69	86	32	216	50	40	24	25	26
Peak Strains 6 mm	51	52	67	117	175	153	385	122	68	44	41	35
Peak Strains 12 mm	69	88	114	182	286	361	583	208	115	67	59	33
Peak Strains 18 mm	271	284	265	360	572	598	825	354	265	122	112	69
Peak Strains 24 mm	692	452	389	532	803	782	1000	466	392	181	181	136
Peak Strains 30 mm	600	521	440	632	1035	953	1213	601	594	339	301	417
Peak Strains 60 mm	898	684	577	933	1702	1570	2733	1080	1065	655	519	796
Peak Strains 90 mm	1115	763	616	1265	2119	4091	2249	1475	1496	842	776	974
Pushover	35	404	233	1105	2072	1048	1058	2320	1437	945	25	1252

Table 4.12 **Comparison of North-South Top Bar Strains**

Bottom North-South Bars
Steel Fibre Specimen
(Average Strains)

Bar	BNS 16	BNS 14	BNS 12	BNS 11	BNS 10	BNS 9	BNS 8	BNS 7	BNS 6	BNS 5	BNS3	BNS 1
Cycle												
Dead Load	22	-12	-23	-15	-25	-31	-31	-20	-8.5	-9	5	31
Peak Strains 6 mm	21	-7	-8	10	13	18	19	18	14	8	11	33
Peak Strains 12 mm	22	0	14	53	74	202	177	75	49	42	24	49
Peak Strains 18 mm	17	0	33	96	156	398	360	157	83	72	49	48
Peak Strains 24 mm	33	12	74	140	276	642	589	345	147	118	67	55
Peak Strains 30 mm	63	38	140	182	408	878	840	530	247	194	100	69
Peak Strains 60 mm	142	93	299	421	884	1344	1390	988	566	582	574	227
Peak Strains 90 mm	204	170	413	767	1315	1747	1872	1304	778	804	765	303
Peak Strains 120.1 mm	303	438	679	1230	2030	1697	1861	1980	1112	1108	868	394
Peak Strains 120.2 mm	367	438	558		1145	490	867	1164	760	760		260
Pushover	412		1177		2178	850	3741	2111	1430	1430		372

Bottom North-South Bars
Control Specimen
(Average Strains)

Bar	BNS 16	BNS 14	BNS 12	BNS 11	BNS 10	BNS 9	BNS 8	BNS 7	BNS 6	BNS 5	BNS3	BNS 1
Cycle												
Dead Load	-14	-17	-16	-15	-11	-8	-5	-33	-20	-21	-12	-10
Peak Strains 6 mm	-13	-15	-3	33	28	16	22	25	14	-6	-7	-8
Peak Strains 12 mm	-7	-4	23	41	88	141	168	113	71	24	6	-3
Peak Strains 18 mm	-13	20	93	166	234	411	438	504	150	67	6	-14
Peak Strains 24 mm	24	199	181	224	347	590	619	875	239	122	15	-26
Peak Strains 30 mm	17	324	231	351	595	507	744	1016	370	223	79	-42
Peak Strains 60 mm	875	512	930	788	1249	761	1177	2021	1358	484	492	1114
Peak Strains 90 mm	1040	601	1578	1340	1740	1914	1091	2550	1952	919	672	1548
Pushover	1050	393	574	458	1061	1383	1294	1177	1116	631	219	277

Table 4.13 **Comparison of North-South Bottom Bar Strains**

Steel Fibre Specimen								
Column Region	Top Bars				Bottom Bars			
Gauge	32	37	38	43	1	2	3	4
Peak Strains 60 mm	205	15	37	294	74	163	115	94
Peak Strains 90 mm	195	30	91	451	82	257	237	136
Pushover	634	234	183	313	388	688	1006	314
Control Specimen								
Column Region	Top Bars				Bottom Bars			
Gauge	32	37	38	43	1	2	3	4
Peak Strains 60 mm	614	353	99	455	180	291		441
Peak Strains 90 mm	781	600	211	434	247	239		460
Pushover	697	753	221	181	266	254		229

Table 4.14 **Comparison of East-West Bar Strains for Various Drift Cycles**

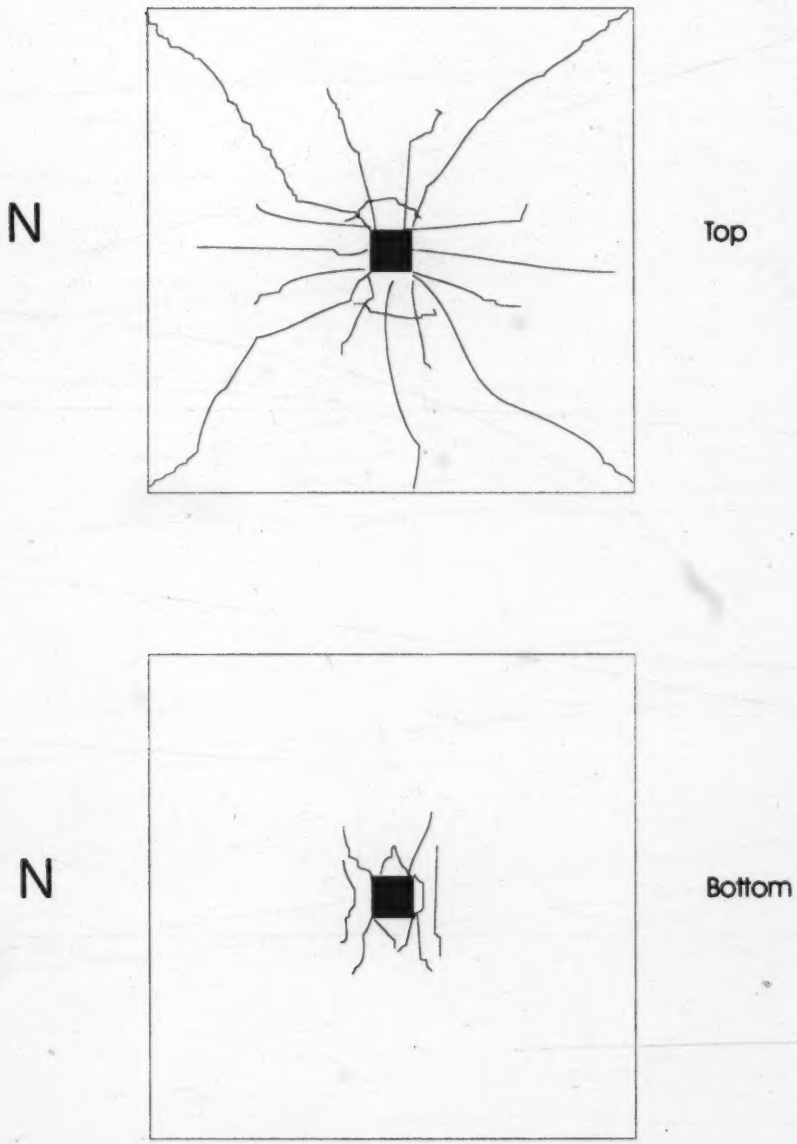

Figure 4.1 Final Crack Pattern of Steel Fibre Specimen

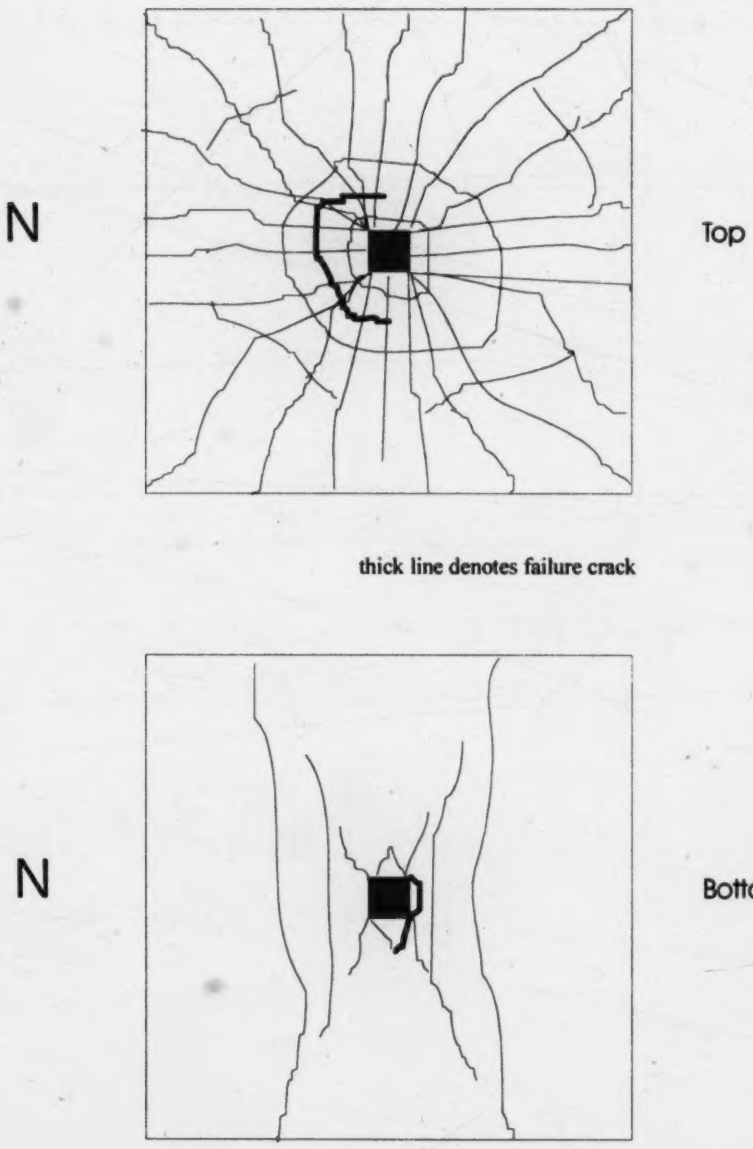

Figure 4.2 Final Crack Pattern of Control Specimen

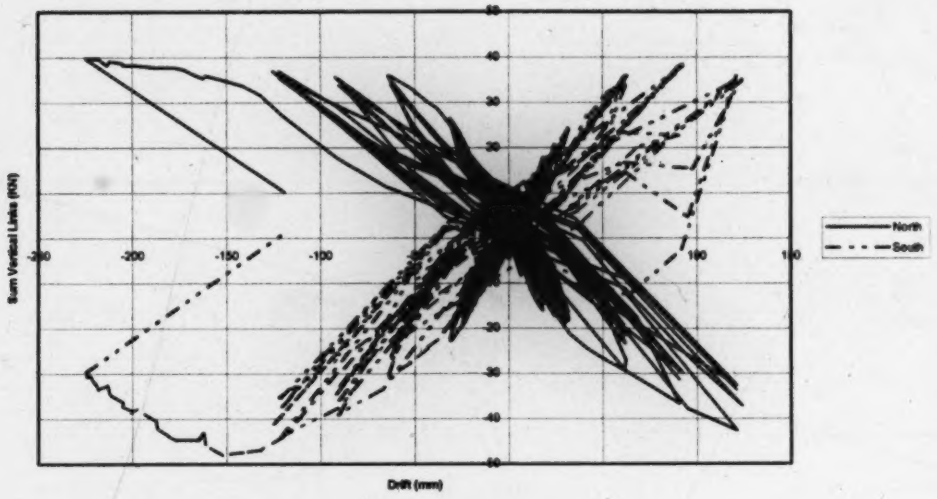

Figure 4.3 Load in Vertical Edge Boundary Links vs. Lateral Drift
Steel Fibre Specimen

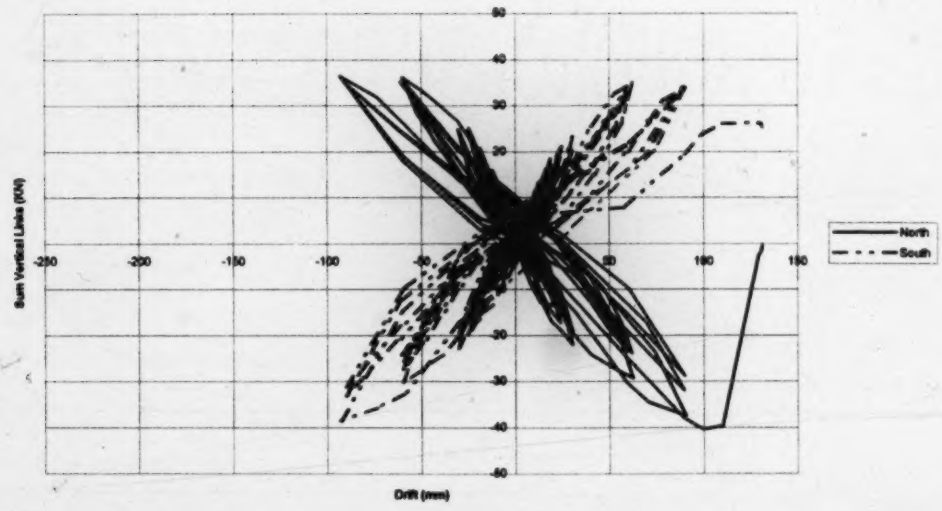

Figure 4.4 Load in Vertical Edge Boundary Links vs. Lateral Drift
Control Specimen

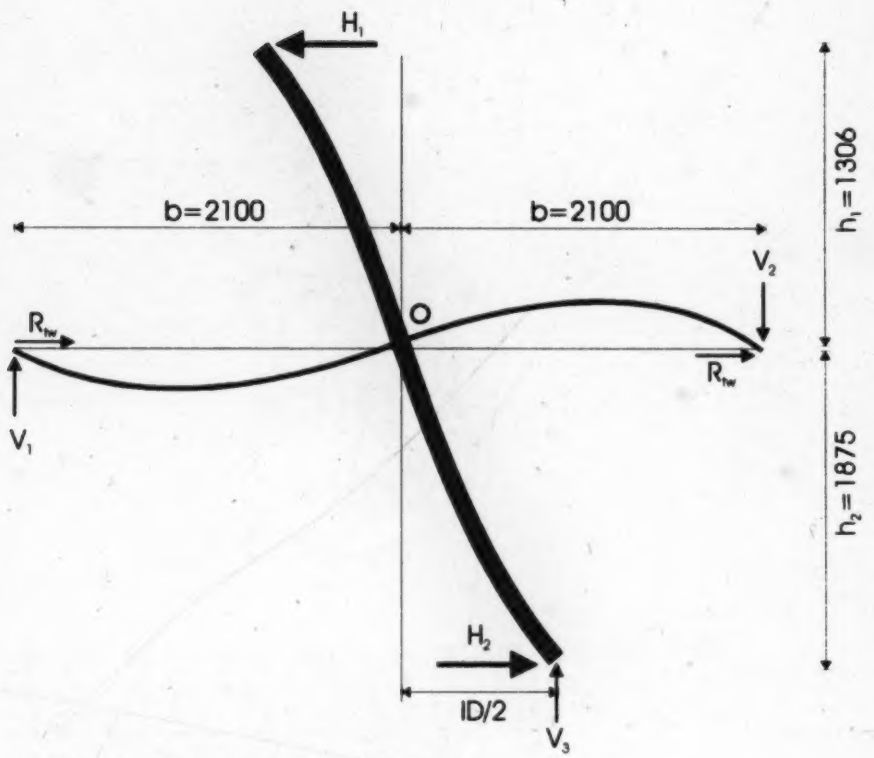

$\Sigma M_o = 0 = H_1h_1 + H_2h_2 - V_1b - V_2b - V_3(ID/2)$

R_{fw} = Resistance due to friction in Twisting Restraints

Figure 4.5 Free-Body Diagram of Specimen

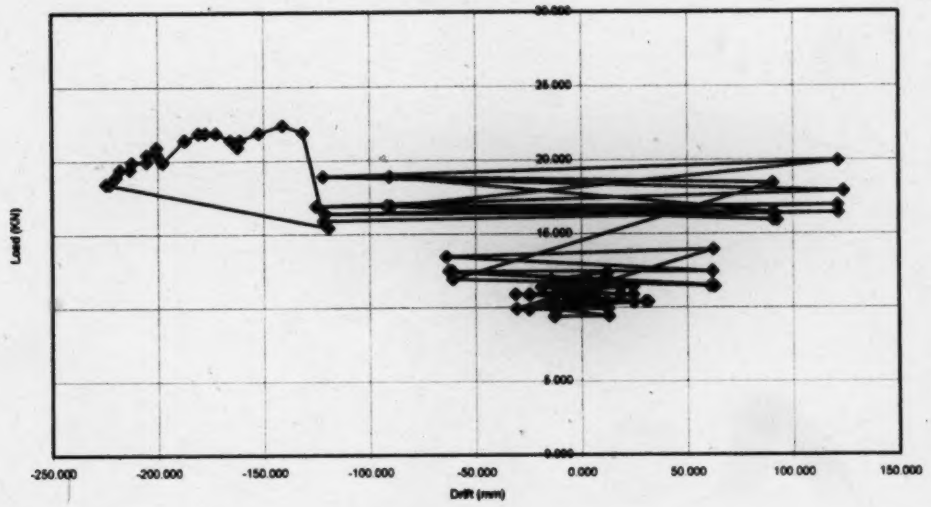

Figure 4.6 Sum of Loads in North-South Edge Restraints (5 to 8) vs. Lateral Drift Steel Fibre Specimen

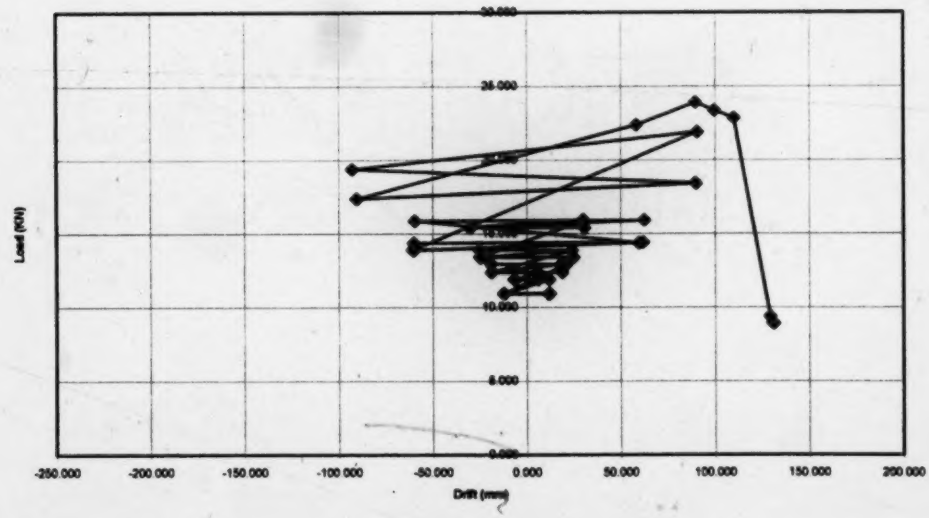

Figure 4.7 Sum of Loads in North-South Edge Restraints (5 to 8) vs. Lateral Drift Control Specimen

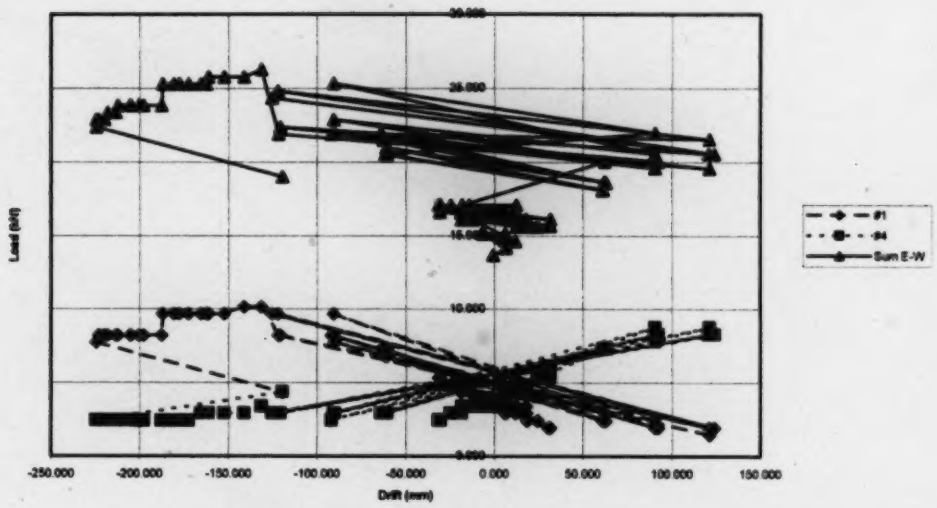

Figure 4.8 Sum of Loads in East-West Edge Restraints (1 to 4) vs. Lateral Drift, And Loads in East-West Edge Restraints 1 and 4 vs. Lateral Drift Steel Fibre Specimen

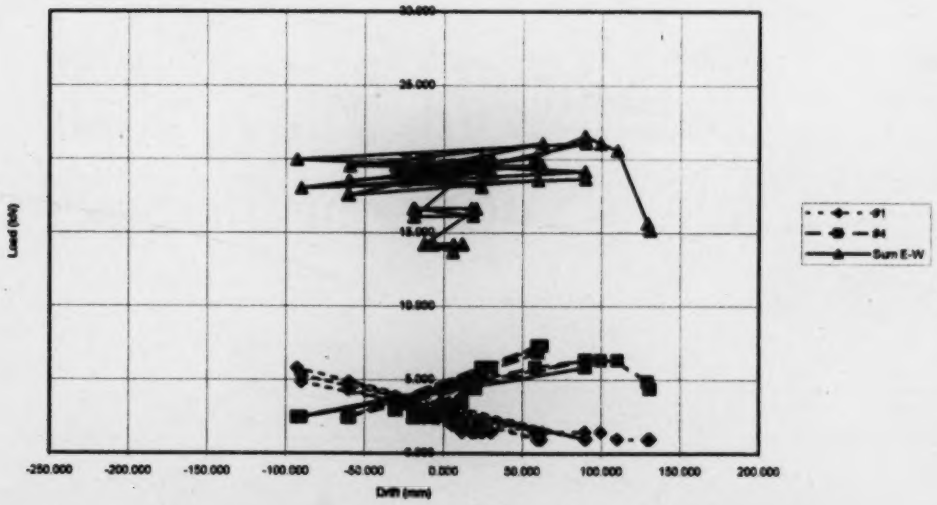

Figure 4.9 Sum of Loads in East-West Edge Restraints (1 to 4) vs. Lateral Drift, And Loads in East-West Edge Restraints 1 and 4 vs. Lateral Drift Control Specimen

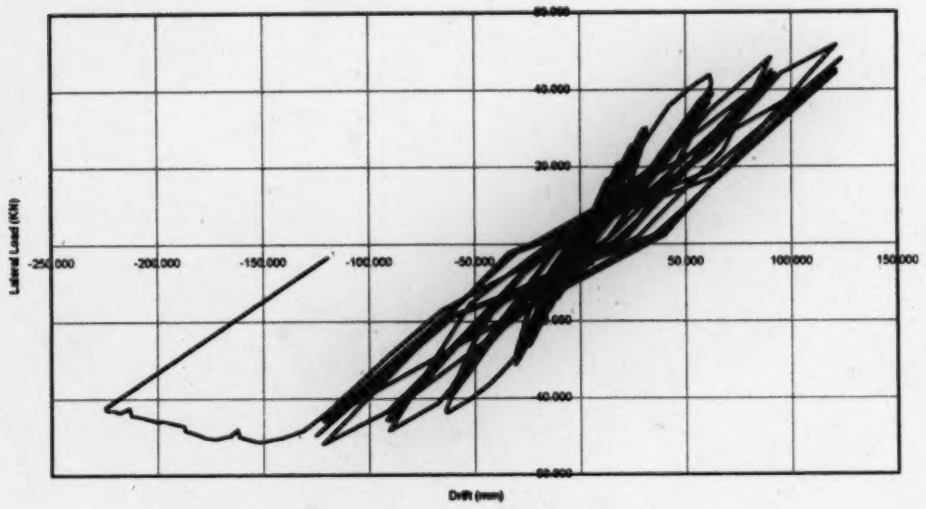

Figure 4.10 Horizontal Load vs. Lateral Drift
Steel Fibre Specimen

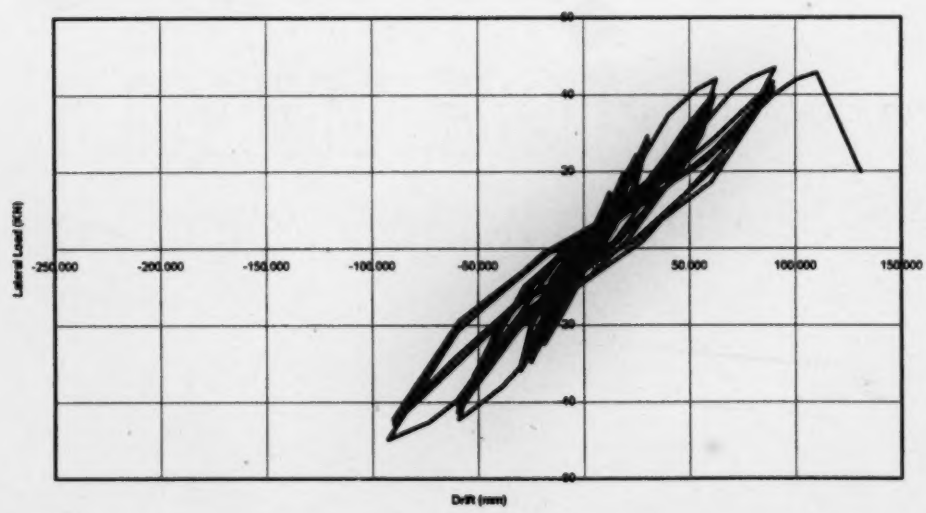

Figure 4.11 Horizontal Load vs. Lateral Drift
Control Specimen

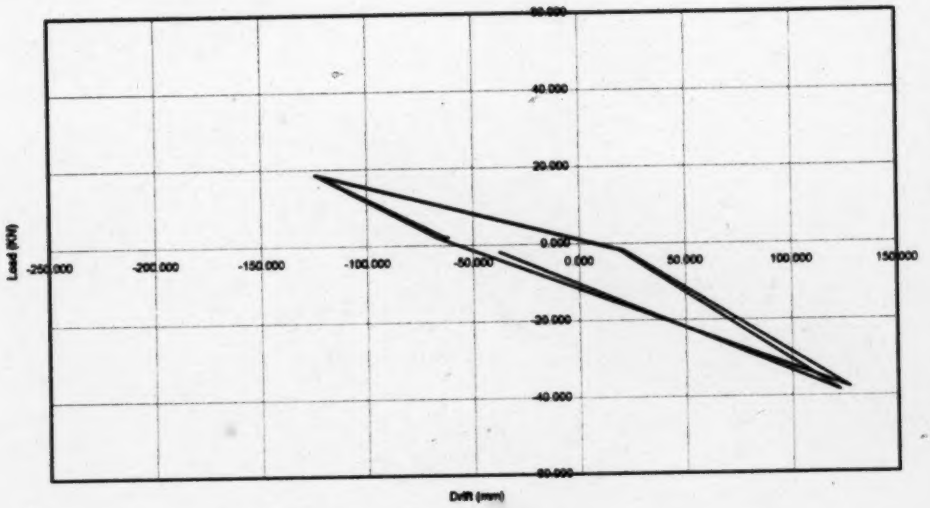

Figure 4.12 Horizontal Load vs. Lateral Drift
Post-Peak Response
Steel Fibre Specimen

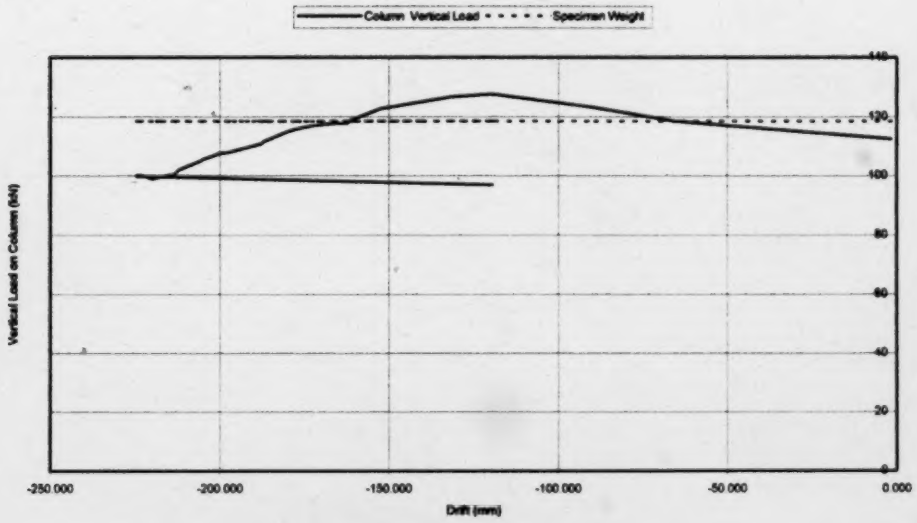

Figure 4.13 Gravity Load Redistribution at Pushover
Column Vertical Load vs. Lateral Drift
Steel Fibre Specimen

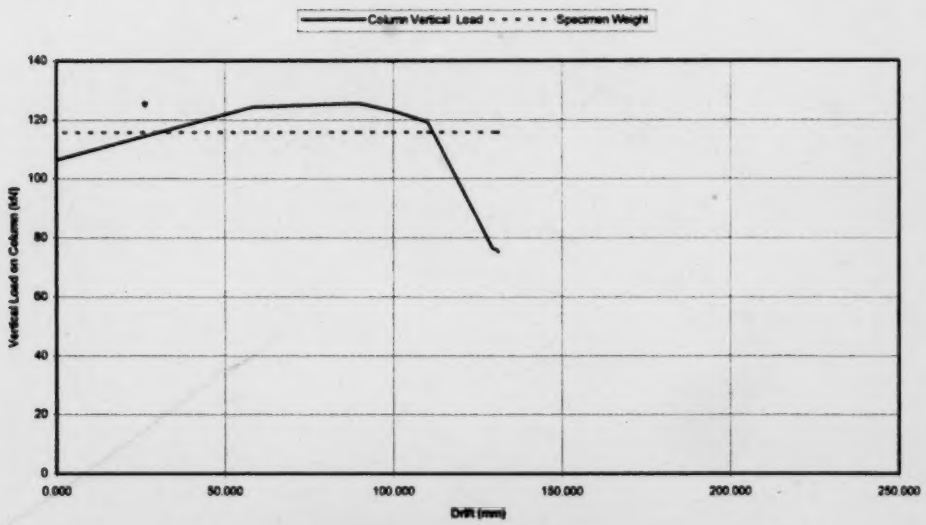

Figure 4.14 Gravity Load Redistribution at Pushover
Column Vertical Load vs. Lateral Drift
Control Specimen

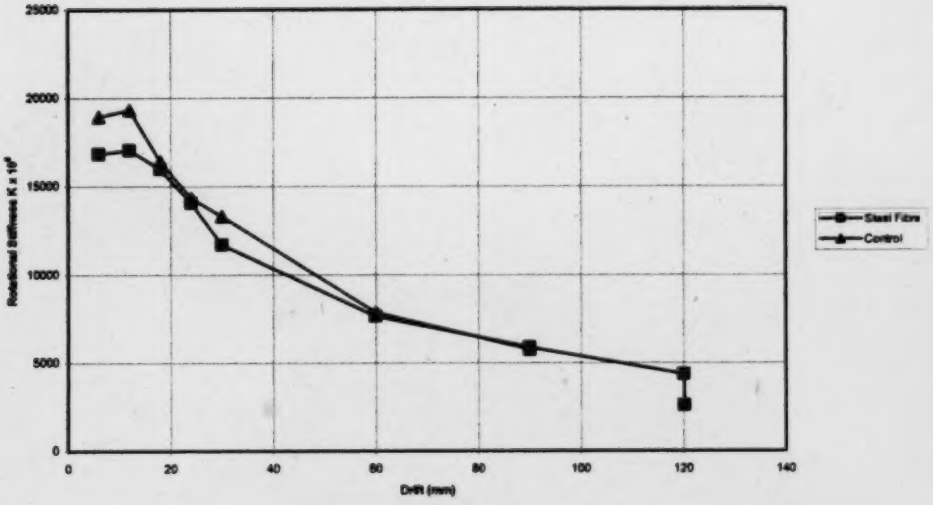

Figure 4.15 Rotational Stiffness of Connection for each Drift Cycle

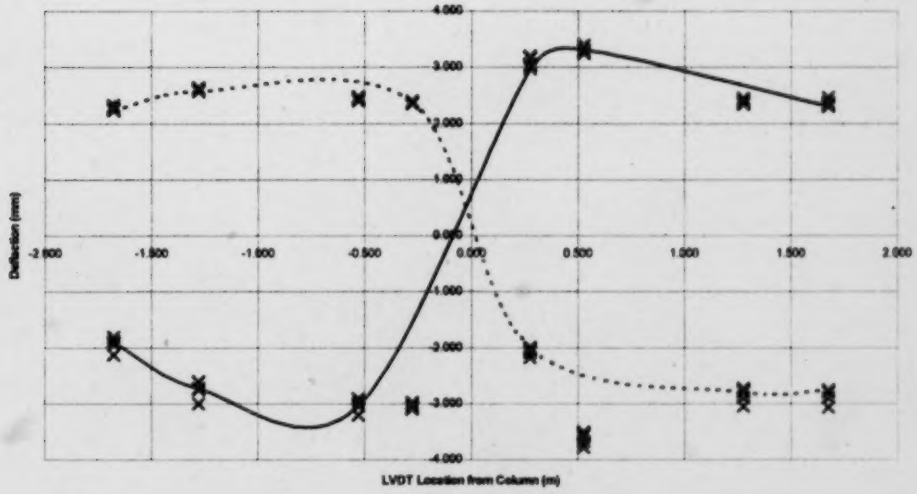

Figure 4.16 Slab Deflections: North-South Direction Vertical LVDT's Steel Fibre Specimen – 60 mm Drift Cycle

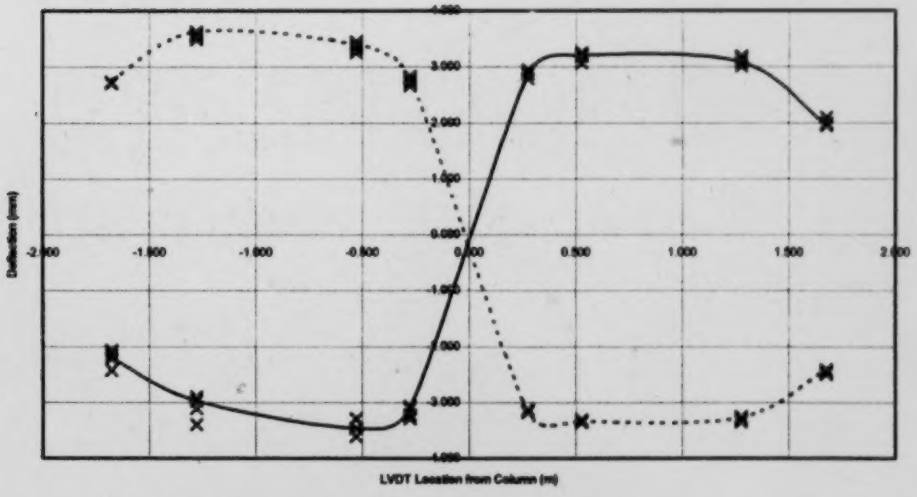

Figure 4.17 Slab Deflections: North-South Direction Vertical LVDT's Control Specimen – 60 mm Drift Cycle

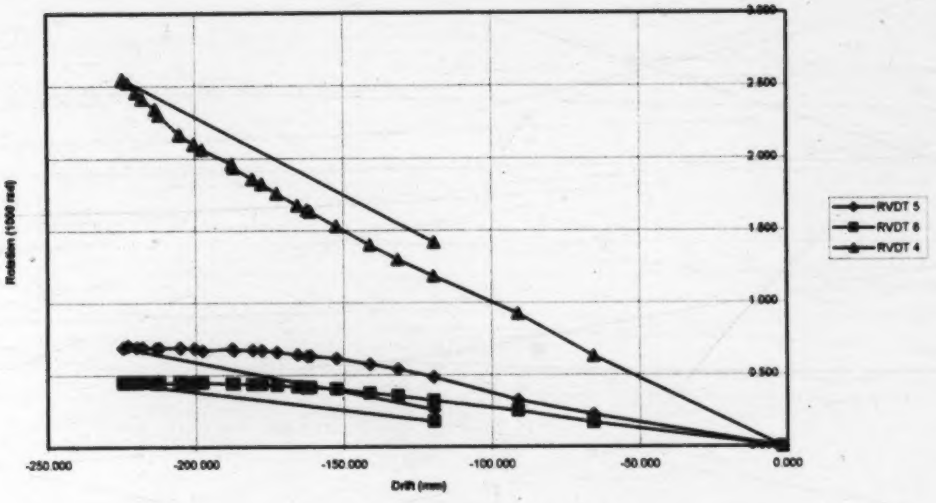

Figure 4.18 Slab Rotation vs. Lateral Drift RVDT 4, 5 & 6
Steel Fibre Specimen – Pushover

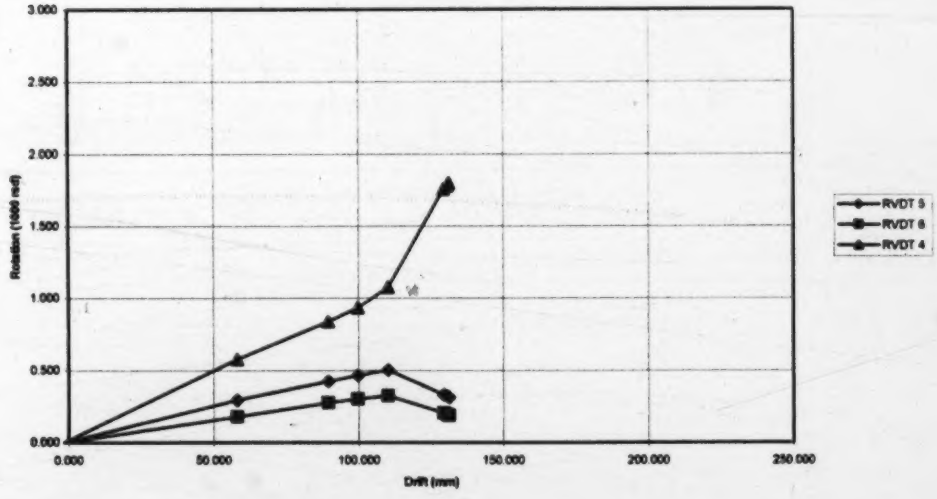

Figure 4.19 Slab Rotation vs. Lateral Drift RVDT 4, 5 & 6
Control Specimen – Failure

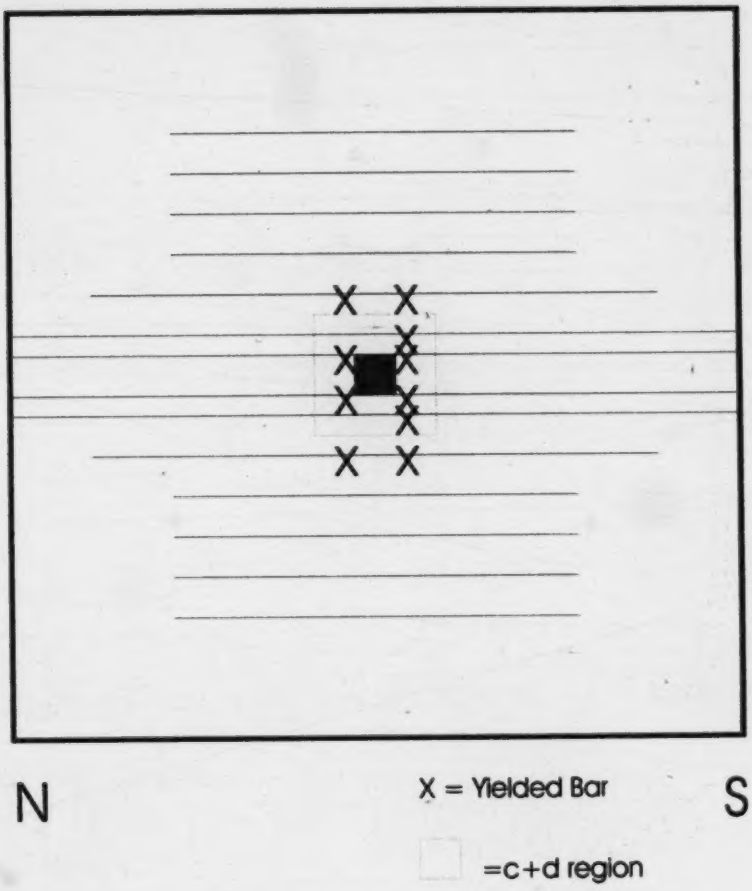

Figure 4.20 Yielded Bar Locations at Failure in Top Mat Steel Fibre Specimen

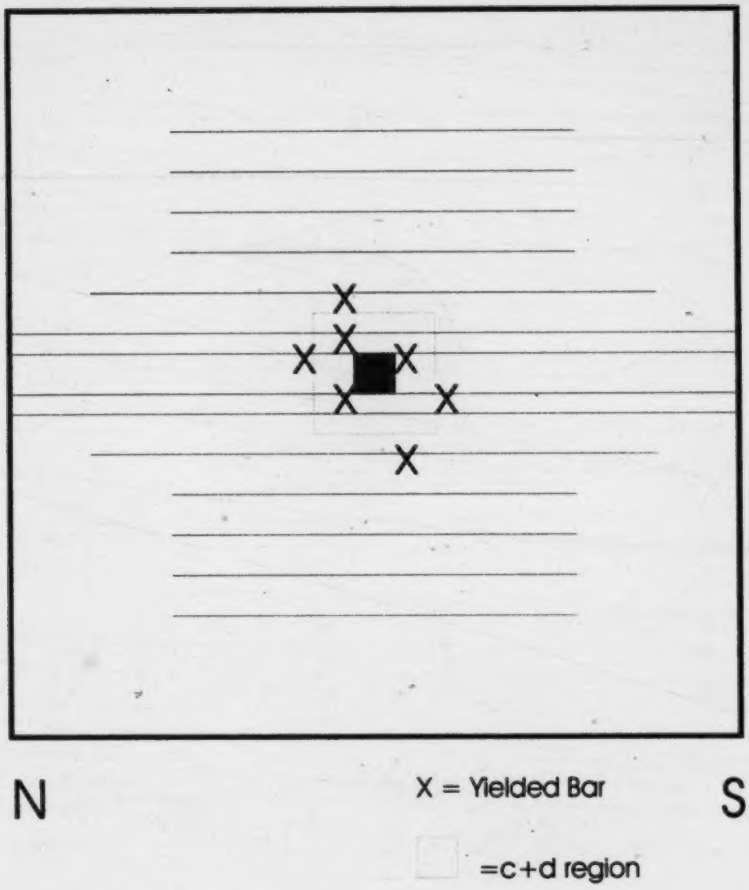

Figure 4.21 Yielded Bar Locations at Failure in Top Mat Control Specimen

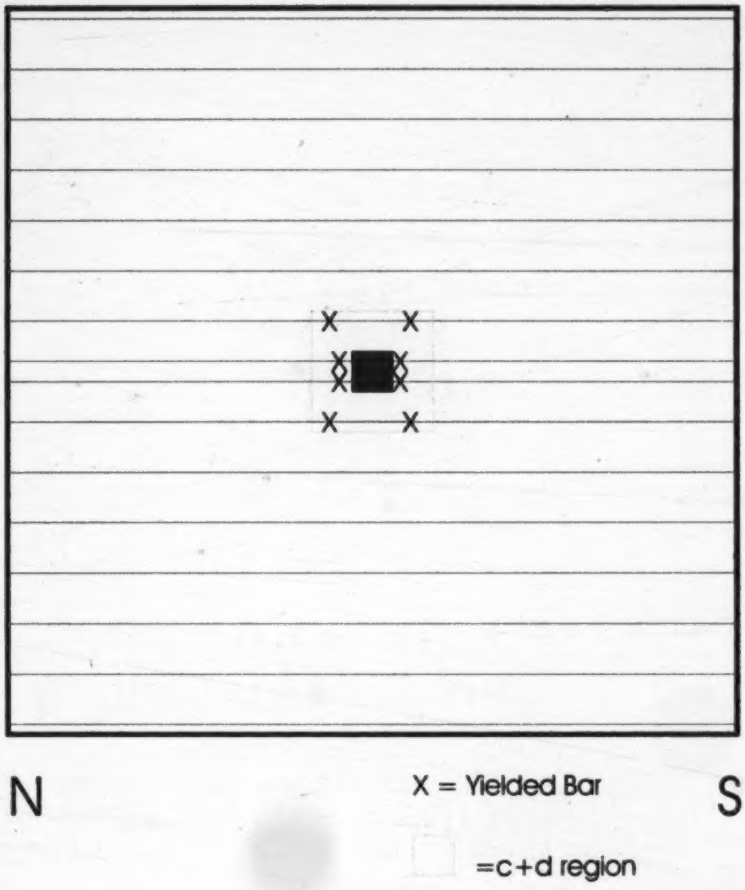

Figure 4.22 Yielded Bar Locations at Failure in Bottom Mat Steel Fibre Specimen

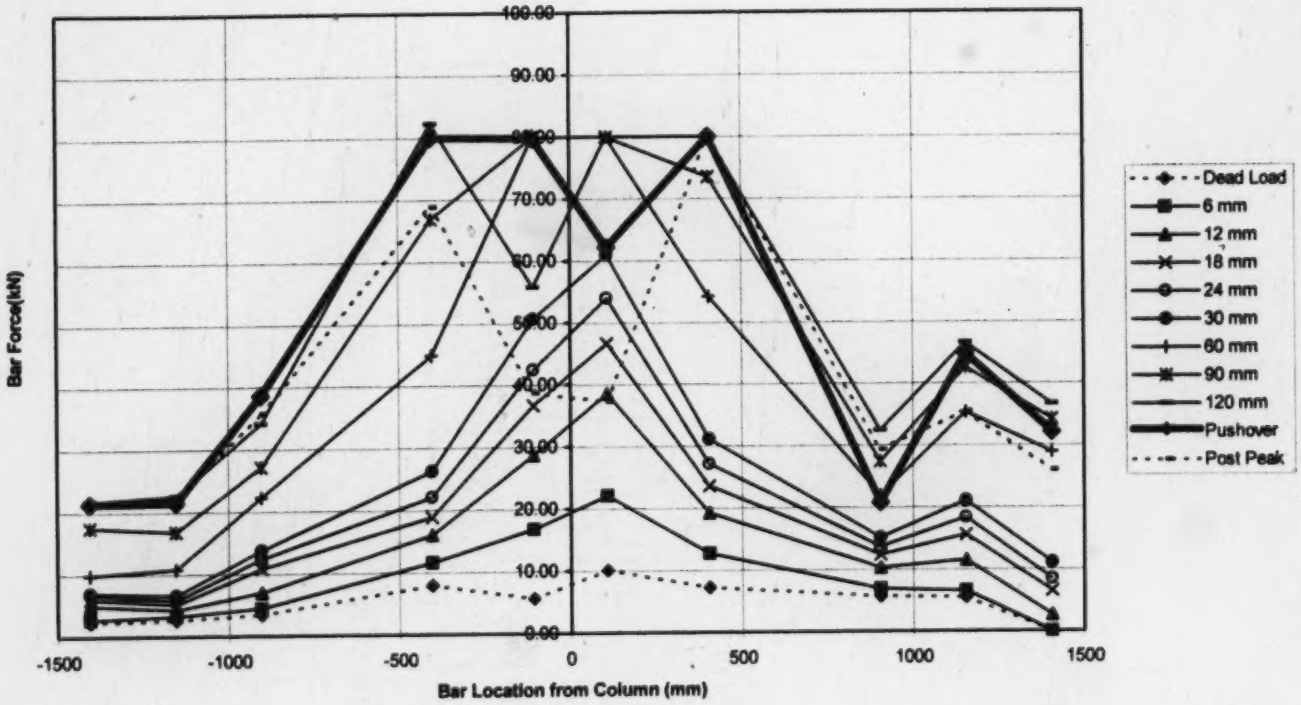

Figure 4.23 Bar Forces in North-South Top Bars across East-West Column Line
For Each Drift Cycle
Steel Fibre Specimen

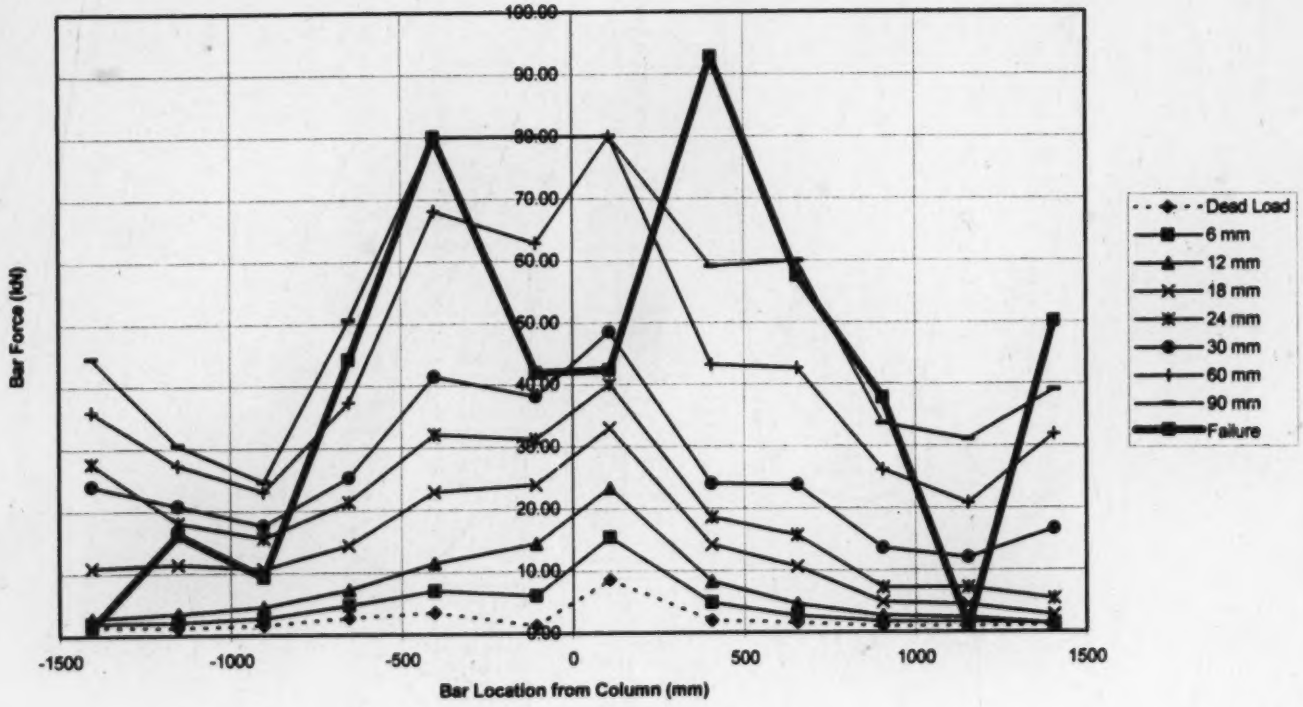

Figure 4.24 Bar Forces in North-South Top Bars across East-West Column Line
For Each Drift Cycle
Control Specimen

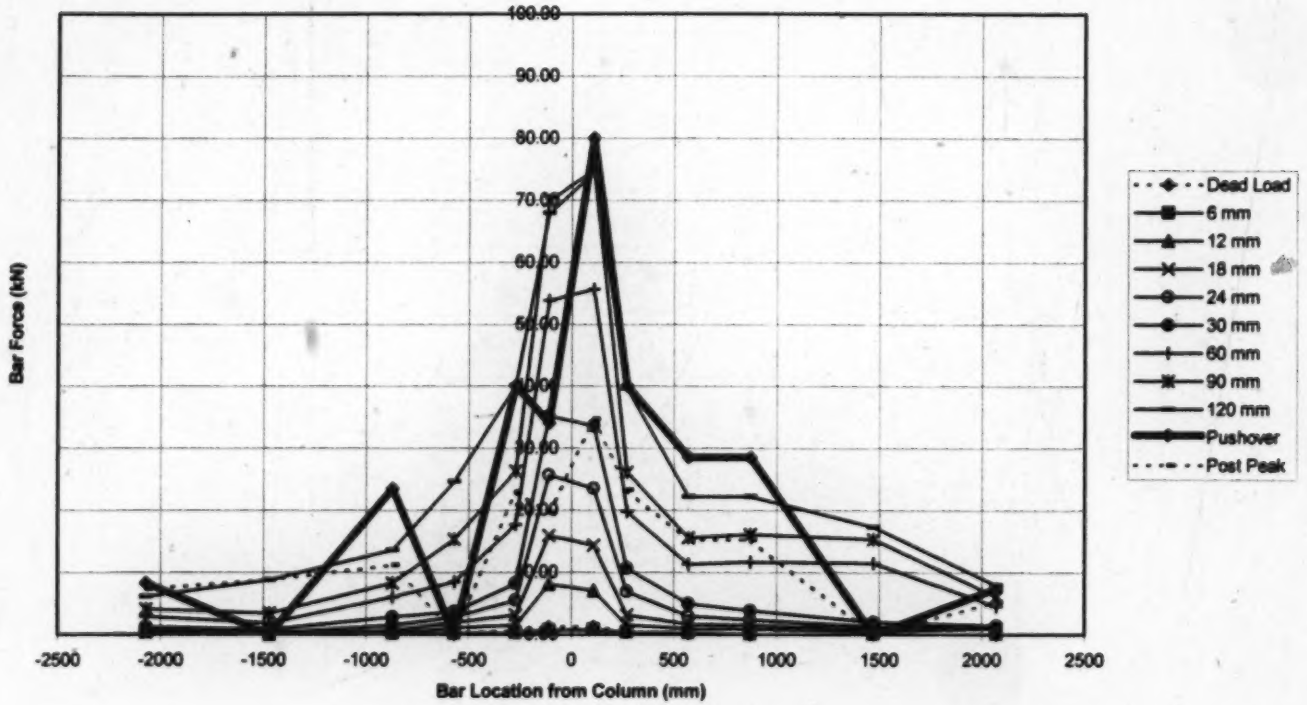

Figure 4.25 Bar Forces in North-South Bottom Bars across East-West Column Line
For Each Drift Cycle
Steel Fibre Specimen

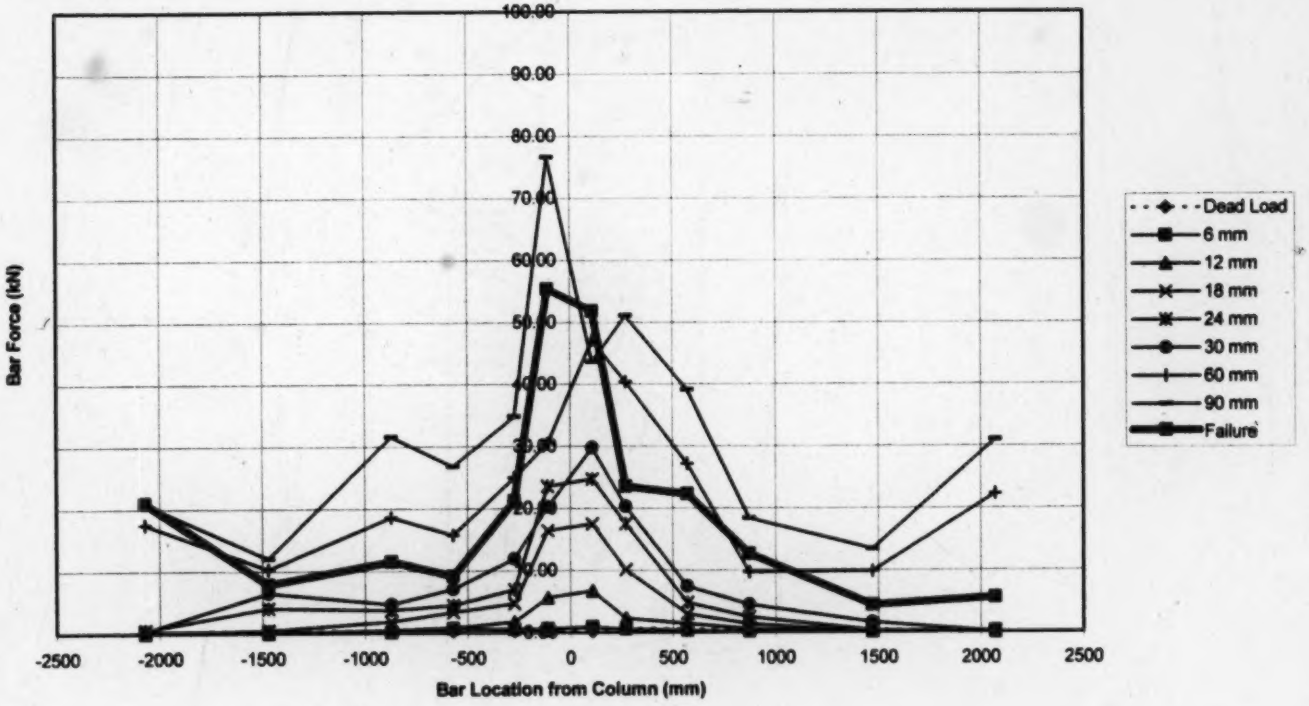

Figure 4.26 Bar Forces in North-South Bottom Bars across East-West Column Line For Each Drift Cycle
Control Specimen

5. DISCUSSION OF TEST RESULTS

5.1 Effects of Steel Fibres

Steel fibres significantly improved the properties of the reinforced concrete. The most important effect of the steel fibres was that they made the connection stronger and more ductile. The steel fibre specimen was able to sustain significantly higher lateral drift and demonstrated ductile properties prior to failure. Even after reaching its peak lateral load, the specimen retained most of its gravity load capacity and performed well while subjected to a number of alternating post-peak cycles of lateral drift.

Steel fibres counteract the formation and growth of tensile cracks and thereby influence cracking and deformation properties in a positive way. Cracking of the steel fibre concrete was delayed, slowed and reduced compared to the control specimen. As cracking occurs, the steel fibres become responsible for the load transfer in those areas and will increase the post cracking strength of the concrete. Steel fibres considerably reduced slab deflections as well as slab rotations.

The particular capacity of steel fibres to counteract the formation and widening of tensile cracks allow tensile stresses to be transferred, while in plain concrete the tensile strength decreases immediately to zero once cracking occurs. The tensile portion of flexural stresses is adequately transferred by traditional bar reinforcement, although steel fibres may be beneficial as well. With punching shear however, a tensile face in the slab is

created at about a 45 degree angle in which plane the bar reinforcement has little effect in transferring tensile stresses. Steel fibres increase the tensile strength of the shear plane, improving the punching strength of the connection. In the experiment, the steel fibres also reduced the demand on the bar reinforcement for the torsional moment transfer.

5.2 Comparison of Test Results to Code Provisions

Both, the steel fibre specimen and the control specimen reached their peak lateral forces of 51.5 kN and 45.6 kN, respectively, at about 4 % drift. The forces were applied at the top of the column and the lateral moment at the connection could be calculated from the force-couple acting on the column. The lateral moments at the joint for the steel fibre and the control specimen were 164 kNm and 155 kNm. The Canadian concrete code CSA A23.3-95 stipulates that for square columns, the portion of the unbalanced moment at the connection, γ_v, that is transferred by shear is 0.4. The shear stress acting on the critical section is given by:

$$v = \frac{V}{b_0 d} + \frac{\gamma_v Me}{J} \qquad (5.1)$$

where:

V = shear force due to gravity loads = 104 kN,

M = unbalanced moment at connection = lateral moment = 164 kNm (steel fibre specimen) or 155 kNm (control specimen),

b_0 = perimeter of critical section = $4\,(c+d)$ = 1844 mm,

d = effective depth of the slab = 106 mm,

c = column dimension = 355 mm,

γ_v = fraction of moment to be transferred by shear = 0.4,

e =distance from the centroid of critical section to critical perimeter = $(c+d)/2$ = 231 mm,

J = polar moment of inertia of the critical section = 7.01×10^9 mm^4.

The polar moment of inertia is calculated as follows:

$$J = \frac{(c+d)d^3}{6} + \frac{(c+d)^3 d}{6} + \frac{d(c+d)^3}{2} \tag{5.2}$$

The first term in equation 5.1 becomes 0.53 MPa for both specimens and the second term for the steel fibre specimen is 2.16 MPa compared to 2.04 MPa for the control specimen. Hence, the respective shear stresses acting on the critical perimeter are 2.69 MPa and 2.57 MPa. Resistance provided by the concrete is calculated according to the concrete code as follows:

$$v_c = 0.4\lambda\phi_c\sqrt{f'_c} \tag{5.3}$$

where λ is taken as unity and f'_c is the compressive strength of the concrete. ϕ_c is a material constant that compensates for the irregularities of the concrete properties and is taken as unity here. The concrete compressive strength was 37.6 MPa for the steel fibre specimen and 34.1 MPa for the control specimen leading to v_c = 2.45 MPa and 2.34 MPa, respectively. The shear strength of the concrete, according to the code model, is lower than the applied shear stresses, suggesting a punching failure should have occurred in

both specimens. However, no punching failure occurred in the steel fibre specimen. The code model appears to be quite conservative, especially since the material constant ϕ_c for concrete is usually taken as 0.6.

5.3 Comparison of Test Results to the Strip Model

The fraction of the moment due to lateral loads transferred to the slab as shear can be estimated from the measured vertical reactions at the north and south edges of the slab. Under lateral loads, punching of the slab will occur most likely on the more heavily loaded side and not around the entire column perimeter. Directly at the north or south column face, the shear force is the sum of the vertical reaction at the slab edge and the gravity load acting on the respective quadrant of the slab. From Table 4.3, the vertical reaction at the edge of the more heavily loaded side was 47.9 kN for the steel fibre specimen and 39.7 kN for the control specimen. The gravity load of both specimens was 104 kN. The shear acting on the more heavily loaded face of the column becomes: V = 47.9 + (0.25)(104) = 73.9 kN (steel fibre specimen), and V = 39.7 + (0.25)(104) = 65.7 kN (control specimen).

Alexander and Simmonds (1999) developed the Strip model to calculate the punching shear resistance of flat slabs. In this model, the slab is divided into four quadrants by radial strips, which extend from the column parallel to the slab reinforcement to a point of zero shear. As each radial strip is loaded on its side faces by the adjacent quadrants; loads can only reach the column if they pass through one of the strips. Each strip is

supported by a vertical reaction P_s at the column end and bending moments, M_{neg} and M_{pos}, at the column and remote ends, respectively. On the side faces, loads are limited to the net internal shear capacity w of the slab. From statics, the vertical reaction P_s can be expressed as:

$$P_s = 2\sqrt{M_s w} \tag{5.4}$$

where M_s is the sum of the negative and positive flexural capacities, M_{neg} and M_{pos}, at the end of the strip. Both, the positive and negative flexural capacities can be estimated from the distribution of the reinforcement ρ in the strip as follows:

$$M = (\rho)(f_y)(0.9cd^2) \tag{5.5}$$

In both specimens the radial strip includes two 15M bars on the top and bottom giving a reinforcement ratio ρ=0.0099 and a resulting moment capacity $M_{neg} = M_{pos} = 16.4$ kNm. The internal shear capacity is calculated by:

$$w = 0.17d\sqrt{f'_c} \tag{5.6}$$

For the steel fibre specimen $w = 118.9$ kN/m and for the control specimen $w = 113.2$ kN/m. The punching strength at the column face becomes $P_s = 124$ kN and $P_s = 121$ kN for the steel fibre specimen and the control specimen, respectively. According to the strip model neither specimen should have failed in shear.

5.4 Slab Forces at Peak Lateral Load

Under lateral load failure of the connection will occur on the more heavily loaded side of the slab. Prior to failure a yield line may form across the slab near the face of the column. From the crack patterns in shown in Figures 4.1 and 4.2 another yield line extending from the corner of the column to the corner of the slab, at a 45 degree angle away from the column face, may also have developed. The former yield line would cross all 14 top bars while the latter yield line only crosses 10 of the top bars. However the maximum negative moment capacity that can possibly develop at the connection would engage all 14 available top bars.

From equilibrium, any tension that is generated in these top bars will have a concrete compression strut framing into the column. Compression struts of bars placed through the column will act directly on the perpendicular column face, while bars away from the column will have their compression struts framing into the side face of the column at about a 45 degree angle as shown in Figure 5.1. These struts on the side face of the column can be divided into their shear and normal components, the latter not being relevant to moment transfer The effective width of the compression block is c_1+c_2, where c_1 is the dimension of the column face parallel to the bar reinforcement and c_2 is the dimension of the perpendicular face of the column. For a square column, where $c_1=c_2=c$, the width of the compression block is $2c$.

The dimension a, the depth of the concrete stress block is given by:

$$a = \frac{A_s f_y}{\alpha_1 f'_c 2c}$$

where:

A_s = area of reinforcing steel = 2800 mm2 (14 No. 15M bars),

f_y = yield strength of reinforcing steel = 400 MPa,

α_1 = stress block parameter = 0.79 (both specimens),

f'_c = concrete strength = 37.6 MPa (steel fibre specimen), 34.1 MPa (control specimen), and

$2c$ = width of compression block = 710 mm.

The depth of the compression block a becomes 53.1 mm for the steel fibre specimen and 58.6 mm for the control specimen. The resisting negative moment M_{res}^- of the connection is calculated from:

$$M_{res}^- = A_s f_y (d - \frac{a}{2})$$

and is 89.0 kNm for the steel fibre specimen and 85.9 kNm for the control specimen.

To calculate the moment acting on the face of the column, the slab can be considered as a cantilever supported from the column. The free body diagram of this cantilever is shown in Figure 5.2 where:

V = shear force at face of the column,

B = weight of 4 concrete blocks = 7.5 kN,

D = self-weight of the slab = 28.8 kN,

R_1 = force in the N-S edge restraint = 22.4 kN (steel fibre specimen) = 23.9 kN (control specimen), and,

R_2 = force in vertical edge boundary links = 47.9 kN (steel fibre specimen) = 39.7 kN (control specimen). Taking the moments of these forces about point O results in a negative moment demand at the face of the column of 102.8 kNm for the steel fibre specimen and 85.0 kNm for the control specimen all of which must frame into the column.

For the control specimen, the negative moment acting on the connection is almost exactly equal to the resisting negative moment suggesting that the connection may have failed because its negative moment capacity was exceeded. Whether the specimen failed in tension by a bond failure of a top bar or in compression by crushing of the compression block is not known. Cyclic loading will likely have caused an internal shear crack in the slab within the critical section. Failure, regardless whether in tension or compression, would have caused the concrete to separate at its weakest location: the internal shear crack. This explains why the failure of the control specimen visually appeared to be a punching shear failure but could in fact have been a flexural failure.

The steel fibre specimen exceeded its negative moment capacity by about 14 kNm. From observations about slab rotations made earlier in the text, it was concluded that the steel fibres caused the slab to behave more uniformly. A reason for this observation is that the steel fibre slab experienced substantially less cracking than the control specimen. Through the reduction of cracking, the steel fibres allowed the torsional stresses to be distributed further away from the column region therefore engaging more of the outlying top bars, resulting in a higher negative moment capacity. Because of this increase in

torsional stiffness, the steel fibres may have increased the flexural capacity of the connection.

Prior to reaching the peak lateral load, successive loading cycles caused yielding in the top bars near the column face allowing them to deform plastically. The positive moment in the reversing half of the drift cycle was not large enough to recover the bar deformation. As a result a crack will grow with each increase in lateral load causing the slab to "grow" as the reinforcement expands.

5.5 Degradation of the Stiffness of the Connection

During the experiment the cyclic lateral drift caused severe degradation of the stiffness of the connection. The stiffness of the connection is directly related to the effective width of the slab. The effective width of the slab is the width of the joint region in the slab into which the lateral forces are transferred from the column. For an elastic frame, the stiffness K at the interior joint of a slab with far ends pinned is given by:

$$K = \frac{12EI_{slab}}{L}$$

where E is the modulus of elasticity of the slab concrete, I_{slab} is the effective moment of inertia of the slab and L is the distance between the centrelines of the adjacent slab bays. The moment of inertia of the slab is defined as:

$$I_{slab} = \frac{bh^3}{12} xC$$

Here, h is the depth of the slab, C is a cracking factor and b is the effective width of the slab. The cracking factor accounts for the loss of stiffness due to the degree of cracking and varies from 1 (initial) to about 1/3 (at about 3 % drift). Since in this case the stiffness K has been determined from measurements during the test, the calculated stiffness already accounts for cracking. The cracking factor is the only variable that is not a constant and the product of the cracking factor and the effective width has been calculated in Table 5.1. Figure 5.3 is a plot of the product of the cracking factor and the effective width of the slab at its respective lateral drift level.

Cracking of the slab under reversed cyclic loading reduces the net shear area available for shear resistance. Durrani et al. (1995) proposed the following equation for the punching shear strength of concrete subjected to cyclic lateral drift (in SI units):

$$v_c = (0.33 - 0.021\Delta)\sqrt{f'_c} \tag{5.7}$$

where Δ is the inter-story drift in percent. At 4 % drift, or about when the peak lateral load occurred in both specimens, the punching strength of the concrete using equation 5.7 becomes 1.51 MPa for the steel fibre specimen and 1.44 MPa for the control specimen. From the test results obtained in this experiment, it appears that the code model presented in section 5.2 is on the conservative side and needs no further reduction in concrete strength accounting for the degradation of stiffness for drift levels up to 4%.

5.6 Proposed Design Equation

The effect of steel fibres on punching shear strength is not discussed in the Canadian concrete code. Shear stresses of both specimens encountered at peak lateral load, calculated using equation 5.1, do not differ significantly. In this experiment, the higher peak lateral load observed in the steel fibre specimen may then be attributed solely to its slightly higher compressive strength of the concrete. Compressive strength of the concrete is not affected by the presence of steel fibres.

Previous test programs discussed in chapter 2 all reported increases in punching strength due to the steel fibres. Shaaban and Gesund (1994) suggested that the shear strength of the steel fibre reinforced concrete is directly related to its splitting strength. In this test, the steel fibre content was 40 kg/m^3 or 0.17 % by weight of concrete. According to equation 2.3 (SI units), $f_{sp} = (0.025W_f + 0.57)\sqrt{f'_c}$, developed by these authors the splitting strength of the concrete would be 3.50 MPa comparing well to the 3.80 MPa determined in the split cylinder test. Since the splitting strength of concrete describes its tensile abilities and shear transfer is increased by the post cracking behaviour of the steel fibre concrete allowing the transfer of tensile stresses in the shear plane to continue, the use of the splitting strength may be more appropriate than the use of the compressive strength of the concrete. However, under numerous cycles of reversed cyclic drift, the connection will still deteriorate. Substituting the $0.33\sqrt{f'_c}$ term in equation 5.7 with the splitting strength may be yield a good approximation for the shear strength of the concrete under reversed cyclic loading (SI units):

$$v_c = f_{sp} - 0.021\Delta\sqrt{f'c} \tag{5.8}$$

or substituting equation 2.3 for the splitting strength f_{sp}:

$$v_c = \left(0.0025\frac{F}{w_c} + 0.57 - 0.021\Delta\right)\sqrt{f'_c} \tag{5.9}$$

where F is the mass of steel fibres per unit volume of plain concrete (kg/m^3) and w_c is the unit weight of plain concrete (kN/m^3). At 4 % drift the shear strength of the steel fibre specimen according to equation 5.9 would be 3.06 MPa.

The code equation predicted a shear strength of 2.45 MPa. The specimen reached its peak lateral load during pushover at a shear stress of 2.64 MPa. Since the specimen did not fail in punching, the actual shear strength of the steel fibre concrete may in fact be higher than predicted by the code equation and probably closer to equation 5.9. Further, the failure surface appeared to start occurring immediately adjacent to the column, where the interface between plain concrete and steel fibre concrete was located. Since the steel fibres may not have contributed fully in this region, the true beneficial effect of the steel fibres may not be reflected in the results obtained here.

Cycle	Specimen	Average Stiffness K for Cycle x10^6	f'_c (MPa)	E (MPa)	I_{slab} (mm^4)	Effective Width x Cracking Factor C x b (mm)
6 mm	Steel Fibre	16835	37.6	24513	2.40E+08	821
	Control	18930	34.1	23353	2.84E+08	969
12 mm	Steel Fibre	17050	37.6	24513	2.43E+08	832
	Control	19322	34.1	23353	2.90E+08	990
18 mm	Steel Fibre	15982	37.6	24513	2.28E+08	780
	Control	16412	34.1	23353	2.46E+08	840
24 mm	Steel Fibre	14083	37.6	24513	2.01E+08	687
	Control	14353	34.1	23353	2.15E+08	735
30 mm	Steel Fibre	11708	37.6	24513	1.67E+08	571
	Control	13309	34.1	23353	1.99E+08	682
60 mm	Steel Fibre	7650	37.6	24513	1.09E+08	373
	Control	7868	34.1	23353	1.18E+08	403
90 mm	Steel Fibre	5879	37.6	24513	8.39E+07	287
	Control	5755	34.1	23353	8.63E+07	295
120 mm	Steel Fibre	4360	37.6	24513	6.22E+07	213
Residual	Steel Fibre	2589	37.6	24513	3.70E+07	126

Table 5.1 Calculation of the Effective Slab Width x Cracking Factor after each Cycle

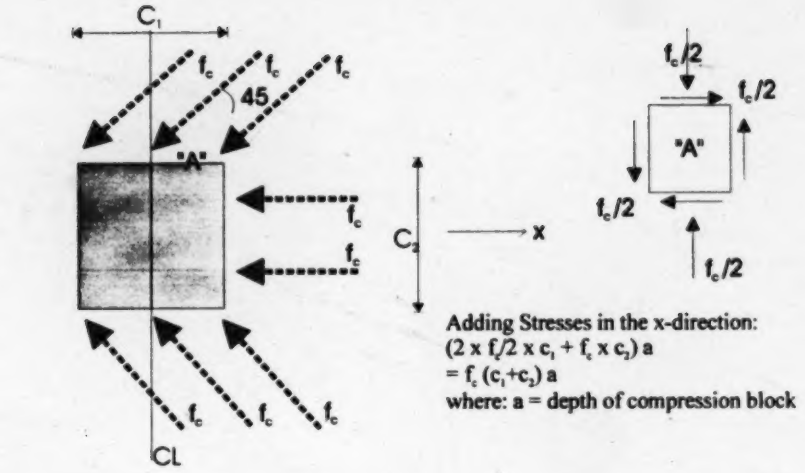

Figure 5.1 Location of Compression Struts

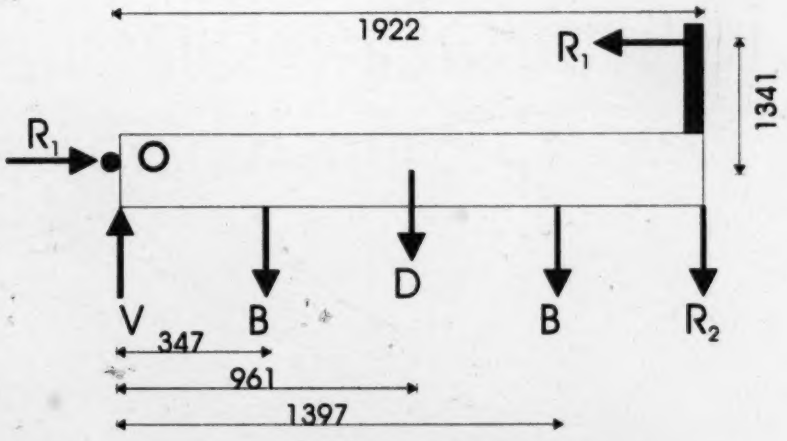

Figure 5.2 Free Body Diagram of Slab Cantilever

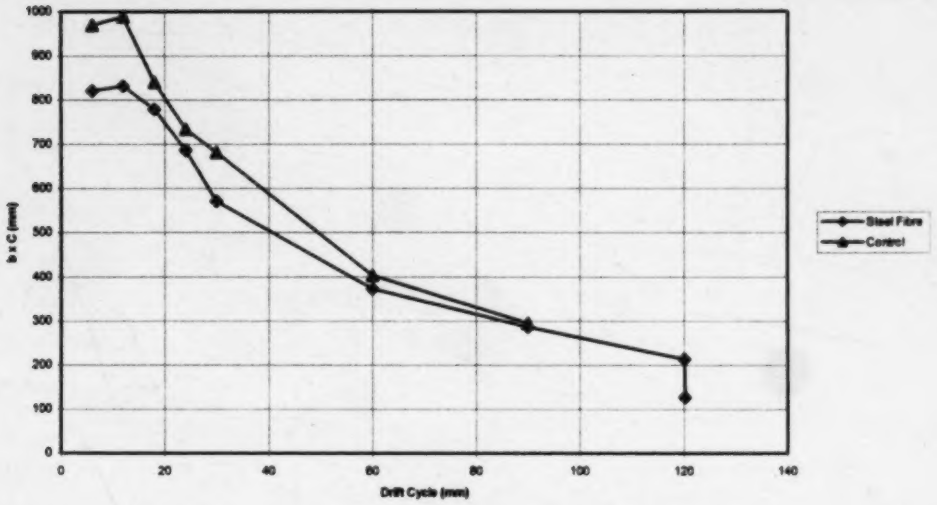

Figure 5.3 Effective Width of Slab "*b*" x Cracking Factor "*C*" after each Cycle

6. SUMMARY, CONCLUSIONS AND RECOMMENDATIONS

6.1 Summary

Although usually not part of the lateral load resisting system, slab column connections must sustain lateral drift during an earthquake without any loss of their gravity load capacity. Such inter-story deflections create a moment at the slab-column joint, part of which is transferred as shear to the slab. The ultimate strength of flat-slab structures is often governed by punching shear and the use of shear reinforcement in the slab may be required to increase the punching strength at the slab column connection under those circumstances.

Steel fibre reinforcement has proven to be an effective and practical type of shear reinforcement. A literature survey showed that steel fibres increase the ultimate strength of the connection and, more importantly, provide for a ductile failure with considerable post-failure reserve strength. Steel fibre reinforced connections performed well under cyclic loading allowing for substantial inter-story drifts without any loss in gravity load capacity. Reductions of slab deflections and rotations are also reported. Steel fibres increase the shear transfer to the column due to post-cracking tension capacity of steel fibre reinforced concrete. Addition of a relatively small amount, between 30 to 60 kg/m^3 of steel fibres proved to be very effective, exceeding this range did not result in any further benefits.

The experimental program involved the testing of two full-scale isolated slab-column connections subjected to reversed cyclic lateral drift. The first specimen contained 40 kg/m^3 of steel fibres placed throughout the entire slab, except in the immediate column region. For comparison purposes, the slab of the second specimen contained only plain concrete. Apart from the steel fibres, the specimens were identical in both fabrication and material properties and were tested under the same conditions. The test itself subjected the two specimens to increasing cycles of reversing lateral inter-story drift while maintaining a constant gravity load. The main objective of this test program was to compare the behaviour of the two specimens and to create a test set-up that accurately reflects prototype conditions. Parameters that were investigated during the test were the load-drift response, degradation of the connection, mode of failure and post-failure resistance.

6.2 Conclusions

1. The steel fibres significantly increased the drift capacity of the slab-column connection. The steel fibre specimen sustained much larger inter-story drifts than did the control specimen

2. The steel fibre specimen demonstrated significant ductility with a gradual failure, while the control specimen experienced precipitous failure.

3. Deterioration of the stiffness of the connection was faster in the control specimen.

4. Slab deflections and slab rotations in the steel fibre specimen were 10 % and 30 % lower, respectively, than in the control specimen.

5. Steel fibres significantly reduced cracking of the slab and increased its post-cracking stiffness.

6. Torsional strains in the bar reinforcement at the connections are reduced and torsional stiffness of the slab is increased by the presence of steel fibres. This may result in an increase of the flexural as well as the shear capacity of the connection as more flexural reinforcement was developed.

7. Cyclic lateral loading caused successive yielding of the top bars at the face of the column, which permanently elongated these bars. This became evident in the steel fibre specimen, where a gap at the joint started to "grow" with increasing drift.

8. The code model is satisfactory in predicting the strength of a slab-column subjected to cyclic lateral loading.

9. In repair situations, placing steel fibres into the column region may prove difficult. Nevertheless, the test has shown that a substantial improvement of the punching strength of the connection is achieved without steel fibres in this region. This suggests that the use of steel fibre concrete is effective in repairing slab-column connections.

6.3 Recommendations

1. Although the presence of steel fibres did increase the strength of the slab-column connection, the mechanism by which the strength is increased is not known. Further testing is required to determine whether the increase in strength is in fact related to the increase in torsional stiffness.

2. Neither of the two specimens developed a punching shear failure, as the slabs were deficient in flexural capacity. In this experiment, the cut-offs of the reinforcement bars in the top mat, while suitable for gravity loads, may not have been long enough for the lateral loads. As a result some bars may not have fully developed. It is suggested, that the bar cut-off lengths be chosen more appropriately to sustain lateral loads to ensure adequate flexural capacity in a future experiment.

3. Further testing should also consider other types of occupancy loads beyond the residential type considered in this experiment.

4. Steel fibres have proven to be very effective in preventing a precipitous punching shear failure of slab-column connections during an earthquake, both in this experiment and in previous test programs. They represent a simple and practical alternative to other methods of improving the punching shear strength. The use of

steel fibre concrete in rehabilitation situations has also been addressed in this experiment with positive results. A test program with only two specimens provides very limited data and further testing in the area of rehabilitation is suggested due to its wide range of applications.

LIST OF REFERENCES

ACI Committee 421, 1999, "Draft Report on Design of Slabs Subjected to Seismic and Dynamic Forces," American Concrete Institute, Detroit, Michigan.

ACI Committee 544, 1989, "Measurements of Properties of Fiber Reinforced Concrete," ACI Materials Journal, Vol. 85, No. 6, pp 583-593.

Alexander, S. D. B. and Simmonds, S. H., 1992, "Punching Shear Tests of Concrete Slab-Column Joints Containing Fiber Reinforcement," ACI Journal, Vol. 89, No. 4, pp. 425-432.

Alexander, S.D.B. and Simmonds, S. H., 1991, "Bond Model for Strength of Slab-Colum Joints," Structural Engineering Report No. 174, Department of Civil Engineering, University of Alberta, Edmonton, pp. 52.

Canadian Standards Association, 1994, "Design of Concrete Structures for Buildings (CSA A23.3-94),"Canadian Standards Association, Rexdale, Ontario.

Durrani, A. J. and Diaz, A. J., 1992, "Seismic Resistance of Fiber-Reinforced Slab-Column Connections." Proceedings, 10th World Conference on Earthquake Engineering, Balkema, A. A., editor, Rotterdam, Vol. 6, pp. 3113-3116.

Durrani, A. J., Du, Y. and Luo, Y. H., 1995, "Seismic Resistance of Nuonductile Slab-Column Connections in Existing Flat-Slab Buildings, ACI Journal, Vol. 92, No. 4, pp. 479-487.

Gardner, N. J., 1990, "Relationship of the Punching Shear Capacity of Reinforced Concrete Slabs," ACI Journal, Vol. 87, No. 1, pp. 66-71.

Gesund, H. and Kaushik, Y. P., 1970, "Analysis of Punching Shear Failures in Slabs," International Association for Bridge and Structural Engineering, Zurich, Vol. 30-I, pp. 41-60.

Maidl, B. R., 1995, "Steel Fibre Reinforced Concrete," Ernst & Sohn, Berlin.

McHarg, P. J., Cook, W. D., Mitchell, D., Yoon, Y., 2000, "Benefits of Concentrated Slab Reinforcement and Steel Fibres on Performance of Slab-Column Connections," ACI Journal, Vol. 97, No. 2, pp. 225-234.

National Research Council of Canada, 1995, "National Building Code of Canada," National Research Council of Canada, Ottawa, Ontario.

Shaaban, A. M. and Gesund, H., 1993, "Splitting Tensile Strength of Steel Fibre Reinforced Concrete Cylinders Consolidated by Rodding or Vibrating," ACI Materials Journal, Vol. 90, No. 4, pp. 366-369.

Shaaban, A. M. and Gesund, H., 1994, "Punching Shear Strength of Steel Fiber Reinforced Concrete Flat Plates," ACI Journal, Vol. 91, No. 4, pp.407-414.

Schaefer, T. C., Editor, 1999, "The Design of Two-way Slabs," ACI Special Publication SP-183, pp. 93-118.

Shehata, I. A. E. M., 1990, "Rational Method for Designing RC Slabs to Resist Punching," ASCE Journal of Structural Engineering, Vol. 116, No. 7, pp. 2055-2060.

Swamy, R. N. and Ali, S. A. R., 1982, "Punching Shear Behavior of Reinforced Slab-Column Connections Made with Steel Fiber Concrete,"ACI Journal, Vol. 79, No. 5, pp. 392-406.

APPENDIX A

DESIGN CALCULATIONS

A.1 Determination of the Lateral Force

The deflected shape of the slab column connection as well as its free body diagram is shown in Figures A.1 and A.2, respectively. The inter-story drift *ID* is twice the deflection *D* due to the slab rotation α plus the deflection of the column ΔD itself under the applied lateral load *V*:

$$ID = 2(D + \Delta D) \tag{A.1}$$

Since the angle of rotation α is relatively small, *D* is related to it by: $d = \alpha (h/2)$.

Summing the moments around the connection gives:

$$6k_s\alpha - 2V\,h/2 = 0 \tag{A.2}$$

where $k_s = \dfrac{(EI)_s}{l}$ = stiffness of the slab. The deflection of the column itself is calculated by:

$$\Delta D = \frac{V(h/2)^3}{3(EI)_c} \tag{A.3}$$

Making all the substitutions and rearranging yields the relationship between the lateral force *V* and the inter-story drift *ID*:

$$V = \frac{ID}{\frac{h^3}{12(EI)_c} + \frac{h^2 l}{6(EI)_s}}$$

(A.4)

For this test the quantities are as follows:

ID = inter-story drift = 60 mm,

h = story height = 3 m,

l = clear span = 4.2 m, and,

E = Modulus of Elasticity of the concrete = 21900 MPa.

The moment of inertia of the slab is estimated from $I_s = CS\frac{lh_s^3}{12}$, where C is a cracking factor of 0.4 (fully cracked), S is an effective width reduction factor which can be taken as 0.3 according to Parker et. al. and h_s is the slab depth. For the column, the moment of inertia is given by: $I_c = C\frac{c^4}{12}$, where again C is the cracking factor (here 0.8) and c is the column dimension. Hence, to achieve an inter-story drift of 2% or 60 mm a lateral force V of 29.3 KN is required.

A.2 Design of Slab Reinforcement

The slab design dead load consists a superimposed uniformly distributed load (UDL) of 0.75 KPa and the slab self-weight of 3.6 KPa totalling 4.35 KPa. The design live load acting on the slab was a UDL of 1.9 KPa. Further, a moment of 88 KNm due to the

lateral force acted on the connection. Slab reinforcement requires was designed according the Direct Design Method.

For the bottom mat only the gravity loads were considered. The factored loads were calculated using a combination of 1.25 x dead loads + 1.5 live loads = 8.3 KPa resulting in a design moment of 18.3 KNm/m. 35% of this moment is taken in the positive moment region requiring a bottom steel amount of 180 mm^2/m. Minimum steel as prescribed by the code requires 304 mm^2/m and thus 10M bars spaced at 300 mm throughout the slab were selected.

The top mat was designed to resist the moment due to earthquake in addition to the gravity loads. 40% is thefraction of the moment that is transferred to the slab as, resulting in a design earthquake moment of 0.6 x 88 KNm = 52.8 KNm. The factored gravity load combination is given by 1.0 x dead load + 1.0 (0.5 x live load + 1.0 x earthquake load) and the gravity design moment was 49.1 KNm, 65% which is resisted in the negative moment region or 31.9 KNm. The total negative design moment is 84.7 KNm requiring 2356 mm^2 of top steel. 14 No. 15M bars were chosen to that effect.

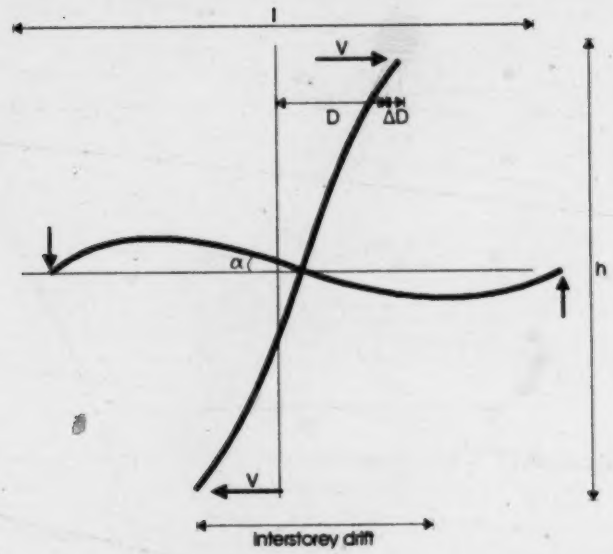

Figure A.1

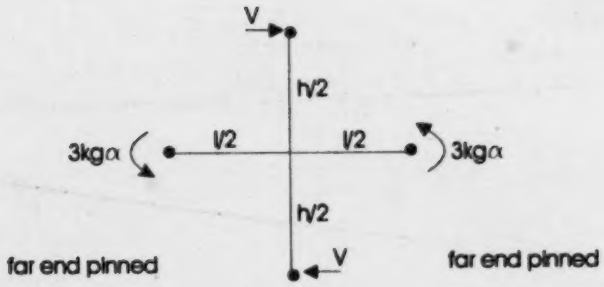

Figure A.2

APPENDIX B

PICTURES OF TEST SPECMENS AND TEST SET-UP

Figure B.1 Edge Boundary Links

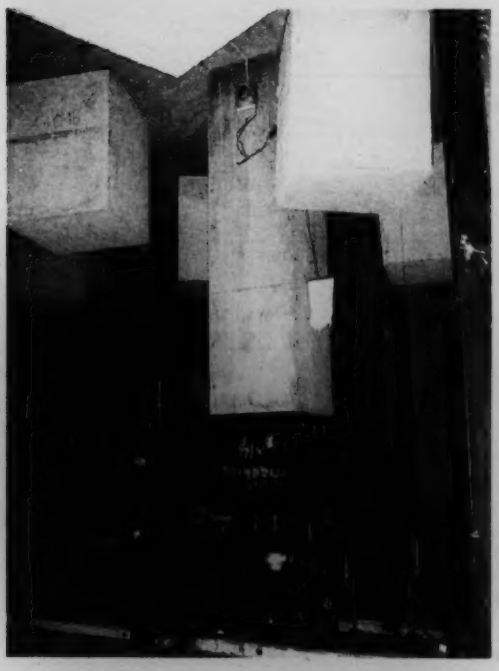

Figure B.2 Bottom Column

Figure B.3 Bottom Support

Figure B.4 Lateral Jack and Edge Restraints

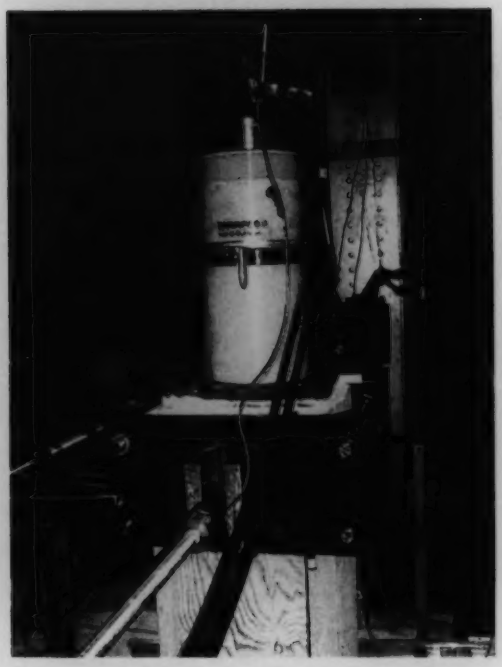

Figure B.5 Top Support

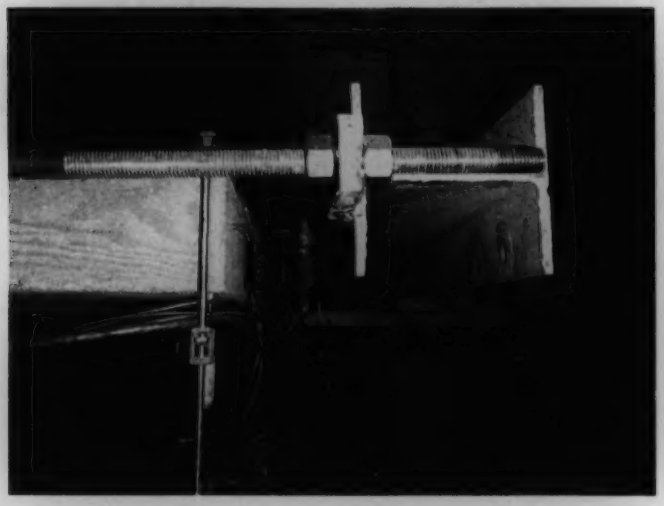

Figure B.6 Twisting Restraints

Figure B.7 Lateral Drift of Steel Fibre Specimen at End of Test

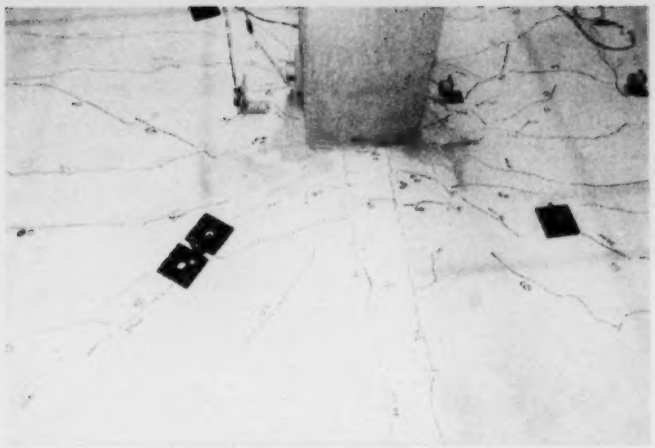

Figure B.8 Cracks at 60 mm Drift – Steel Fibre Specimen (Looking North)

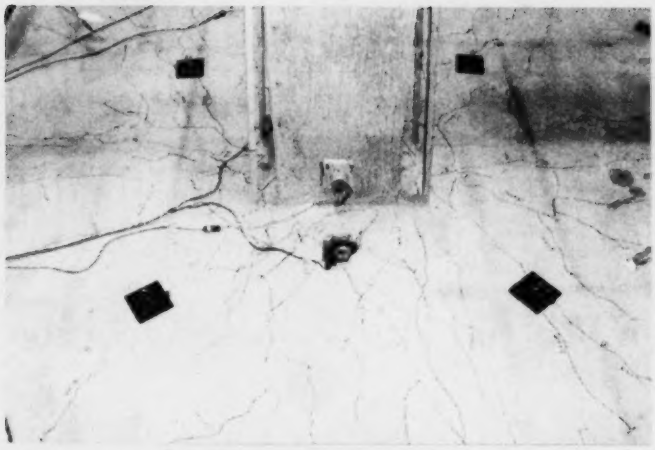

Figure B.9 Cracks at 60 mm Drift – Control Specimen (Looking East)

Figure B.10 Cracks at Pushover – Steel Fibre Specimen
(Looking East)

Figure B.11 Cracks at Pushover, Underside of Slab – Steel Fibre Specimen
(Looking East)

Figure B.12 Cracks at Failure – Control Specimen
(Looking South)

Figure B.13 Cracks at Failure, Underside of Slab – Control Specimen
(Looking East)

Figure B.14 Cracks at Failure – Control Specimen
(Looking South-East)

Figure B.15 Cracks at Failure, Underside of Slab – Control Specimen
(Looking North-West)